UNIVERSIDADE D
COIMBRA

Tiago Emanuel Anjo de Oliveira Custódio

Low Density Warm Stellar Matter With Light Clusters And Hyperclusters, Hyperons And Delta Isobars

Dissertação no âmbito do Mestrado em Física Nuclear e de Partículas orientada pela Professora Doutora Maria Constança Mendes Pinheiro da Providência Santarém e Costa e Doutora Helena Sofia de Castro Felga Ramos Pais e apresentada ao Departamento de Física da Faculdade de Ciências e Tecnologia.

Outubro de 2021

Low Density Warm Stellar Matter with Light Clusters and Hyperclusters, Hyperons and Delta Isobars

Tiago Emanuel Anjo de Oliveira Custódio

A thesis submitted for the degree of Master in Nuclear and Particle Physics

Supervisors:
Prof. Doutora Maria Constança Mendes Pinheiro da Providência Santarém e Costa
Doutora Helena Sofia de Castro Felga Ramos Pais

Department of Physics
University of Coimbra
Portugal

October 2021

Resumo

A abundância de agregados leves, hiperões e partículas Δ produzidas em ambientes estelares tais como supernovas e colisões de duas estrelas de neutrões é calculada a baixas densidades no âmbito de modelos relativistas de campo médio não lineares e com acoplamentos dependentes da densidade. Em relação aos agregados leves, consideraram-se cinco agregados puramente nucleónicos e três hiperagregados. Verifica-se que a introdução de hiperões e partículas Δ empurra a dissolução dos agregados leves para densidades mais altas, aumentando também a sua abundância. Este efeito é tanto maior quanto menor for a fração de carga do sistema e quanto maior a temperatura. Por outro lado, as abundâncias de hiperões e partículas Δ são também afetadas pela presença de agregados leves no sistema, fazendo com que os hiperões e Δs de carga positiva ou neutra diminuam de quantidade, enquanto que os de carga negativa aumentam. Também se observa que a dissolução dos agregados menos abundantes ocorre a densidades mais elevadas fruto da redução dos efeitos de Pauli-blocking. De um modo geral, os hiperagregados apenas se formam a temperaturas superiores a 25 MeV, sendo que dependendo da temperatura e composiçao química do sistema, podem chegar a ser mais abundantes que o ^{4}He ou mesmo mais abundantes que outros agregados mais pesados. Também se verifica que para alguns valores dos acoplamentos das partículas Δ aos mesões, a massa efetiva do nucleão torna-se zero a baixas densidades, impedindo a equação de estado correspondente de atingir a estrela de massa máxima. Quando tal acontece, a equação de estado correspondente a esses acoplamentos não serve para descrever estrelas de neutrões.

Palavras-chave: Teoria Relativista Nuclear de Campo Médio, Matéria de Supernovas e Colisões de Estrelas de Neutrões, Agregados Leves e Hiperagregados, Bariões Pesados, Matéria Hadrónica Quente Não Homogénea

Abstract

The abundance of light nuclei, hyperons and Δ isobars that are produced in stellar environments such as supernova or binary neutron star mergers, is calculated within both nonlinear and density-dependent relativistic mean-field models in low-density matter. Five purely nucleonic light nuclei (^{2}H, ^{3}H, ^{3}He, ^{4}He, ^{6}He) are considered, together with three light hypernuclei ($^3_\Lambda$H, $^4_\Lambda$H, $^4_\Lambda$He). We show that the presence of hyperons and Δs shifts the dissolution of clusters to larger densities, and increases the amount of clusters. This effect is larger the smaller the charge fraction, and the higher the temperature. The abundance of hyperons and Δs is also affected by the cluster formation: neutral and positively charged hyperons and Δs suffer a reduction, and the negatively charged ones an increase. We also observe that the dissolution of the less-abundant clusters occurs at larger densities due to smaller Pauli-blocking effects. Overall, hypernuclei set in at temperatures above 25 MeV, and depending on the temperature and chemical composition, they may be more abundant than ^{4}He, or even more abundant than other heavier clusters. It is also seen that for some values of the couplings of the Δs, the nucleon effective mass becomes zero at too low densities, preventing the corresponding EoS of reaching the maximum mass star, therefore not being adequate to describe neutron stars.

Keywords: Relativistic Nuclear Mean Field Theory, Supernova and Neutron Star Merger Matter, Light Nuclei and Hypernuclei, Heavy Baryons, Warm Non-homogeneous Hadronic Matter

Acknowledgements

First and foremost, I would like to show my deepest gratitude to my supervisors, Professor Constança Providência and Helena Pais, for all their teachings, time devoted and patience. Their deep knowledge about this field of Physics is remarkable and it was a pleasure to learn from them.

To my friends, who showed me how to de-stress and enjoy the good things in life.

Finally, to my family, whose unconditional support and love have brought me to this point in my life, I whole-heartedly thank you.

This thesis was supported with funds from FCT/MCTES under the project POCI-01-0145-FEDER-029912.

Contents

List of Figures

List of Tables

List of Abbreviations

NS Neutron Star

EoS Equation of State

RMF Relativistic Mean Field

HIC Heavy-Ion Collisions

CCS Core-Collapse Supernova

BNSM Binary Neutron Star Mergers

LHC Large Hadron Collider

RHIC Relativistic Heavy Ion Collider

Chapter 1

Introduction

Neutron stars are produced as a result of core-collapse supernova (CCS) corresponding to the late stage of massive stars (typically $M > 8M_\odot$ [1]). Right after the core-collapse, the young neutron star (NS) reaches high temperatures of up to tens of MeV. However, in a matter of a few seconds, neutrinos and photons diffuse out of the star and it cools down to less than 1 MeV, leading the star matter to reach its ground state configuration in chemical equilibrium (also known as β-equilibrium) [1]. Since the temperature in equilibrium is below 1 MeV, the star is cold on the nuclear level and the temperature can be approximated to zero. In this case, the strong nuclear reactions that conserve strangeness can no longer occur, whereas weak interactions not conserving strangeness still take place, resulting in the star having a net strangeness. On the other hand, the baryon number and electrical charge are globally conserved in a NS [1].

Matter inside a NS is subject to incredibly high densities, reaching several times the nuclear saturation density (n_0) in the innermost layers of the star. This implies that masses of $1.5-2M_\odot$ can fit in a radius of the order of $\sim$10km (typical values of a NS). NSs show a onion-like structure. The layers, from the surface to the center, comprise an outer crust, an inner crust, and a core, with an atmosphere constituted by a lattice of ionized atomic nuclei (mainly ^{56}Fe, produced in nuclear fusion reactions by the progenitor star) with electrons filling up the gaps between the nuclei [2]. As we go deeper into the star, we reach the outer crust, where the increasing density leads the protons inside the nuclei to capture surrounding electrons making the nuclei richer in neutrons through the inverse β-decay [2, 3]. However, as the density further increases, the increase of neutrons is such that, due to the symmetry term, neutrons start to leave the nuclei (neutron drip). This line sets the border between the outer and inner crusts. In the inner crust, heavy neutron rich clusters are expected to be formed, immersed in a gas of neutrons and electrons [2, 3]. These clusters become heavier up to a point where the competition between the nuclear and the Coulomb forces is so strong that they form geometrical structures that resemble the Italian pasta, and were coined the nuclear pasta phase [4–6]. Light clusters, such as ^{2}H, ^{3}H, ^{3}He, ^{4}He, ^{6}He, are also expected to be present in the inner crust for temperatures above 1 MeV [7]. As the density increases even further, these heavy clusters will eventually melt (at densities of $\sim 0.5n_0$). This sets the transition to the core of the star. In this region, the composition of the star corresponds to uniform nuclear matter made of neutrons, protons, electrons and muons [3]. In the inner core of the star (densities of the order of $\sim 2n_0$), exotic degrees of freedom such as hyperons (Λ, $\Sigma^{-,0,+}$, $\Xi^{-,0}$) and delta isobars ($\Delta^{-,0,+,++}$), or even deconfined quark matter, may appear [3].

Hyperons are baryons with at least one quark s; together with the nucleons they form the spin-1/2 baryonic octet. Delta isobars are spin-3/2 baryons formed by u and d quarks that

usually decay via the strong force into a nucleon and a pion. Both hyperons and Δs are heavier than nucleons. These exotic degrees of freedom appear because, as the density increases, the chemical potentials of the nucleons also increase since as fermions they obey the Pauli exclusion principle. Thus, the nucleons at the top of their Fermi levels will be highly energetic and it becomes energetically favorable to convert them into more massive particles such as hyperons and Δs since they will start by filling their low momentum Fermi levels, reducing the pressure of the system. Therefore, when the increasing chemical potentials of the nucleons approach the effective mass of hyperons and Δs, nucleons will start to be converted to these new degrees of freedom.

As we mentioned above, once the star cools down to $T = 0$ MeV, β-equilibrium is reached and the star will remain in equilibrium unless it is perturbed by some external phenomena, such as a collision with another NS. Just like in the CCS, when two binary NSs collide and merge β-equilibrium is not necessarily achieved and temperatures as high as 50 to 100 MeV may be attained. At such high temperatures, exotic degrees of freedom such as hyperons and Δ isobars may appear at much lower densities compared to the case where the NS is in β-equilibrium. In fact, a finite temperature allows for the presence of excited states of the nucleons, which will then convert into heavier baryons at lower densities. Therefore, to describe both CCS and BNSM it is necessary to consider a wide range of charge fractions, temperatures and densities.

In this work, we will be mainly interested in studying the presence of light nuclei in matter that has not yet achieved β-equilibrium, such as CCS and BNSM matter. However, these light nuclei are also present at subsaturation densities in the inner crust of proto NS and have been detected in heavy-ion collisions (HIC) in several experiments, such as ALICE at the Large Hadron Collider (LHC), STAR at the Relativistic Heavy Ion Collider (RHIC), or J-PARC, from the E13 collaboration. Some of these states, like the deuteron, the hypertriton [8], the hyperhydrogen 4 [9] or the hyperhelium4 [10] are loosely bound objects with quite a large radius. It is still not understood why these states are well described within a thermal approach with a temperature production of the order of 150 MeV, much larger than their binding energy [11]. At RHIC and LHC, the baryonic chemical potential is quite low. The formation of light clusters at much smaller temperatures, of the order of 5 to 12 MeV, but larger densities, below 0.1 fm^{-3}, has been measured by the multi-detectors NIMROD at the Texas A&M University [12] and INDRA [13] at GANIL. This experimental data set constraints on the low-density nuclear matter equation of state (EoS) at temperatures and densities of interest to the evolution of CCS and BNSM. In fact, it is important to know the abundances of these light nuclei when studying both CCS and BNSM because their presence may impact the evolution of these systems by affecting the rate at which the weak reactions take place during the core collapse [14, 15], or the dissolution of the remnant torus of accreted matter that is formed around the high mass NS after a BNSM [16]. Light clusters could also influence the dissipative processes that determine the post-merger evolution and mass ejection from the remnant [17, 18].

Besides reducing the Fermi pressure, the introduction of hyperons decreases the free energy of matter as mentioned in Refs. [19, 20], where it was also shown that at low densities hyperons compete with light clusters and that the minimization of the free energy should allow for the appearance of hyperons at very low densities, which, however was not implemented. In Ref. [21], the possible appearance of hyperons in the density region of the non-homogeneous matter that forms the inner crust of a NS was analyzed. Temperatures below the melting temperature of the heavy clusters that form this region were considered, i.e $T \lesssim 15$ MeV. It was found that only very small amounts of hyperons, like Λ fractions below 10^{-5}, were present in the background

gas. The low-density EoS of stellar matter including light clusters and heavy baryons was also studied in Ref. [22]. In addition to hyperons, the author also considered Δ baryons, pions, and the presence of a representative heavy cluster. It was shown that, depending on temperature and density, the composition of matter may shift from a greater abundance of light clusters to a heavy-baryon predominance.

Therefore, in the present work we are going to simultaneously calculate, in a consistent way, the abundance of purely nucleonic light clusters (^{2}H, ^{3}H, ^{3}He, ^{4}He and ^{6}He) and hyperclusters ($^3_\Lambda$H, $^4_\Lambda$H, $^4_\Lambda$He) as well as hyperons and Δ isobars within relativistic mean-field models. The introduction of clusters is going to follow the approach first presented in Ref. [23], where the effect of the medium on the binding energy of the clusters is considered through the introduction of a binding energy shift, together with a universal coupling of the $\sigma-$meson to the different clusters, that was chosen so that the equilibrium constants of the NIMROD experiment [12] were reproduced. In Refs. [24, 25], the same approach was applied to the description of the INDRA data [13] including the medium effects on the data analysis. It was verified that, in this case, the equilibrium constants could be reproduced only if a larger $\sigma-$meson coupling was introduced. The calibration of the $\sigma-$meson to the clusters coupling was later performed for other models in Ref. [26].

This work is organized as follows: in Chapter 2 we introduce the formalism to describe NS matter in β-equilibrium and $T = 0$ MeV for two types of RMF models: nonlinear and density-dependent. In Chapter 3, we derive the formalism used to introduce light nucleonic clusters and hyperclusters, for finite temperatures and fixed charge fraction. In Chapter 4, we present the results for different scenarios: the effect of temperature, charge fraction, and density, and the inclusion of hyperons, Δs, light clusters and hyperclusters are discussed. The results presented in Sections 4.2-4.4 are based on a recently published work [27]. Finally, in Chapter 5, we draw some conclusions.

Chapter 2

Relativistic Nuclear Field Theory for zero temperature and β-equilibrium

In this chapter, we will derive the formalism to describe stellar matter at $T = 0$ MeV and β-equilibrium in the scope of Relativistic Nuclear Field Theory.

In Relativistic Nuclear Field Theory each baryon B is represented by a Dirac Spinor. In our present approach, the interactions between the different baryons are mediated by four different mesons: the isoscalar-scalar σ meson; the isoscalar-vector ω^μ meson; the isoscalar-vector ϕ^μ and the isovector-vector $\vec{\rho^\mu}$.

The σ meson provides the attractive strong force between the baryons whereas the ω^μ meson is responsible for the repulsive strong force. Besides the repulsion given by the ω^μ meson, the interaction between two hyperons is also mediated by the strange ϕ^μ meson that gives extra repulsion for these interactions. Since we will be dealing with highly asymmetric matter (NS matter), we are required to have a $\vec{\rho^\mu}$ meson that accounts for the isospin dependence of the interaction.

As for the baryons, we are going to consider the spin-1/2 baryonic octet composed of protons p, neutrons n and the Λ, $\Sigma^{-,0,+}$, $\Xi^{-,0}$ hyperons as well as the four spin-3/2 Δ isobars $\Delta^{-,0,+,++}$. Finally, electrons e^- and muons μ^- will also be taken into account.

To describe these systems, we will consider two different model approaches to the Relativistic Nuclear Field Theory: the nonlinear models and the density-dependent models. Let us start by considering the nonlinear models.

2.1 Nonlinear RMF Models

2.1.1 Lagrangian Density

The Lagrangian density for such a system is given by [20, 28, 29]:

$$\mathcal{L} = \sum_b \mathcal{L}_b + \sum_\Delta \mathcal{L}_\Delta + \sum_l \mathcal{L}_l + \mathcal{L}_m, \tag{2.1}$$

where $\mathcal{L}_b$, $\mathcal{L}_\Delta$, $\mathcal{L}_l$, $\mathcal{L}_m$ are the Lagrangian densities for the baryon octet ($b = p, n, \Lambda, \Sigma^{-,0,+}, \Xi^{-,0}$), Δ quartet ($\Delta = \Delta^{-,0,+,++}$), leptons ($l = e^-, \mu^-$) and free mesons, respectively. $\mathcal{L}_b$, $\mathcal{L}_\Delta$, $\mathcal{L}_l$, $\mathcal{L}_m$

	n	p	Λ	Σ^-	Σ^0	Σ^+	Ξ^-	Ξ^0	Δ^-	Δ^0	Δ^+	Δ^{++}
J	1/2	1/2	1/2	1/2	1/2	1/2	1/2	1/2	3/2	3/2	3/2	3/2
I_3	−1/2	1/2	0	−1	0	1	−1/2	1/2	−3/2	−1/2	1/2	3/2

Table 2.1: Spin (J) and isospin projection (I_3) quantum numbers for the baryons considered in our system.

are thus given by [1]:

$$\begin{aligned}\mathcal{L}_b &= \bar{\Psi}_b(x)\left[i\gamma_\mu\partial^\mu - m_b + g_{\sigma b}\sigma(x) - g_{\omega b}\gamma_\mu\omega^\mu(x)\right. \\ &\left. -g_{\rho b}\gamma_\mu\vec{I}_b\cdot\vec{\rho^\mu}(x) - g_{\phi b}\gamma_\mu\phi^\mu(x)\right]\Psi_b(x) \end{aligned} \tag{2.2}$$

$$\begin{aligned}\mathcal{L}_\Delta &= \bar{\Psi}_\Delta(x)\left[i\gamma_\mu\partial^\mu - m_\Delta + g_{\sigma\Delta}\sigma(x) - g_{\omega\Delta}\gamma_\mu\omega^\mu(x)\right. \\ &\left. -g_{\rho\Delta}\gamma_\mu\vec{I}_\Delta\cdot\vec{\rho^\mu}(x)\right]\Psi_\Delta(x) \end{aligned} \tag{2.3}$$

$$\mathcal{L}_l = \bar{\Psi}_l(x)\left[i\gamma_\mu\partial^\mu - m_l\right]\Psi_l(x) \tag{2.4}$$

$$\begin{aligned}\mathcal{L}_m &= \frac{1}{2}\partial_\mu\sigma(x)\partial^\mu\sigma(x) - \frac{1}{2}m_\sigma^2\sigma^2(x) - \frac{\kappa}{3!}g_{\sigma N}^3\sigma^3(x) - \frac{\lambda}{4!}g_{\sigma N}^4\sigma^4(x) \\ &-\frac{1}{4}\Omega^{\mu\nu}(x)\Omega_{\mu\nu}(x) + \frac{1}{2}m_\omega^2\omega_\mu(x)\omega^\mu(x) + \frac{\zeta}{4!}g_{\omega N}^4(\omega_\mu(x)\omega^\mu(x))^2 \\ &-\frac{1}{4}\vec{R}^{\mu\nu}(x)\cdot\vec{R}_{\mu\nu}(x) + \frac{1}{2}m_\rho^2\vec{\rho}_\mu(x)\cdot\vec{\rho}^\mu(x) \\ &+\Lambda_\omega g_{\rho N}^2\vec{\rho}_\mu(x)\cdot\vec{\rho}^\mu(x)g_{\omega N}^2\omega_\mu(x)\omega^\mu(x) \\ &-\frac{1}{4}\vec{P}^{\mu\nu}(x)\vec{P}_{\mu\nu}(x) + \frac{1}{2}m_\phi^2\phi_\mu(x)\phi^\mu(x), \end{aligned} \tag{2.5}$$

where $\Omega_{\mu\nu}(x) = \partial_\mu\omega_\nu(x) - \partial_\nu\omega_\mu(x)$, $R_{\mu\nu}(x) = \partial_\mu\vec{\rho}_\nu(x) - \partial_\nu(x)\vec{\rho}_\mu(x) + g_\rho(\vec{\rho}_\mu\times\vec{\rho}_\nu)$, $P_{\mu\nu}(x) = \partial_\mu\phi_\nu(x) - \partial_\nu\phi_\mu(x)$.

$\vec{I_B}$ is the isospin operator (B=b,Δ). The spin and isospin projection quantum numbers for the baryonic octet and Δ particles can be found in Table 2.1. Ψ_b is the baryon Dirac field for the baryon octet whereas Ψ_Δ is the Rarita-Schwinger field for the Δ isobars. Ψ_l is the lepton Dirac field.

We take for the vacuum proton and neutron mass an average value, $m = m_n = m_p = 939$ MeV. The values of the masses for all baryons can be found in Table 2.2.

The g_{mB} ($m = \sigma, \omega, \phi, \rho$) correspond to the coupling constants of the interaction between the baryons and the four different mesons. These coupling constants tell us the strength of the interaction and can be determined algebraically in terms of the properties of nuclear matter at saturation density [1].

The nonlinear terms in the meson fields are introduced in order to take into account the impact of the variation of the density in the interaction. These terms are only nonzero for the nonlinear models. Later we will also consider the density-dependent models for which these nonlinear terms in the meson fields vanish and the variation of the density is instead accounted through the density dependence of the coupling parameters.

The terms with the couplings κ and λ are self-interactions of the σ meson introduced in

[1] x≡(t,x,y,z)

	n	p	Λ	Σ^-	Σ^0	Σ^+	Ξ^-	Ξ^0	Δ^-	Δ^0	Δ^+	Δ^{++}
m_B	939	939	1115.683	1197	1193	1189	1321	1315	1232	1232	1232	1232

Table 2.2: Masses of the baryonic octet and four Δ isobars.

Ref. [30]. They are included to better control the compression modulus and the effective nucleon mass of the theory. The term with the coupling ζ is a self-interaction of the ω meson and is related to the softening of the high density sector of the EoS [31]. Finally, the Λ_ω coupling of the interaction between the ω and ρ mesons allows us to control the density dependence of the nuclear symmetry energy [32–34].

In Section 4.1 we take a closer look at the values of the coupling constants and parameters mentioned above.

2.1.2 Equations of Motion

The equations of motion for the baryonic and mesonic fields are obtained by solving the usual Euler-Lagrange equation:

$$\partial_\mu \left(\frac{\partial \mathcal{L}}{\partial \left(\partial_\mu \Phi \right)} \right) = \frac{\partial \mathcal{L}}{\partial \Phi} \tag{2.6}$$

The equations of motions for the mesons are then:

$$\partial_\mu \partial^\mu \sigma(x) + m_\sigma^2 \sigma(x) + \frac{\kappa}{2} g_{\sigma N}^3 \sigma^2(x) + \frac{\lambda}{3!} g_{\sigma N}^4 \sigma^3(x) = \sum_{B=b,\Delta} g_{\sigma B} \bar{\Psi}_B(x) \Psi_B(x) \tag{2.7}$$

$$\begin{aligned} &\partial_\alpha \Omega^{\alpha\beta}(x) + m_\omega^2 \omega^\beta(x) + \frac{\zeta}{3!} g_{\omega N}^4 \omega_\mu(x) \omega^\mu(x) \omega^\beta(x) \\ &+ 2\Lambda_\omega g_{\rho N}^2 g_{\omega N}^2 \omega^\beta(x) \vec{\rho}_\mu(x) \cdot \vec{\rho}^\mu(x) = \sum_{B=b,\Delta} g_{\omega B} \bar{\Psi}_B(x) \gamma^\beta \Psi_B(x) \end{aligned} \tag{2.8}$$

$$\partial^\nu R_{\nu\mu}(x) + m_\rho^2 \vec{\rho}_\mu(x) + 2\Lambda_\omega g_{\rho N}^2 g_{\omega N}^2 \omega_\beta(x) \omega^\beta(x) \vec{\rho}_\mu(x) = \sum_{B=b,\Delta} g_{\rho B} \bar{\Psi}_B(x) \gamma_\mu \vec{I}_B \Psi_B(x) \tag{2.9}$$

$$\partial_\alpha P^{\alpha\beta}(x) + m_\phi^2 \phi^\beta(x) = \sum_{B=b} g_{\phi B} \bar{\Psi}_B(x) \gamma^\beta \Psi_B(x) \tag{2.10}$$

The equations of motion for the baryon octet are:

$$\left[i\gamma_\mu \partial^\mu - m_b + g_{\sigma b}\sigma(x) - g_{\omega b}\gamma_\mu \omega^\mu(x) - g_{\rho b}\gamma_\mu \vec{I}_b \cdot \vec{\rho^\mu}(x) - g_{\phi b}\gamma_\mu \phi^\mu(x) \right] \Psi_b(x) = 0 \tag{2.11}$$

The equations of motion for the Δ isobars read:

$$\left[i\gamma_\mu \partial^\mu - m_\Delta + g_{\sigma\Delta}\sigma(x) - g_{\omega\Delta}\gamma_\mu \omega^\mu(x) - g_{\rho\Delta}\gamma_\mu \vec{I}_\Delta \cdot \vec{\rho^\mu}(x) \right] \Psi_\Delta(x) = 0 \tag{2.12}$$

Finally, the equations of motion for the leptons are given by:

$$\left[i\gamma_\mu \partial^\mu - m_l \right] \Psi_l(x) = 0 \tag{2.13}$$

2.1.3 Relativistic Mean-Field Approximation

Since the above coupled nonlinear differential equations are difficult to solve, we will now introduce an approximation known as the Relativistic Mean-Field approximation (RMF). Furthermore, we are interested in a system of static uniform matter in its ground state.

Thus, the RMF approximation consists of replacing the meson fields by their mean values in their ground state:

$$\sigma(x) \rightarrow \langle\sigma\rangle \tag{2.14}$$

$$\omega^{\mu}(x) \rightarrow \langle\omega^{\mu}\rangle \tag{2.15}$$

$$\vec{\rho}^{\mu}(x) \rightarrow \langle\vec{\rho}^{\mu}\rangle \tag{2.16}$$

$$\phi^{\mu}(x) \rightarrow \langle\phi^{\mu}\rangle \tag{2.17}$$

In static uniform matter, the source currents $\bar{\Psi}_B(x)\Psi_B(x)$ and $\bar{\Psi}_B(x)\gamma^{\mu}\Psi_B(x)$ are independent of x. The same happens for the meson mean fields. As a result, the meson equations of motion are reduced to:

$$m_{\sigma}^2\langle\sigma\rangle + \frac{\kappa}{2}g_{\sigma N}^3\langle\sigma\rangle^2 + \frac{\lambda}{3!}g_{\sigma N}^4\langle\sigma\rangle^3 = \sum_{B=b,\Delta} g_{\sigma B}\left\langle\bar{\Psi}_B\Psi_B\right\rangle \tag{2.18}$$

$$m_{\omega}^2\langle\omega_0\rangle + \frac{\zeta}{3!}g_{\omega N}^4\langle\omega_0\rangle^3 + 2\Lambda_{\omega}g_{\rho N}^2g_{\omega N}^2\langle\omega_0\rangle\langle\rho_{03}\rangle^2 = \sum_{B=b,\Delta} g_{\omega B}\left\langle\Psi_B^{\dagger}\Psi_B\right\rangle \tag{2.19}$$

$$m_{\rho}^2\langle\rho_{03}\rangle + 2\Lambda_{\omega}g_{\rho N}^2g_{\omega N}^2\langle\omega_0\rangle^2\langle\rho_{03}\rangle = \sum_{B=b,\Delta} g_{\rho B}\left\langle\bar{\Psi}_B\gamma_0 I_{3B}\Psi_B\right\rangle \tag{2.20}$$

$$m_{\phi}^2\langle\phi_0\rangle = \sum_{B=b} g_{\phi B}\left\langle\Psi_B^{\dagger}\Psi_B\right\rangle \tag{2.21}$$

The expectation values for the spatial components of the ω and ϕ mesons vanish due to rotational invariance. Thus, in the RMF approximation for static uniform matter in its ground state, only the temporal components of the meson fields are nonzero. For the ρ meson, only the temporal component of the third isospin component is nonzero.

Therefore, in the RMF approximation, the Lagrangian given in Eq.(2.1) reduces to [2]:

$$\begin{aligned}\mathcal{L}_{RMF} = &- \frac{1}{2}m_{\sigma}^2\sigma^2 - \frac{\kappa}{3!}g_{\sigma N}^3\sigma^3 - \frac{\lambda}{4!}g_{\sigma N}^4\sigma^4 + \frac{1}{2}m_{\omega}^2\omega_0^2 + \frac{\zeta}{4!}g_{\omega N}^4\omega_0^4 \\ &+ \frac{1}{2}m_{\rho}^2\rho_{03}^2 + \Lambda_{\omega}g_{\rho N}^2g_{\omega N}^2\rho_{03}^2\omega_0^2 + \frac{1}{2}m_{\phi}^2\phi_0^2\end{aligned} \tag{2.22}$$

2.1.4 Energy Spectrum

In the RMF approximation of uniform static matter, each baryon field Ψ_B satisfies an equation with no x-dependent terms, which means that these baryonic fields are momentum

[2] $\langle\sigma\rangle \equiv \sigma$, $\langle\omega_0\rangle \equiv \omega_0$, $\langle\rho_{03}\rangle \equiv \rho_{03}$, $\langle\phi_0\rangle \equiv \phi_0$

eigenstates that can be written as [3]:

$$\Psi_B(x) = \Psi_B(\vec{k})e^{-ik\cdot x} \tag{2.23}$$

Substituting in Eq.(2.11) yields:

$$\left[\gamma_\mu k^\mu - m_b + g_{\sigma b}\sigma - g_{\omega b}\gamma_\mu\omega^\mu - g_{\rho b}\gamma_\mu\vec{I}_b\cdot\vec{\rho^\mu} - g_{\phi b}\gamma_\mu\phi^\mu\right]\Psi_b(\vec{k}) = 0. \tag{2.24}$$

Following the method used in Ref. [1], let us define the following quantities:

$$K^\mu = k^\mu - g_{\omega b}\omega^\mu - g_{\rho b}\vec{I}_b\cdot\vec{\rho^\mu} - g_{\phi b}\phi^\mu \tag{2.25}$$

$$m_b^* = m_b - g_{\sigma b}\sigma \tag{2.26}$$

where m_b^* is the effective mass of each baryon b.

Rewriting Eq.(2.24) using Eqs.(2.25) and (2.26) yields:

$$\left[\gamma_\mu K^\mu - m_b^*\right]\Psi_b(\vec{k}) = 0 \tag{2.27}$$

As usual, the eigenvalues can be obtained by rationalizing the Dirac operator. Multiplying Eq.(2.27) by $(\gamma_\mu K^\mu + m_b^*)$ and considering the γ matrices properties ($\{\gamma_\mu,\gamma_\nu\} = 2g_{\mu\nu}$) gives:

$$\begin{aligned}
\left(\gamma_\mu K^\mu + m_b^*\right)\left(\gamma_\mu K^\mu - m_b^*\right) &= \gamma_\mu K^\mu\gamma_\nu K^\nu - m_b^*\gamma_\mu K^\mu + m_b^*\gamma_\mu K^\mu - m_b^{*2} \\
&= \gamma_\mu K^\mu\gamma_\nu K^\nu - m_b^{*2} \\
&= \frac{\gamma_\mu K^\mu\gamma_\nu K^\nu + \gamma_\nu K^\nu\gamma_\mu K^\mu}{2} - m_b^{*2} \\
&= K^\mu K^\nu\frac{\gamma_\mu\gamma_\nu + \gamma_\nu\gamma_\mu}{2} - m_b^{*2} \\
&= K^\mu K^\nu\frac{2g_{\mu\nu}}{2} - m_b^{*2} \\
&= K^\mu K_\mu - m_b^{*2}
\end{aligned} \tag{2.28}$$

As a result, Eq.(2.27) can now be written as

$$\left[K^\mu K_\mu - m_b^{*2}\right]\Psi_b(\vec{k}) = 0, \tag{2.29}$$

where $(K^\mu K_\mu - m_b^{*2})$ is no longer an operator acting on $\Psi_b(\vec{k})$, which means that it must be equal to zero. Thus,

$$\begin{aligned}
K^\mu K_\mu - m_b^{*2} = 0 &\Leftrightarrow K_0K_0 - K_iK_i - m_b^{*2} = 0 \\
&\Leftrightarrow K_0^2 - K_i^2 - m_b^{*2} = 0.
\end{aligned} \tag{2.30}$$

As we have seen before, in the RMF approximation only the σ, ω_0, ρ_{03} and ϕ_0 components

[3] $k\cdot x \equiv k_0 t - \vec{k}\cdot\vec{r}$

of the mesons are nonzero. Then, Eq.(2.30) is simply [4]:

$$\begin{aligned} & (k_0 - g_{\omega b}\omega_0 - g_{\rho b} I_{3b}\rho_{03} - g_{\phi b}\phi_0)^2 - k_i^2 - m_b^{*2} = 0 \\ \Leftrightarrow\ & (k_0 - g_{\omega b}\omega_0 - g_{\rho b} I_{3b}\rho_{03} - g_{\phi b}\phi_0)^2 = k_i^2 + m_b^{*2} \\ \Leftrightarrow\ & k_0 = g_{\omega b}\omega_0 + g_{\rho b} I_{3b}\rho_{03} + g_{\phi b}\phi_0 \pm \sqrt{k^2 + m_b^{*2}}\ . \end{aligned} \tag{2.31}$$

From here, we can now write the energy eigenvalues for each particle ($E_b^+(k)$) and anti-particle ($E_b^-(k)$) of the baryonic octet:

$$E_b^{\pm}(k) = g_{\omega b}\omega_0 + g_{\rho b} I_{3b}\rho_{03} + g_{\phi b}\phi_0 \pm \sqrt{k^2 + m_b^{*2}}\ \ ,\ \ b = n, p, \Lambda, \Sigma^{-,0,+}, \Xi^{-,0}\ . \tag{2.32}$$

Following a similar procedure, we can obtain the energy eigenvalues for the Δ quartet

$$E_\Delta^{\pm}(k) = g_{\omega\Delta}\omega_0 + g_{\rho\Delta} I_{3\Delta}\rho_{03} \pm \sqrt{k^2 + m_\Delta^{*2}}\ \ ,\ \ \Delta = \Delta^{-,0,+,++} \tag{2.33}$$

and for the leptons

$$E_l^{\pm}(k) = \pm\sqrt{k^2 + m_l^{*2}}\ \ ,\ \ l = e^-, \mu^-. \tag{2.34}$$

2.1.5 Baryonic and Scalar Density

As we can see, for example in Eq.(2.32) for the baryon octet, we need to know the values of the mesons fields given by their equations of motion ((2.18),(2.19),(2.20),(2.21)) in order to calculate the particle's energy spectrum.

However, to solve the meson equations we first need to calculate the baryon currents $\left\langle \bar{\Psi}_b \Psi_b \right\rangle$ and $\left\langle \Psi_b^\dagger \Psi_b \right\rangle$ whose eigenvalues depend on the meson fields themselves.

To do so, we will follow the method described in Ref. [1]. We start by realizing that, in this theory, each single-particle state is characterized by a momentum $\vec{k}$ and a spin projection which we will denote by κ. Then, the expectation value of an operator Γ in the ground state of the many-particle system $\left\langle \bar{\Psi}_b \Gamma \Psi_b \right\rangle$ can be written as a function of the expectation value of the single-particle state $\left(\bar{\Psi}_b \Gamma \Psi_b\right)_{\vec{k},\kappa}$:

$$\left\langle \bar{\Psi}_b \Gamma \Psi_b \right\rangle = \sum_\kappa \int \frac{d\vec{k}}{(2\pi)^3} \left(\bar{\Psi}_b \Gamma \Psi_b\right)_{\vec{k},\kappa} \Theta\left(\mu_b - E(\vec{k})\right), \tag{2.35}$$

where the sum over κ is the sum over the spin states of the occupied momentum states, μ_b is the chemical potential of baryon b and $\Theta\left(\mu_b - E(\vec{k})\right)$ is a step function defined as

$$\Theta\left(\mu_b - E(\vec{k})\right) = \begin{cases} 1 & \text{if } |\vec{k}| \le k_{F,b} \\ 0 & \text{if } |\vec{k}| > k_{F,b} \end{cases} \tag{2.36}$$

where $k_{F,b}$ is the Fermi momentum of baryon b.

For the cases we are interested in, the operator Γ usually appears in the Dirac Hamiltonian, H_D. The Dirac Hamiltonian can be determined using Eq.(2.27) and considering the gamma

[4] $k_i^2 \equiv k^2$

matrices properties ($\gamma_0\gamma_0 = \mathbb{1}$):

$$\begin{aligned}
&\left[\gamma_\mu(k^\mu - g_{\omega b}\omega^\mu - g_{\rho b}\vec{I}_b\cdot\vec{\rho^\mu} - g_{\phi b}\phi^\mu) - m_b^*\right]\Psi_b(\vec{k}) = 0\\
\Leftrightarrow &\left[\gamma_0(k^0 - g_{\omega b}\omega^0 - g_{\rho b}I_{3b}\rho_3^0 - g_{\phi b}\phi^0) - \gamma_i k^i - m_b^*\right]\Psi_b(\vec{k}) = 0\\
\Leftrightarrow &\left[\gamma_0 g_{\omega b}\omega^0 + \gamma_0 g_{\rho b}I_{3b}\rho_3^0 + \gamma_0 g_{\phi b}\phi^0 + \gamma_i k^i + m_b^*\right]\Psi_b(\vec{k}) = \gamma_0 k^0\Psi_b(\vec{k})\\
\Leftrightarrow &\gamma_0\left[\gamma_0 g_{\omega b}\omega^0 + \gamma_0 g_{\rho b}I_{3b}\rho_3^0 + \gamma_0 g_{\phi b}\phi^0 + \gamma_i k^i + m_b^*\right]\Psi_b(\vec{k}) = \gamma_0\gamma_0 k^0\Psi_b(\vec{k})\\
\Leftrightarrow &\gamma_0\left[\gamma_0 g_{\omega b}\omega^0 + \gamma_0 g_{\rho b}I_{3b}\rho_3^0 + \gamma_0 g_{\phi b}\phi^0 + \gamma_i k^i + m_b^*\right]\Psi_b(\vec{k}) = E(k)\Psi_b(\vec{k})\\
\Leftrightarrow &H_D\Psi_b(\vec{k}) = E(k)\Psi_b(\vec{k}).
\end{aligned} \tag{2.37}$$

The Dirac Hamiltonian is thus given by:

$$H_D = \gamma_0\left[\gamma_0 g_{\omega b}\omega^0 + \gamma_0 g_{\rho b}I_{3b}\rho_3^0 + \gamma_0 g_{\phi b}\phi^0 + \gamma_i k^i + m_b^*\right] \tag{2.38}$$

We already know that the expectation value of the Dirac Hamiltonian in the ground state for a single-particle state of given $\vec{k}$ and κ will be the energy eigenvalue described in Eq.(2.32). So:

$$\left(\Psi_b^\dagger H_D\Psi_b\right)_{\vec{k},\kappa} = E(k) = g_{\omega b}\omega_0 + g_{\rho b}I_{3b}\rho_{03} + g_{\phi b}\phi_0 + \sqrt{k^2 + m_b^{*2}} \tag{2.39}$$

On the other hand, if we develop the left-hand side of Eq.(2.39) taking into account Eq.(2.37), we get:

$$\left(\Psi_b^\dagger H_D\Psi_b\right)_{\vec{k},\kappa} = \left(\Psi_b^\dagger E(k)\Psi_b\right)_{\vec{k},\kappa} = E(k)\left(\Psi_b^\dagger\Psi_b\right)_{\vec{k},\kappa} \tag{2.40}$$

Equations (2.39) and (2.40) immediately set the following normalization condition:

$$\left(\Psi_b^\dagger\Psi_b\right)_{\vec{k},\kappa} = 1 \tag{2.41}$$

Taking the derivative of the left-hand side of Eq.(2.40) with respect to any given variable ζ present in the Hamiltonian yields:

$$\begin{aligned}
\frac{\partial}{\partial\zeta}\left(\Psi_b^\dagger H_D\Psi_b\right)_{\vec{k},\kappa} &= \left(\frac{\partial\Psi_b^\dagger}{\partial\zeta}H_D\Psi_b\right)_{\vec{k},\kappa} + \left(\Psi_b^\dagger\frac{\partial H_D}{\partial\zeta}\Psi_b\right)_{\vec{k},\kappa} + \left(\Psi_b^\dagger H_D\frac{\partial\Psi_b}{\partial\zeta}\right)_{\vec{k},\kappa}\\
&= E(k)\left(\frac{\partial\Psi_b^\dagger}{\partial\zeta}\Psi_b\right)_{\vec{k},\kappa} + \left(\Psi_b^\dagger\frac{\partial H_D}{\partial\zeta}\Psi_b\right)_{\vec{k},\kappa} + E(k)\left(\Psi_b^\dagger\frac{\partial\Psi_b}{\partial\zeta}\right)_{\vec{k},\kappa}\\
&= \left(\Psi_b^\dagger\frac{\partial H_D}{\partial\zeta}\Psi_b\right)_{\vec{k},\kappa} + E(k)\left(\left(\frac{\partial\Psi_b^\dagger}{\partial\zeta}\Psi_b\right)_{\vec{k},\kappa} + \left(\Psi_b^\dagger\frac{\partial\Psi_b}{\partial\zeta}\right)_{\vec{k},\kappa}\right)\\
&= \left(\Psi_b^\dagger\frac{\partial H_D}{\partial\zeta}\Psi_b\right)_{\vec{k},\kappa} + E(k)\frac{\partial}{\partial\zeta}\left(\Psi_b^\dagger\Psi_b\right)_{\vec{k},\kappa}\\
&= \left(\Psi_b^\dagger\frac{\partial H_D}{\partial\zeta}\Psi_b\right)_{\vec{k},\kappa}
\end{aligned} \tag{2.42}$$

where $\frac{\partial}{\partial\zeta}\left(\Psi_b^\dagger\Psi_b\right)_{\vec{k},\kappa} = 0$ because Ψ_b is a normalized eigenstate, see Eq.(2.41).

From now on, we can take the result of Eq.(2.42) to calculate derivatives of the left-hand

side of Eq.(2.40). Combining Eqs.(2.40), (2.41) and (2.42) we get:

$$\left(\Psi_b^\dagger \frac{\partial H_D}{\partial \zeta}\Psi_b\right)_{\vec{k},\kappa} = \frac{\partial}{\partial \zeta}E(k)\ . \tag{2.43}$$

Let us now calculate $\left\langle \Psi_b^\dagger \Psi_b \right\rangle$, taking into account Eqs.(2.35) and (2.41):

$$\begin{aligned}
\left\langle \Psi_b^\dagger \Psi_b \right\rangle &= \sum_\kappa \int \frac{d\vec{k}}{(2\pi)^3} \left(\Psi_b^\dagger \Psi_b\right)_{\vec{k},\kappa} \Theta\left(\mu_b - E(\vec{k})\right) \\
&= \sum_\kappa \int \frac{d\vec{k}}{(2\pi)^3} \Theta\left(\mu_b - E(\vec{k})\right) \\
&= (2J_b+1)\int_0^{k_{F,b}} \frac{d\vec{k}}{(2\pi)^3} \\
&= (2J_b+1)\int_0^{k_{F,b}} \frac{4\pi k^2 dk}{(2\pi)^3} \\
&= \frac{(2J_b+1)}{2\pi^2}\int_0^{k_{F,b}} k^2 dk \\
&= \frac{(2J_b+1)}{6\pi^2} k_{F,b}^3,
\end{aligned} \tag{2.44}$$

where J_b is the spin of particle b and $(2J_b+1)$ the corresponding degeneracy. The result obtained in Eq.(2.44) corresponds to the density of each baryon b of the baryonic octet, ρ_b. Then:

$$\rho_b = \left\langle \Psi_b^\dagger \Psi_b \right\rangle = \frac{(2J_b+1)}{2\pi^2}\int_0^{k_{F,b}} k^2 dk = \frac{(2J_b+1)}{6\pi^2} k_{F,b}^3 \ \ , \ \ b = n, p, \Lambda, \Sigma^{-,0,+}, \Xi^{-,0}\ . \tag{2.45}$$

We can also calculate $\left\langle \bar{\Psi}_b \Psi_b \right\rangle$. To do so, we first need to calculate $\left(\bar{\Psi}_b \Psi_b\right)_{\vec{k},\kappa}$ using Eq.(2.43):

$$\begin{aligned}
&\left(\Psi_b^\dagger \frac{\partial H_D}{\partial m_b}\Psi_b\right)_{\vec{k},\kappa} = \frac{\partial}{\partial m_b}E(k) \\
\Leftrightarrow &\left(\Psi_b^\dagger \frac{\partial}{\partial m_b}\left[\gamma_0\left(\gamma_0 g_{\omega b}\omega^0 + \gamma_0 g_{\rho b} I_{3b}\rho_3^0 + \gamma_0 g_{\phi b}\phi^0 + \gamma_i k^i + m_b - g_{\sigma b}\sigma\right)\right]\Psi_b\right)_{\vec{k},\kappa} = \frac{\partial}{\partial m_b}E(k) \\
\Leftrightarrow &\left(\Psi_b^\dagger \gamma_0 \Psi_b\right)_{\vec{k},\kappa} = \frac{\partial}{\partial m_b}\left[g_{\omega b}\omega_0 + g_{\rho b} I_{3b}\rho_{03} + g_{\phi b}\phi_0 + \sqrt{k^2 + (m_b - g_{\sigma b}\sigma)^2}\right] \\
\Leftrightarrow &\left(\bar{\Psi}_b \Psi_b\right)_{\vec{k},\kappa} = \frac{m_b^*}{\sqrt{k^2 + m_b^{*2}}}\ .
\end{aligned} \tag{2.46}$$

Then, using Eqs.(2.35) and (2.46), we have:

$$\begin{aligned}
\left\langle \bar{\Psi}_b \Psi_b \right\rangle &= \sum_\kappa \int \frac{d\vec{k}}{(2\pi)^3} \left(\bar{\Psi}_b \Psi_b\right)_{\vec{k},\kappa} \Theta\left(\mu_b - E(\vec{k})\right) \\
&= (2J_b+1)\int \frac{d\vec{k}}{(2\pi)^3} \frac{m_b^*}{\sqrt{k^2 + m_b^{*2}}} \Theta\left(\mu_b - E(\vec{k})\right) \\
&= \frac{(2J_b+1)}{2\pi^2}\int_0^{k_{F,b}} \frac{m_b^*}{\sqrt{k^2 + m_b^{*2}}} k^2 dk\ .
\end{aligned} \tag{2.47}$$

The result obtained in Eq.(2.47) corresponds to the scalar density of each baryon b of the baryonic octet, ρ_b^s. Then:

$$\rho_b^s = \left\langle \bar{\Psi}_b \Psi_b \right\rangle = \frac{(2J_b+1)}{2\pi^2} \int_0^{k_{F,b}} \frac{m_b^*}{\sqrt{k^2+m_b^{*2}}} k^2 dk \ \ , \ \ b = n, p, \Lambda, \Sigma^{-,0,+}, \Xi^{-,0} \ . \tag{2.48}$$

Following a similar procedure, we can obtain the density and scalar density for the Δ quartet particles

$$\rho_\Delta = \left\langle \Psi_\Delta^\dagger \Psi_\Delta \right\rangle = \frac{(2J_\Delta+1)}{2\pi^2} \int_0^{k_{F,\Delta}} k^2 dk = \frac{(2J_\Delta+1)}{6\pi^2} k_{F,\Delta}^3 \ \ , \ \ \Delta = \Delta^{-,0,+,++} \tag{2.49}$$

$$\rho_\Delta^s = \left\langle \bar{\Psi}_\Delta \Psi_\Delta \right\rangle = \frac{(2J_\Delta+1)}{2\pi^2} \int_0^{k_{F,\Delta}} \frac{m_\Delta^*}{\sqrt{k^2+m_\Delta^{*2}}} k^2 dk \ \ , \ \ \Delta = \Delta^{-,0,+,++} \tag{2.50}$$

and for the leptons

$$\rho_l = \left\langle \Psi_l^\dagger \Psi_l \right\rangle = \frac{(2J_l+1)}{2\pi^2} \int_0^{k_{F,l}} k^2 dk = \frac{(2J_l+1)}{6\pi^2} k_{F,l}^3 \ \ , \ \ l = e^-, \mu^- \tag{2.51}$$

$$\rho_l^s = \left\langle \bar{\Psi}_l \Psi_l \right\rangle = \frac{(2J_l+1)}{2\pi^2} \int_0^{k_{F,l}} \frac{m_l^*}{\sqrt{k^2+m_l^{*2}}} k^2 dk \ \ , \ \ l = e^-, \mu^- \ . \tag{2.52}$$

Having determined how to calculate the baryon currents, which as we saw are simply the densities and scalar densities of the various particles, we can rewrite the equations of motion of the meson fields ((2.18),(2.19),(2.20),(2.21)) in terms of these densities as:

$$m_\sigma^2 \sigma + \frac{\kappa}{2} g_{\sigma N}^3 \sigma^2 + \frac{\lambda}{3!} g_{\sigma N}^4 \sigma^3 = \sum_{B=b,\Delta} g_{\sigma B} \rho_B^s \tag{2.53}$$

$$m_\omega^2 \omega_0 + \frac{\zeta}{3!} g_{\omega N}^4 \omega_0^3 + 2\Lambda_\omega g_{\rho N}^2 g_{\omega N}^2 \omega_0 \rho_{03}^2 = \sum_{B=b,\Delta} g_{\omega B} \rho_B \tag{2.54}$$

$$m_\rho^2 \rho_{03} + 2\Lambda_\omega g_{\rho N}^2 g_{\omega N}^2 \omega_0^2 \rho_{03} = \sum_{B=b,\Delta} g_{\rho B} I_{3B} \rho_B \tag{2.55}$$

$$m_\phi^2 \phi_0 = \sum_{B=b} g_{\phi B} \rho_B \tag{2.56}$$

The only thing that is missing so that we are able to solve the meson equations of motion ((2.53),(2.54),(2.55),(2.56)) is to find out the value of the Fermi momentum $k_{F,B}$ for each particle.

2.1.6 Cold Neutron Star Matter in Beta Equilibrium

As we mentioned in the Introduction, after the formation of a NS, its temperature falls down to less than 1 MeV in just a few seconds. Following this rapid cooling (in which neutrinos and photons diffuse out of the star), the star matter reaches chemical equilibrium corresponding to the ground state configuration (also known as β-equilibrium).

Since the temperature in equilibrium is below 1 MeV, the star is cold on the nuclear level (which basically corresponds to zero temperature, $T = 0$ MeV) meaning that strong reactions

that conserve the strangeness quantum number no longer occur. On the other hand, weak interactions can still occur. The fact that weak interactions do not conserve strangeness, will result in the star having a net strangeness. Therefore, strangeness is not conserved in a NS.

Just like strangeness, lepton quantum number is not conserved in the scale of the star because neutrinos generated in cooling processes diffuse out of the star.

Therefore, the only two quantum numbers conserved in the scale of the star are the baryon number and the electric charge number.

As a result, all particle chemical potentials can be written in terms of the chemical potentials corresponding to these two conserved charges [5]. That is, for any given particle c, its chemical potential is simply a linear combination of the baryon and electric charge chemical potentials:

$$\mu_c = b_c\mu_n - q_c\mu_e \tag{2.57}$$

where b_c is the baryon number of particle c; q_c is the electrical charge (in units of $+e$); and μ_n, μ_e the baryon and electrical charge chemical potentials, respectively.

Since $\mu_e = \mu_n - \mu_p$, the hyperon chemical potentials can be written in terms of the nucleon chemical potentials:

$$\mu_\Lambda = \mu_n \tag{2.58}$$

$$\mu_{\Sigma^-} = 2\mu_n - \mu_p, \quad \mu_{\Sigma^0} = \mu_n, \quad \mu_{\Sigma^+} = \mu_p \tag{2.59}$$

$$\mu_{\Xi^-} = 2\mu_n - \mu_p, \quad \mu_{\Xi^0} = \mu_n \ . \tag{2.60}$$

Similarly, for the Δ isobars we have:

$$\mu_{\Delta^-} = 2\mu_n - \mu_p, \quad \mu_{\Delta^0} = \mu_n, \quad \mu_{\Delta^+} = \mu_p, \quad \mu_{\Delta^{++}} = 2\mu_p - \mu_n \ . \tag{2.61}$$

As we know, for $T = 0$ MeV, the chemical potential of a particle c corresponds to the Fermi energy, which corresponds to the energy eigenvalue whose momentum is the Fermi momentum $k_{F,c}$. Then, in order to find out the value of the Fermi momentum for each particle c, we simply have to equate Eq.(2.57) to the corresponding energy eigenvalue equations (2.32), (2.33) and (2.34), taking $k = k_{F,c}$:

$$\mu_c = E_c(k_{F,c}) \ . \tag{2.62}$$

Then, for a particle b of the baryonic octet, the chemical potential can also be written as:

$$\mu_b = g_{\omega b}\omega_0 + g_{\rho b}I_{3b}\rho_{03} + g_{\phi b}\phi_0 + \sqrt{k_{F,b}^2 + m_b^{*2}} \ . \tag{2.63}$$

If we define an effective chemical potential μ_b^* as

$$\mu_b^* = \sqrt{k_{F,b}^2 + m_b^{*2}} = \mu_b - g_{\omega b}\omega_0 - g_{\rho b}I_{3b}\rho_{03} - g_{\phi b}\phi_0 \ , \tag{2.64}$$

the Fermi momentum $k_{F,b}$ is simply given by:

$$k_{F,b} = \sqrt{\mu_b^{*2} - m_b^{*2}} \ . \tag{2.65}$$

[5] The neutrino chemical potential, μ_ν, is set to zero because neutrinos diffuse out of the star; the strangeness chemical potential, μ_S, is also zero because strangeness is not conserved.

Similarly, for the Δ particles we have

$$\mu_\Delta = g_{\omega\Delta}\omega_0 + g_{\rho\Delta} I_{3\Delta}\rho_{03} + \sqrt{k_{F,\Delta}^2 + m_\Delta^{*2}} \tag{2.66}$$

$$k_{F,\Delta} = \sqrt{\mu_\Delta^{*2} - m_\Delta^{*2}} \tag{2.67}$$

and for the leptons:

$$\mu_l = \sqrt{k_{F,l}^2 + m_l^{*2}} \tag{2.68}$$

$$k_{F,l} = \sqrt{\mu_l^2 - m_l^{*2}} \ . \tag{2.69}$$

Having determined the Fermi momentum of the particles, we are now capable of solving the meson equations of motion ((2.53),(2.54),(2.55),(2.56)). For that, we only need to make sure that for any given total baryonic density of the system, n_B, given by

$$n_B = \sum_{c=b,\Delta,l} \rho_c \ , \tag{2.70}$$

the equations ((2.53),(2.54),(2.55),(2.56)) are solved self-consistently taking into account the β-equilibrium condition of Eq.(2.57) as well as the conservation of the electrical charge:

$$\sum_{c=b,\Delta,l} q_c \rho_c = 0 \ . \tag{2.71}$$

2.1.7 Equation of State

To obtain the EoS for this system, we first consider the energy-momentum tensor $T^{\mu\nu}$ usually given by:

$$T^{\mu\nu} = \left(\frac{\partial \mathcal{L}}{\partial(\partial_\mu \Phi_i)} \right) \partial^\nu \Phi_i - g^{\mu\nu}\mathcal{L} \ . \tag{2.72}$$

For a perfect fluid in its rest frame, $T^{\mu\nu}$ reduces to [1]:

$$T^{\mu\nu} = \begin{pmatrix} \epsilon & 0 & 0 & 0 \\ 0 & p & 0 & 0 \\ 0 & 0 & p & 0 \\ 0 & 0 & 0 & p \end{pmatrix},$$

where ϵ is the energy density of the system and p the pressure. Both ϵ and p are expectation values of the respective components of the energy-momentum tensor.

Thus, the energy density is given by ($g^{00} = 1$):

$$\begin{aligned} \epsilon = T^{00} &= \left(\frac{\partial \mathcal{L}}{\partial(\partial_0 \Psi_i)} \right) \partial^0 \Psi_i - g^{00}\mathcal{L} \\ &= \bar{\Psi}_i i\gamma_0 \partial^0 \Psi_i - \mathcal{L} \\ &= \bar{\Psi}_i \gamma_0 k_0 \Psi_i - \mathcal{L} \end{aligned} \tag{2.73}$$

The ground state expectation value of the energy density is then

$$\epsilon = \left\langle \bar{\Psi}_i \gamma_0 k_0 \Psi_i \right\rangle - \langle \mathcal{L} \rangle \tag{2.74}$$

$$= \left\langle \bar{\Psi}_i \gamma_0 k_0 \Psi_i \right\rangle - \mathcal{L}_{RMF} \tag{2.75}$$

where $\mathcal{L}_{RMF}$ is given by Eq.(2.22).

Using the method to calculate expectation values derived in Section 2.1.5, we find that:

$$\left\langle \bar{\Psi}_i \gamma_0 k_0 \Psi_i \right\rangle = \sum_{i=b,\Delta,l} \left[\frac{2J_i+1}{2\pi^2} \int_0^{k_{F,i}} k^2 \sqrt{k^2 + m_i^{*2}} dk + g_{\omega i} \omega_0 \rho_i \right. \tag{2.76}$$
$$\left. + g_{\rho i} \rho_{03} I_{3i} \rho_i + g_{\phi i} \phi_0 \rho_i \right]$$

Then, the energy density of the system is given by

$$\epsilon = \sum_{i=b,\Delta,l} \left[\frac{2J_i+1}{2\pi^2} \int_0^{k_{F,i}} k^2 \sqrt{k^2 + m_i^{*2}} dk + g_{\omega i} \omega_0 \rho_i \right. \tag{2.77}$$
$$\left. + g_{\rho i} \rho_{03} I_{3i} \rho_i + g_{\phi i} \phi_0 \rho_i \right] - \mathcal{L}_{RMF} \ .$$

On the other hand, the pressure reads ($g^{nn} = -3$):

$$p = \frac{1}{3} T^{nn} = \frac{1}{3} \left(\frac{\partial \mathcal{L}}{\partial(\partial_n \Psi_i)} \right) \partial^n \Psi_i - \frac{1}{3} g^{nn} \mathcal{L} \tag{2.78}$$

$$= \bar{\Psi}_i i \gamma_n \partial^n \Psi_i + \mathcal{L}$$

$$= \bar{\Psi}_i \gamma_n k^n \Psi_i + \mathcal{L}$$

The ground state expectation value of pressure is then

$$p = \left\langle \bar{\Psi}_i \gamma_n k^n \Psi_i \right\rangle + \langle \mathcal{L} \rangle \tag{2.79}$$

$$= \left\langle \bar{\Psi}_i \gamma_n k^n \Psi_i \right\rangle + \mathcal{L}_{RMF} \tag{2.80}$$

Once more, using the method to calculate expectation values derived in Section 2.1.5, we find that:

$$\left\langle \bar{\Psi}_i \gamma_n k^n \Psi_i \right\rangle = \sum_{i=b,\Delta,l} \frac{2J_i+1}{2\pi^2} \int_0^{k_{F,i}} \frac{k^4 dk}{\sqrt{k^2 + m_i^{*2}}} \tag{2.81}$$

Then, the pressure of the system follows

$$p = \frac{1}{3} \sum_{i=b,\Delta,l} \frac{2J_i+1}{2\pi^2} \int_0^{k_{F,i}} \frac{k^4 dk}{\sqrt{k^2 + m_i^{*2}}} + \mathcal{L}_{RMF}. \tag{2.82}$$

The relation between the energy density given by Eq.(2.77) and the pressure (2.82) corre-

sponds to the EoS of the system.

2.2 Density-Dependent RMF Models

In Section 2.1 we discussed nonlinear Relativistic Mean-Field models. We will now turn to a different type of models known as density-dependent Relativistic Mean-Field models. Nevertheless, the majority of the methods used for nonlinear models are still valid to deal with density-dependent models. Therefore, in this section we will only take a look at what is different in a density-dependent model when compared to a nonlinear one.

2.2.1 Lagrangian Density

As mentioned in Section 2.1.1 for the nonlinear models, the effect of the variation of the density on the interactions was taken into account through the addition of some nonlinear terms in the mesonic fields (Eq.2.5). In the case of the density-dependent models, the density dependence of the interactions is instead taken into account by considering that the coupling parameters of the particles to the meson fields depend on the density of the system. That is, the coupling parameters to the mesons ($g_{mB} = g_{mB}(\varrho)$) will be functionals of the vector density operator ϱ [35, 36]:

$$\varrho = \sqrt{J^\mu J_\mu}, \tag{2.83}$$

where

$$J^\mu = \sum_{c=b,\Delta} \bar{\Psi}_c \gamma^\mu \Psi_c \tag{2.84}$$

is the total baryon vector current (baryonic octet and Δ isobars).

As a result, the nonlinear terms previously considered in Eq.(2.5) vanish, since they are no longer needed to account for the density dependence. Then, the counterpart of Eq.(2.5) is simply:

$$\begin{aligned} \mathcal{L}_m &= \frac{1}{2}\partial_\mu\sigma(x)\partial^\mu\sigma(x) - \frac{1}{2}m_\sigma^2\sigma^2(x) \\ &\quad -\frac{1}{4}\Omega^{\mu\nu}(x)\Omega_{\mu\nu}(x) + \frac{1}{2}m_\omega^2\omega_\mu(x)\omega^\mu(x) \\ &\quad -\frac{1}{4}\vec{R}^{\mu\nu}(x)\cdot\vec{R}_{\mu\nu}(x) + \frac{1}{2}m_\rho^2\vec{\rho}_\mu(x)\cdot\vec{\rho}^\mu(x) \\ &\quad -\frac{1}{4}\vec{P}^{\mu\nu}(x)\vec{P}_{\mu\nu}(x) + \frac{1}{2}m_\phi^2\phi_\mu(x)\phi^\mu(x). \end{aligned} \tag{2.85}$$

The Lagrangian densities for the baryonic octet and Δ isobars are similar to Eqs.(2.2) and (2.3)

$$\begin{aligned} \mathcal{L}_b &= \bar{\Psi}_b(x)\left[i\gamma_\mu\partial^\mu - m_b + g_{\sigma b}\sigma(x) - g_{\omega b}\gamma_\mu\omega^\mu(x)\right. \\ &\quad \left. -g_{\rho b}\gamma_\mu\vec{I}_b\cdot\vec{\rho^\mu}(x) - g_{\phi b}\gamma_\mu\phi^\mu(x)\right]\Psi_b(x) \end{aligned} \tag{2.86}$$

$$\begin{aligned} \mathcal{L}_\Delta &= \bar{\Psi}_\Delta(x)\left[i\gamma_\mu\partial^\mu - m_\Delta + g_{\sigma\Delta}\sigma(x) - g_{\omega\Delta}\gamma_\mu\omega^\mu(x)\right. \\ &\quad \left. -g_{\rho\Delta}\gamma_\mu\vec{I}_\Delta\cdot\vec{\rho^\mu}(x)\right]\Psi_\Delta(x) \end{aligned} \tag{2.87}$$

the only difference being the fact that now the coupling parameters are functionals of ϱ.

Usually, the functional dependence of the nucleon couplings on the total density of the system n_B is defined as in Ref. [37]:

$$g_{iN}(n_B) = g_{iN}(n_0)a_i\frac{1+b_i(x+d_i)^2}{1+c_i(x+d_i)^2}, \;\; i=\sigma,\,\omega \tag{2.88}$$

$$g_{iN}(n_B) = g_{iN}(n_0)\exp[-a_\rho(x-1)], \;\; i=\rho \tag{2.89}$$

where the parameters a_i, b_i, c_i, d_i are specific for each density dependent RMF model, n_0 is the symmetric nuclear saturation density (which is also model dependent) and $x = n_B/n_0$.

For the hyperon and Δ couplings, we will assume the same density dependence of the nucleon couplings, since their couplings are defined in terms of the nucleon couplings.

Finally, the Lagrangian density of the leptons remains the same as Eq.(2.4).

2.2.2 Equations of Motion

Following the same procedure as we have done for the nonlinear models, the equations of motion for the mesonic fields are

$$m_\sigma^2\sigma = \sum_{c=b,\Delta} g_{\sigma c}\rho_c^s \tag{2.90}$$

$$m_\omega^2\omega_0 = \sum_{c=b,\Delta} g_{\omega c}\rho_c \tag{2.91}$$

$$m_\rho^2\rho_{03} = \sum_{c=b,\Delta} g_{\rho c}I_{3c}\rho_c \tag{2.92}$$

$$m_\phi^2\phi_0 = \sum_{c=b} g_{\phi c}\rho_c \;, \tag{2.93}$$

where the couplings now depend on the total baryonic density of the system. The densities ρ_c and scalar densities ρ_c^s are also given by the same expressions as for the nonlinear models (Eqs.(2.45),(2.48),(2.49),(2.50)), the only difference being the calculation of the Fermi momenta k_F, which we will take a look later.

As for the equations of motion of the baryonic octet, the fact that the coupling constants depend on ϱ will originate some modifications with respect to Eq.(2.11). Solving the Euler-Lagrange equations (Eq.(2.6)) in the RMF Approximation for a density-dependent model yields:

$$\begin{aligned} 0 = {} & \left[\gamma_\mu k^\mu - m_b + g_{\sigma b}\sigma - g_{\omega b}\gamma_0\omega^0 - g_{\rho b}\gamma_0 I_{3b}\rho_3^0 - g_{\phi b}\gamma_0\phi^0\right]\Psi_b(\vec{k}) \\ & + \sum_{c=b,\Delta}\bar{\Psi}_c(\vec{k})\frac{\partial g_{\sigma c}(\varrho)}{\partial\varrho}\frac{\partial\varrho}{\partial\bar{\Psi}_b}\sigma\Psi_c(\vec{k}) - \sum_{c=b,\Delta}\bar{\Psi}_c(\vec{k})\frac{\partial g_{\omega c}(\varrho)}{\partial\varrho}\frac{\partial\varrho}{\partial\bar{\Psi}_b}\gamma_0\omega^0\Psi_c(\vec{k}) \\ & - \sum_{c=b,\Delta}\bar{\Psi}_c(\vec{k})\frac{\partial g_{\rho c}(\varrho)}{\partial\varrho}\frac{\partial\varrho}{\partial\bar{\Psi}_b}\gamma_0 I_{3c}\rho_3^0\Psi_c(\vec{k}) - \sum_{c=b,\Delta}\bar{\Psi}_c(\vec{k})\frac{\partial g_{\phi c}(\varrho)}{\partial\varrho}\frac{\partial\varrho}{\partial\bar{\Psi}_b}\gamma_0\phi^0\Psi_c(\vec{k}) \end{aligned} \tag{2.94}$$

Since $\frac{\partial\varrho}{\partial\bar{\Psi}_b} = \gamma_0\Psi_b$ and taking into account the baryonic (Eq.(2.45)) and scalar densities

(Eq.(2.48)) previously defined, Eq.(2.94) yields

$$\begin{aligned} 0 \;=\; & \Bigg[\gamma_\mu k^\mu - m_b + g_{\sigma b}\sigma + \gamma_0 \sum_{c=b,\Delta} \frac{\partial g_{\sigma c}}{\partial \varrho}\sigma\rho_c^s - g_{\omega b}\gamma_0\omega^0 \\ & -\gamma_0 \sum_{c=b,\Delta} \frac{\partial g_{\omega c}}{\partial \varrho}\omega^0\rho_c - g_{\rho b}\gamma_0 I_{3b}\rho_3^0 - \gamma_0 \sum_{c=b,\Delta} \frac{\partial g_{\rho c}}{\partial \varrho}\rho_3^0 I_{3c}\rho_c \\ & -g_{\phi b}\gamma_0\phi^0 - \gamma_0 \sum_{c=b,\Delta} \frac{\partial g_{\phi c}}{\partial \varrho}\phi^0\rho_c\Bigg]\,\Psi_b(\vec{k})\ . \end{aligned} \tag{2.95}$$

Similarly, the equations of motion for the Δ isobars are:

$$\begin{aligned} 0 \;=\; & \Bigg[\gamma_\mu k^\mu - m_\Delta + g_{\sigma\Delta}\sigma + \gamma_0 \sum_{c=b,\Delta} \frac{\partial g_{\sigma c}}{\partial \varrho}\sigma\rho_c^s - g_{\omega\Delta}\gamma_0\omega^0 \\ & -\gamma_0 \sum_{c=b,\Delta} \frac{\partial g_{\omega c}}{\partial \varrho}\omega^0\rho_c - g_{\rho\Delta}\gamma_0 I_{3\Delta}\rho_3^0 - \gamma_0 \sum_{c=b,\Delta} \frac{\partial g_{\rho c}}{\partial \varrho}\rho_3^0 I_{3c}\rho_c\Bigg]\,\Psi_\Delta(\vec{k})\ . \end{aligned} \tag{2.96}$$

The equations of motion for the leptons remain the same as (2.13).

2.2.3 Energy Spectrum

If we now apply the same method used in Section 2.1.4 to Eq.(2.95), we find the energy eigenvalues for the baryonic octet particles and antiparticles for a density-dependent RMF model:

$$E_b^{\pm}(k) = g_{\omega b}\omega_0 + g_{\rho b}I_{3b}\rho_{03} + g_{\phi b}\phi_0 + \Sigma_0^R \pm \sqrt{k^2 + m_b^{*2}}\ , \tag{2.97}$$

where

$$\Sigma_0^R = \sum_{c=b,\Delta}\Big(\frac{\partial g_{\omega c}}{\partial \varrho}\omega_0\rho_c + I_{3c}\frac{\partial g_{\rho c}}{\partial \varrho}\rho_{03}\rho_c + \frac{\partial g_{\phi c}}{\partial \varrho}\phi_0\rho_c - \frac{\partial g_{\sigma c}}{\partial \varrho}\sigma\rho_c^s\Big) \tag{2.98}$$

is the so-called rearrangement term. The rearrangement term is only present in models with density-dependent couplings and is crucial for the maintenance of the system's thermodynamical consistency.

Similarly, the energy eigenvalues for the Δ isobars are

$$E_\Delta^{\pm}(k) = g_{\omega\Delta}\omega_0 + g_{\rho\Delta}I_{3\Delta}\rho_{03} + \Sigma_0^R \pm \sqrt{k^2 + m_\Delta^{*2}}\ . \tag{2.99}$$

The energy eigenvalues for the leptons remain the same as in nonlinear models (Eq.(2.34)).

2.2.4 Chemical Potentials

The chemical potentials calculated by Eq.(2.62) will also suffer some modifications in a density-dependent RMF model. In fact, if we rewrite Eq.(2.62) taking into account Eq.(2.97), we have:

$$\mu_b = g_{\omega b}\omega_0 + g_{\rho b}I_{3b}\rho_{03} + g_{\phi b}\phi_0 + \Sigma_0^R + \sqrt{k_{F,b}^2 + m_b^{*2}}\ . \tag{2.100}$$

Then, the effective chemical potentials μ_b^* for the baryonic octet will be:

$$\mu_b^* = \sqrt{k_{F,b}^2 + m_b^{*2}} = \mu_b - g_{\omega b}\omega_0 - g_{\rho b} I_{3b}\rho_{03} - g_{\phi b}\phi_0 - \Sigma_0^R \ . \tag{2.101}$$

Finally, the Fermi momentum $k_{F,b}$ reads:

$$k_{F,b} = \sqrt{\mu_b^{*2} - m_b^{*2}} \ \ . \tag{2.102}$$

Similarly, for the Δ particles we have:

$$\mu_\Delta = g_{\omega\Delta}\omega_0 + g_{\rho\Delta} I_{3\Delta}\rho_{03} + \Sigma_0^R + \sqrt{k_{F,\Delta}^2 + m_\Delta^{*2}} \tag{2.103}$$

$$k_{F,\Delta} = \sqrt{\mu_\Delta^{*2} - m_\Delta^{*2}} \tag{2.104}$$

The lepton chemical potentials and Fermi momentum suffer no changes from Eqs.(2.68) and (2.69).

The densities and scalar densities of the various baryons are calculated in the same way as for the nonlinear models, the only difference being the definition of their Fermi momenta.

2.2.5 Equation of State

Following the same method used in Section 2.1.7, the energy density in a density-dependent RMF model is similar to what we had for nonlinear models:

$$\epsilon = \sum_{i=b,\Delta,l} \left[\frac{2J_i+1}{2\pi^2} \int_0^{k_{F,i}} k^2 \sqrt{k^2 + m_i^{*2}} dk + g_{\omega i}\omega_0\rho_i \right. \tag{2.105}$$
$$\left. + g_{\rho i}\rho_{03} I_{3i}\rho_i + g_{\phi i}\phi_0\rho_i \right] + \sum_{c=b,\Delta} \Sigma_0^R \rho_c - \mathcal{L}_{RMF}$$

whereas the pressure has an extra term with the rearrangement term:

$$p = \frac{1}{3} \sum_{i=b,\Delta,l} \frac{2J_i+1}{2\pi^2} \int_0^{k_{F,i}} \frac{k^4 dk}{\sqrt{k^2 + m_i^{*2}}} + \mathcal{L}_{RMF} \ , \tag{2.106}$$

where $\mathcal{L}_{RMF}$ is the Lagrangian density for a density-dependent model in the RMF approximation:

$$\mathcal{L}_{RMF} = -\frac{1}{2} m_\sigma^2 \sigma^2 + \frac{1}{2} m_\omega^2 \omega_0^2 + \frac{1}{2} m_\rho^2 \rho_{03}^2 + \frac{1}{2} m_\phi^2 \phi_0^2 + \sum_{c=b,\Delta} \Sigma_0^R \rho_c \ . \tag{2.107}$$

Chapter 3

Relativistic Mean-Field Models with Light Clusters and Hyperclusters for finite temperature and fixed charge fraction

The thermodynamical conditions that describe the stellar matter EoS that applies to astrophysical sites, like CCSN matter or BNSM, are finite temperatures and fixed charge fractions. In the low-density regime (i.e. below nuclear saturation density), and as mentioned in the Introduction, besides considering a gas of unbound protons, neutrons and electrons, one also needs to take into account the presence of light and heavy nuclei. In this work, we restrict ourselves to light clusters (^{2}H, ^{3}H, ^{3}He, ^{4}He, ^{6}He), and we also include light hypernuclei ($^3_\Lambda$H, $^4_\Lambda$H, $^4_\Lambda$He). Since the charge fraction is fixed, we do not include any leptons. In the following, we present the formalism under the framework of both nonlinear and density-dependent relativistic mean-field models with light clusters and hyperclusters for finite temperature and fixed charge fraction.

3.1 Nonlinear RMF Models with Light Clusters

To begin with, we first study a system consisting of a gas with unbound protons and neutrons as well as the six hyperons previously considered (Λ, $\Sigma^{-,0,+}$, $\Xi^{-,0}$) and the four Δ isobars ($\Delta^{-,0,+,++}$). Immersed in this gas, we consider five purely nucleonic light nuclei with $Z \leq 2$: ^{2}H, ^{3}H, ^{3}He, ^{4}He, ^{6}He. The spin and isospin projection quantum numbers for each purely nucleonic light cluster can be found in Table 3.1.

3.1.1 Lagrangian Density

For the low densities studied here, the five nucleonic light nuclei are considered to be point-like particles due to their small size[1]. As a result, these light nuclei will be treated as new degrees of freedom of the theory.

Then, adding the contribution of the light clusters to Eq.(2.1), the Lagrangian Density of

[1]This is valid as long as the volume occupied by a cluster is much larger than its own volume.

	^{2}H	^{3}H	^{3}He	^{4}He	^{6}He
J	1	1/2	1/2	0	0
I_3	0	−1/2	1/2	0	−1

Table 3.1: Spin (J) and isospin projection (I_3) quantum numbers for the purely nucleonic light clusters.

this system reads [23,37], see also Eq.(2.1):

$$\mathcal{L} = \sum_{\substack{b=baryonic\\octet}} \mathcal{L}_b + \sum_{\Delta} \mathcal{L}_\Delta + \sum_{\substack{i=light\\nuclei}} \mathcal{L}_i + \sum_{m=\sigma,\omega,\phi,\rho} \mathcal{L}_m. \tag{3.1}$$

The Lagrangian densities $\mathcal{L}_b$, $\mathcal{L}_\Delta$ and $\mathcal{L}_m$ are exactly the same as Eqs.(2.2), (2.3) and (2.5), respectively. As for the light clusters, their Lagrangian density $\mathcal{L}_i$ is defined according to the spin of the clusters: two of them are fermions (^{3}H, ^{3}He) and are described by a Lagrangian density equivalent to the one taken for the baryons; two of them are bosons with spin 0 and are described by the Klein-Gordon Lagrangian for scalar fields; and finally, the deuteron has spin 1 and is described by the Proca Lagrangian.

Then, following Refs. [23, 37, 38], the Lagrangian density for the fermionic spin-1/2 light nuclei, reads

$$\mathcal{L}_i = \bar{\Psi}_i \left[\gamma_\mu i D_i^\mu - M_i^*\right] \Psi_i, \; i = {}^3\mathrm{H}, {}^3\mathrm{He} \tag{3.2}$$

The Lagrangian density for the bosonic light nuclei with spin 0 and spin 1 is given by, respectively,

$$\mathcal{L}_i = \frac{1}{2}\left(iD_i^\mu \Psi_i\right)^* \left(iD_{\mu i}\Psi_i\right) - \frac{1}{2}\Psi_i^*(M_i^*)^2\Psi_i, \quad i = {}^4\mathrm{He}, {}^6\mathrm{He} \tag{3.3}$$

$$\begin{aligned}\mathcal{L}_i = {} & \frac{1}{4}\left(iD_i^\mu \Psi_i^\nu - iD_i^\nu \Psi_i^\mu\right)^* \left(iD_{\mu i}\Psi_{\nu i} - iD_{\nu i}\Psi_{\mu i}\right) \\ & -\frac{1}{2}\Psi_i^{\mu *}(M_i^*)^2\Psi_{\mu i}, \quad i = {}^2\mathrm{H}\end{aligned} \tag{3.4}$$

with

$$iD_i^\mu = i\partial^\mu - g_{\omega i}\omega^\mu - g_{\rho i}\vec{I}_i \cdot \vec{\rho^\mu} \; . \tag{3.5}$$

$g_{\omega i}$ and $g_{\rho i}$ are the couplings of cluster i to the ω and ρ mesons, respectively. They are defined as

$$g_{\omega i} = A_i g_{\omega N} \tag{3.6}$$

$$g_{\rho i} = g_{\rho N} \; , \tag{3.7}$$

A_i being the cluster mass number and $g_{\omega N}$, $g_{\rho N}$ the couplings of the nucleons to the mesons.

Since the coupling parameters of the light clusters to the ρ meson are the same as the one of nucleons, what differentiates each cluster concerning this coupling is their isospin projection. The same will be true for the light hyperclusters introduced later. The effective mass M_i^* will be defined in the next subsection.

i	B_i^0 [MeV]
^{2}H	2.224566
^{3}H	8.481798
^{3}He	7.718043
^{4}He	28.29566
^{6}He	29.271114

Table 3.2: Vacuum binding energies, B_i^0, for each light cluster i [39].

3.1.2 Light Clusters Binding Energies and Mass Shifts

In this section, we follow the formalism for the inclusion of in-medium effects in the low-density EoS for warm stellar matter, which was first introduced in Refs. [23, 38].

The total binding energy B_i for a purely nucleonic light cluster i is given by [23, 38]:

$$B_i = A_i m^* - M_i^*, \; i = {}^2\mathrm{H}, {}^3\mathrm{H}, {}^3\mathrm{He}, {}^4\mathrm{He}, {}^6\mathrm{He} \tag{3.8}$$

where $m^* = m - g_{\sigma N}$ is the nucleon effective mass and M_i^* the effective mass of cluster i, which is determined by the σ-cluster coupling $g_{\sigma i}$ as well as by a binding energy shift δB_i:

$$M_i^* = A_i m - g_{\sigma i}\sigma - (B_i^0 + \delta B_i), \tag{3.9}$$

where

$$g_{\sigma i} = x_s A_i g_{\sigma N} \tag{3.10}$$

is the σ-cluster coupling.

As discussed in Ref. [23], in a RMF model the nucleons are considered to be independent particles with no correlations. However, when we introduce correlations via the addition of bound clusters, the couplings of the nucleons inside a cluster to the meson fields may suffer some modifications and a priori we cannot say that the couplings g_{mi} of the clusters to the meson fields will simply be the sum of the individual nucleon couplings that constitute a given cluster. In fact, the couplings $g_{\sigma i}$, $g_{\omega i}$ are new parameters of the model that need to be fitted to experimental data or to results of microscopic theories. Here, we choose to include all the modifications due to the correlations in the σ-cluster coupling by introducing a universal fraction x_s that needs to be fitted to experimental data. Therefore, we consider the ω-cluster coupling defined in Eq.(3.6) to be simply the sum of the individual nucleon couplings as if they were unbound nucleons. B_i^0 is the tabulated vacuum binding energy of light cluster i (Table 3.2) and δB_i is the binding energy shift introduced to account in an effective way for Pauli blocking effects.

Following the method used in Ref. [23], the binding energy shift δB_i of a purely nucleonic light cluster i is defined as:

$$\delta B_i = \frac{Z_i}{\rho_0}(\epsilon_p^* - m\rho_p^*) + \frac{N_i}{\rho_0}(\epsilon_n^* - m\rho_n^*) \tag{3.11}$$

with Z_i, N_i the number of protons and neutrons present at cluster i, respectively.

Defining the binding energy shift as in Eq.(3.11) means that we are excluding from the cluster binding energy the nucleon energy states already occupied by the gas. Therefore, we avoid double counting the nucleons present in the gas or inside the clusters.

Then, we define the gas energy density ϵ_k^* and nucleonic density ρ_k^*, $k = n, p$, associated with the already occupied gas lowest energy states as

$$\epsilon_k^* = \frac{1}{\pi^2}\int_0^{p_{F_k}(\text{gas})} p^2 e_k(p)(f_{k+}(p) + f_{k-}(p))dp \tag{3.12}$$

$$\rho_k^* = \frac{1}{\pi^2}\int_0^{p_{F_k}(\text{gas})} p^2 (f_{k+}(p) + f_{k-}(p))dp. \tag{3.13}$$

where $p_{F_k}(\text{gas}) = (3\pi^2\rho_k)^{1/3}$ is the Fermi momentum of nucleon k defined using the zero temperature relation between density and Fermi momentum (Eq.(2.45)). This definition of $p_{F_k}(\text{gas})$ is only valid in a range of temperatures for which the Fermi distribution of particles is close to a step function.

The functions $f_{k\pm}$ are the Fermi distribution functions for the nucleons and respective antiparticles for finite temperatures given as

$$f_{k\pm}(p) = \frac{1}{\exp[(e_k \mp \mu_k^*)/T] + \eta} \tag{3.14}$$

where $e_k = \sqrt{p_k^2 + m^{*2}}$ is the single-particle energy of the nucleon k, μ_k^* is the effective chemical potential given by Eq.(2.64), T is the temperature of the system and $\eta = 1$ for fermions and $\eta = -1$ for bosons.

3.1.3 Equations of Motion

The introduction of a binding energy shift that depends on the medium (that is the nucleon densities) will modify the equations of motion of the mesonic fields. In order to avoid further complications with rearrangement contributions, we will follow the method used in [37] and substitute the dependence of the binding energy shift on the densities with a dependence on the vector meson fields. In this way, we can treat the binding shifts as we have done for the single particle shifts with respect to the vacuum.

For that, we consider a system made up only of unbound protons and neutrons and solve the vector meson equations (2.54) and (2.55) to obtain the following nucleon pseudo-densities:

$$\rho_n^{\text{ps}} = \frac{m_\omega^2}{2g_{\omega N}}\omega_0 - \frac{m_\rho^2}{g_{\rho N}}\rho_{03} \tag{3.15}$$

$$\rho_p^{\text{ps}} = \frac{m_\omega^2}{2g_{\omega N}}\omega_0 + \frac{m_\rho^2}{g_{\rho N}}\rho_{03}. \tag{3.16}$$

Here we have neglected the nonlinear contributions of the mesons, considering only the more significant linear terms[2]. The binding energy shift, $\delta B_i(\rho_n^{\text{ps}}, \rho_p^{\text{ps}})$, will then depend on the vector mesons through the pseudo-densities ρ_n^{ps} and ρ_n^{ps}.

The presence in the Lagrangian density of a binding energy shift that depends on the ω and ρ vector meson fields, will modify the previously obtained equations of motion for these mesons (Eqs.(2.54),(2.55)).

In fact, solving the Euler-Lagrange equations for the Lagrangian density of Eq.(3.1) results

[2]In fact, we are only looking for an effective way of replacing the dependence on the densities with a dependence on the vector fields so we can define our ansatz considering only the linear terms.

in the following modified equations of motion for the ω and ρ vector meson fields:

$$
\begin{aligned}
m^2_{\omega,\mathrm{eff}}\omega_0 &= \sum_b g_{\omega b}\rho_b + \sum_\Delta g_{\omega\Delta}\rho_\Delta + \sum_i g_{\omega i}\rho_i \\
&\quad - \sum_{\substack{i=^2\mathrm{H},^3\mathrm{H},^3\mathrm{He},\\ ^4\mathrm{He},^6\mathrm{He}}} \rho_i^s \left[\frac{\partial(\delta B_i)}{\partial\rho_n^{\mathrm{ps}}}\frac{\partial\rho_n^{\mathrm{ps}}}{\omega_0} + \frac{\partial(\delta B_i)}{\partial\rho_p^{\mathrm{ps}}}\frac{\partial\rho_p^{\mathrm{ps}}}{\omega_0} \right]
\end{aligned}
\tag{3.17}
$$

$$
\begin{aligned}
m^2_{\rho,\mathrm{eff}}\rho_{03} &= g_{\rho N}\left[\sum_b I_{3b}\rho_b + \sum_\Delta I_{3\Delta}\rho_\Delta + \sum_i I_{3i}\rho_i \right] \\
&\quad - \sum_{\substack{i=^2\mathrm{H},^3\mathrm{H},^3\mathrm{He},\\ ^4\mathrm{He},^6\mathrm{He}}} \rho_i^s \left[\frac{\partial(\delta B_i)}{\partial\rho_n^{\mathrm{ps}}}\frac{\partial\rho_n^{\mathrm{ps}}}{\rho_{03}} + \frac{\partial(\delta B_i)}{\partial\rho_p^{\mathrm{ps}}}\frac{\partial\rho_p^{\mathrm{ps}}}{\rho_{03}} \right]
\end{aligned}
\tag{3.18}
$$

where

$$
m^2_{\omega,\mathrm{eff}} = m^2_\omega + \frac{\zeta}{3!}g^4_{\omega N}\omega_0^2 + 2\Lambda_\omega g^2_{\rho N} g^2_{\omega N}\rho_{03}^2 \tag{3.19}
$$

$$
m^2_{\rho,\mathrm{eff}} = m^2_\rho + 2\Lambda_\omega g^2_{\rho N} g^2_{\omega N}\omega_0^2. \tag{3.20}
$$

Taking the results derived in Appendix A.1, the equations of motion for the ω and ρ mesons read:

$$
\begin{aligned}
m^2_{\omega,\mathrm{eff}}\omega_0 &= \sum_b g_{\omega b}\rho_b + \sum_\Delta g_{\omega\Delta}\rho_\Delta + \sum_i g_{\omega i}\rho_i \\
&\quad -\frac{1}{\rho_0}\left(\frac{m^2_\omega}{2g_{\omega N}}\right)(\rho^s_{^2\mathrm{H}}+\rho^s_{^3\mathrm{H}}+\rho^s_{^3\mathrm{He}}+2\rho^s_{^4\mathrm{He}}+2\rho^s_{^6\mathrm{He}})\left[\frac{\partial\epsilon^*_n}{\partial\rho_n^{\mathrm{ps}}}-\frac{m\partial\rho^*_n}{\partial\rho_n^{\mathrm{ps}}}+\frac{\partial\epsilon^*_p}{\partial\rho_p^{\mathrm{ps}}}-\frac{m\partial\rho^*_p}{\partial\rho_p^{\mathrm{ps}}}\right] \\
&\quad -\frac{1}{\rho_0}\left(\frac{m^2_\omega}{2g_{\omega N}}\right)(\rho^s_{^3\mathrm{H}}+2\rho^s_{^6\mathrm{He}})\left[\frac{\partial\epsilon^*_n}{\partial\rho_n^{\mathrm{ps}}}-\frac{m\partial\rho^*_n}{\partial\rho_n^{\mathrm{ps}}}\right] \\
&\quad -\frac{1}{\rho_0}\left(\frac{m^2_\omega}{2g_{\omega N}}\right)\rho^s_{^3\mathrm{He}}\left[\frac{\partial\epsilon^*_p}{\partial\rho_p^{\mathrm{ps}}}-\frac{m\partial\rho^*_p}{\partial\rho_p^{\mathrm{ps}}}\right]
\end{aligned}
\tag{3.21}
$$

$$
\begin{aligned}
m^2_{\rho,\mathrm{eff}}\rho_{03} &= g_{\rho N}\left[\sum_b I_{3b}\rho_b + \sum_\Delta I_{3\Delta}\rho_\Delta + \sum_i I_{3i}\rho_i \right] \\
&\quad -\frac{1}{\rho_0}\left(\frac{m^2_\rho}{g_{\rho N}}\right)(\rho^s_{^2\mathrm{H}}+\rho^s_{^3\mathrm{H}}+\rho^s_{^3\mathrm{He}}+2\rho^s_{^4\mathrm{He}}+2\rho^s_{^6\mathrm{He}})\left[-\frac{\partial\epsilon^*_n}{\partial\rho_n^{\mathrm{ps}}}+\frac{m\partial\rho^*_n}{\partial\rho_n^{\mathrm{ps}}}+\frac{\partial\epsilon^*_p}{\partial\rho_p^{\mathrm{ps}}}-\frac{m\partial\rho^*_p}{\partial\rho_p^{\mathrm{ps}}}\right] \\
&\quad -\frac{1}{\rho_0}\left(\frac{m^2_\rho}{g_{\rho N}}\right)(\rho^s_{^3\mathrm{H}}+2\rho^s_{^6\mathrm{He}})\left[-\frac{\partial\epsilon^*_n}{\partial\rho_n^{\mathrm{ps}}}+\frac{m\partial\rho^*_n}{\partial\rho_n^{\mathrm{ps}}}\right] \\
&\quad -\frac{1}{\rho_0}\left(\frac{m^2_\rho}{g_{\rho N}}\right)\rho^s_{^3\mathrm{He}}\left[\frac{\partial\epsilon^*_p}{\partial\rho_p^{\mathrm{ps}}}-\frac{m\partial\rho^*_p}{\partial\rho_p^{\mathrm{ps}}}\right]
\end{aligned}
\tag{3.22}
$$

As for the equation of motion for the σ meson, the only modification in relation to Eq.(2.53) will be an additional term for the light clusters:

$$
m^2_\sigma\sigma + \frac{\kappa}{2}g^3_{\sigma N}\sigma^2 + \frac{\lambda}{3!}g^4_{\sigma N}\sigma^3 = \sum_{c=b,\Delta,i} g_{\sigma c}\rho^s_c\ . \tag{3.23}
$$

Since the five purely nucleonic light clusters do not couple to the ϕ meson, its equation of motion will be the same as Eq.(2.56). The equations of motion for the baryonic octet and Δ particles are the same as Eqs.(2.11) and (2.12).

As for the light clusters, the fermionic spin-1/2 ones ($i = {}^3\mathrm{H}, {}^3\mathrm{He}$) will have a Dirac equation similar to the nucleons:

$$[\gamma_\mu i D_i^\mu - M_i^*]\,\Psi_i(x) = 0 \ , \ i = {}^3\mathrm{H}, {}^3\mathrm{He} \ . \tag{3.24}$$

To the bosonic light clusters with spin 0 ($i = {}^4\mathrm{H}, {}^6\mathrm{He}$) corresponds a Klein-Gordon equation of motion:

$$\Big[- i D_i^\mu i D_{\mu i} + M_i^{*2} \Big] \Psi_i = 0 \ , \ i = {}^4\mathrm{He}, {}^6\mathrm{He} \ . \tag{3.25}$$

Finally, the cluster ${}^2\mathrm{H}$ is a boson with spin 1, thus having a Proca equation of motion:

$$-i D_{\mu i} \Big[i D_i^\mu \Psi_i^\nu - i D_i^\nu \Psi_i^\mu \Big] + M_i^{*2} \Psi_i^\nu = 0 \ , \ i = {}^2\mathrm{H} \ . \tag{3.26}$$

The quantities ρ_c, ρ_c^s ($c = b, \Delta, i$) appearing in Eqs.(3.17),(3.18),(3.21),(3.22),(3.23) are the particle baryonic and scalar densities, respectively, at finite temperature given by:

$$\rho_c = \frac{(2J_c+1)}{2\pi^2} \int_0^\infty k^2 dk [f_{k+} - f_{k-}] \tag{3.27}$$

$$\rho_c^s = \frac{(2J_c+1)}{2\pi^2} \int_0^\infty \frac{M_c^*}{\sqrt{k^2 + M_c^{*2}}} k^2 dk [f_{k+} + f_{k-}], \tag{3.28}$$

which were obtained by following a similar procedure to the one derived in Section 2.1.5, the only difference being that now we have to include the Fermi distribution functions from Eq.(3.14) since we are considering finite temperatures.

3.1.4 Mass and Charge Fractions

As we mentioned before, instead of considering a system in β-equilibrium, we will consider a system in which the charge fraction Y_Q is fixed. The reason to do so lies in the fact that in both CCS and BNSM β-equilibrium is not necessarily achieved, as was mentioned in the Introduction. Then, by fixing the charge fractions for several values we can use our system to try and describe these phenomena.

Thus, in the system we are considering, the charge fraction Y_Q is fixed and defined as:

$$Y_Q = \sum_b q_b Y_b + \sum_\Delta q_\Delta Y_\Delta + \sum_i \frac{q_i}{A_i} Y_i \tag{3.29}$$

where q_b, q_Δ, q_i are the electric charges (in units of $+e$) of baryon b from the baryonic octet, Δ isobar and light cluster i, respectively. The quantities Y_b, Y_Δ and Y_i correspond to the mass fractions of the different particles and are given by:

$$Y_b = \frac{\rho_b}{n_B} \tag{3.30}$$

$$Y_\Delta = \frac{\rho_\Delta}{n_B} \tag{3.31}$$

$$Y_i \;=\; A_i \frac{\rho_i}{n_B} \; . \tag{3.32}$$

3.1.5 Light Clusters Chemical Potentials

As mentioned before in Section 2.1.6, the chemical potentials of the baryonic octet particles b and Δ isobars are given by Eqs.(2.57-2.61).

For a light cluster i, their chemical potential μ_i can also be defined as a function of μ_n and μ_p as

$$\mu_i = N_i \mu_n + Z_i \mu_p \; . \tag{3.33}$$

Their effective chemical potential μ_i^* follows

$$\mu_i^* = \mu_i - g_{\omega i}\omega_0 - g_{\rho i} I_{3i} \rho_{03} \; . \tag{3.34}$$

3.1.6 Equation of State with Light Clusters

Following the same method used in Section 2.1.7, the energy density of a system with the baryonic octet ($b = \Lambda, \Sigma^{-,0,+}, \Xi^{-,0}$), Δ isobars ($\Delta = \Delta^{-,0,+,++}$) and the five purely nucleonic light clusters ($i = {}^2$H, ^{3}H, ^{3}He, ^{4}He, ^{6}He) reads

$$\epsilon = \sum_{c=b,\Delta,i} \left[\frac{2J_c+1}{2\pi^2} \int_0^{k_{F,c}} k^2 \sqrt{k^2 + m_c^{*2}} dk + g_{\omega c}\omega_0 \rho_c \right. \tag{3.35}$$
$$\left. + g_{\rho c}\rho_{03} I_{3c} \rho_c + g_{\phi c}\phi_0 \rho_c \right] - \mathcal{L}_{RMF}$$

whereas the pressure is

$$p = \frac{1}{3} \sum_{c=b,\Delta,i} \frac{2J_c+1}{2\pi^2} \int_0^{k_{F,c}} \frac{k^4 dk}{\sqrt{k^2 + m_c^{*2}}} + \mathcal{L}_{RMF} \; . \tag{3.36}$$

3.2 Nonlinear RMF Models with Light Clusters and Hyperclusters

We are now going to add light hypernuclei to the system presented in Section 3.1. Hypernuclei are similar to the light nuclei mentioned above except for the fact than one of their nucleons was replaced by an hyperon.

We will consider three different hypernuclei: the ${}^3_\Lambda$H hypertriton, the ${}^4_\Lambda$H hyper-hydrogen4 and the hyperhelium4 ${}^4_\Lambda$He. As we can see, for each one of these three hypernuclei, a nucleon was replaced by a Λ hyperon.

The spin and isospin projection quantum numbers for each hypercluster can be found in Table 3.3.

3.2.1 Lagrangian Density

The light hyperclusters j will be introduced in a similar way to the purely nucleonic light clusters. That is, they will be considered as point-like particles, adding new degrees of freedom to the system. We will follow the formalism recently published in Ref. [27].

	${}^{3}_{\Lambda}$H	${}^{4}_{\Lambda}$H	${}^{4}_{\Lambda}$He
J	1/2	0	0
I_3	0	−1/2	1/2

Table 3.3: Spin (J) and isospin projection (I_3) quantum numbers for all particles considered in our system.

One of the hyperclusters, ${}^{3}_{\Lambda}$H, has spin 1/2 and is described by a Dirac Lagrangian, and the other two, ${}^{4}_{\Lambda}$H and ${}^{4}_{\Lambda}$He, have spin 0 and are described by a Klein-Gordon Lagrangian.

Then, the Lagrangian density for the fermionic light hypercluster $j = {}^{3}_{\Lambda}$H is:

$$\mathcal{L}_j = \bar{\Psi}_j \left[\gamma_\mu i D_j^\mu - M_j^*\right] \Psi_j, \quad j = {}^{3}_{\Lambda}\text{H} \ , \tag{3.37}$$

whereas for the bosonic light hyperclusters, $j = {}^{4}_{\Lambda}$H, ${}^{4}_{\Lambda}$He, the Lagrangian density is given by

$$\mathcal{L}_j = \frac{1}{2}\Big(iD_j^\mu \Psi_j\Big)^* \Big(iD_{\mu j}\Psi_j\Big) - \frac{1}{2}\Psi_j^*(M_j^*)^2\Psi_j, \quad j = {}^{4}_{\Lambda}\text{H}, {}^{4}_{\Lambda}\text{He} \tag{3.38}$$

with

$$iD_j^\mu = i\partial^\mu - g_{\omega j}\omega^\mu - g_{\phi j}\phi^\mu - g_{\rho i}\vec{I}_j \cdot \vec{\rho^\mu} \ . \tag{3.39}$$

We follow an approach similar to the one used to define the couplings of purely nucleonic light clusters in Section 3.1.1. The coupling to the ω-meson is determined from the sum of the meson coupling to each one of the baryons that constitute the cluster. For a purely nucleonic light cluster this implies that the ω-cluster coupling is the ω-nucleon coupling times the number of nucleons A_i. When hypernuclei are considered it must be taken into account that the coupling of the ω meson to the hyperons is not so strong. We, thus, define the coupling of the hyperclusters to the ω meson as

$$g_{\omega j} = (A_j - 1)g_{\omega N} + g_{\omega\Lambda} \ . \tag{3.40}$$

The coupling to the ϕ meson is considered to be equal to the Λ coupling to ϕ ("ideal mixing" case, see Section 4.1):

$$g_{\phi j} = g_{\phi\Lambda} \ . \tag{3.41}$$

Once again, the coupling to the ρ meson is taken to be the same as the one of nucleons:

$$g_{\rho j} = g_{\rho N} \ . \tag{3.42}$$

The effective mass M_j^* is defined in the next subsection.

3.2.2 Hyperclusters Binding Energies and Mass Shifts

To find the binding energies for the hyperclusters, we first notice that the vacuum mass M_j of an hypercluster j is given by:

$$M_j = (A_j - 1)m + m_\Lambda - B_j^0 \ . \tag{3.43}$$

The vacuum masses for the hypertriton, ${}^{3}_{\Lambda}$H, the hyper-hydrogen4, ${}^{4}_{\Lambda}$H, and the hyperhelium4,

${}^{4}_{\Lambda}$He, were taken from Refs. [8], [9], [10], respectively:

$$M_{{}^{3}_{\Lambda}\mathrm{H}} = 2990.89 \text{ MeV} \tag{3.44}$$

$$M_{{}^{4}_{\Lambda}\mathrm{H}} = 3922.49 \text{ MeV} \tag{3.45}$$

$$M_{{}^{4}_{\Lambda}\mathrm{He}} = 3921.70 \text{ MeV} . \tag{3.46}$$

Their vacuum binding energies are then:

$$B^0_{{}^{3}_{\Lambda}\mathrm{H}} = 2.793 \text{ MeV} \tag{3.47}$$

$$B^0_{{}^{4}_{\Lambda}\mathrm{H}} = 10.198 \text{ MeV} \tag{3.48}$$

$$B^0_{{}^{4}_{\Lambda}\mathrm{He}} = 10.981 \text{ MeV} . \tag{3.49}$$

We can now can write the effective mass of hypercluster j in a similar way to Eq.(3.9) as

$$M^*_j = (A_j - 1)m + m_\Lambda - g_{\sigma j}\sigma - (B^0_j + \delta B_j) \tag{3.50}$$

where

$$g_{\sigma j} = x_s((A_j - 1)g_{\sigma N} + g_{\sigma\Lambda}) \tag{3.51}$$

is the σ-hypercluster coupling. From Ref. [40] we see that the experimental production ratio between ${}^{3}_{\Lambda}$H and ^{3}H (${}^{3}_{\Lambda}\mathrm{H}/{}^{3}\mathrm{H}$) is 0.75 ± 0.07. Since this ratio must be proportional to the square of the interaction and considering the $g_{\sigma\Lambda}$ couplings given in Table 4.4, we find that $(g_{\sigma^{3}_{\Lambda}\mathrm{H}}/g_{\sigma^{3}\mathrm{H}})^2 \sim 0.76$, which suggests that the way we define the σ-hypercluster couplings is in good accordance with experimental data.

As for the hypercluster binding energy shifts, following the same procedure as we did for the light nucleonic clusters, we get a similar expression to Eq.(3.11):

$$\delta B_j = \frac{Z_j}{\rho_0}(\epsilon^*_p - m\rho^*_p) + \frac{N_j}{\rho_0}(\epsilon^*_n - m\rho^*_n) + \frac{\Lambda_j}{\rho_0}(\epsilon^*_\Lambda - m_\Lambda\rho^*_\Lambda) \tag{3.52}$$

4 where Λ_j is the number of Λ hyperons present at hypercluster j (for the three hyperclusters we consider here Λ_j is always equal to 1). Then, we will now have similar expressions to Eqs.(3.12) and (3.13), but for $k = n, p, \Lambda$.

3.2.3 Equations of Motion

From Eq.(3.52) we can see that in the presence of an hypercluster, the binding energy shift will not only depend on the nucleon densities but also on the Λ hyperon density.

Following the same method as in Section 3.1.3, we consider a gas made up of unbound protons and neutrons as well as Λ hyperons and obtain the following pseudo-densities:

$$\rho^{\mathrm{ps}}_n = \frac{m^2_\omega}{2g_{\omega N}}\omega_0 - \frac{g_{\omega\Lambda}}{g_{\phi\Lambda}}\frac{m^2_\phi}{2g_{\omega N}}\phi_0 - \frac{m^2_\rho}{g_{\rho N}}\rho_{03} \tag{3.53}$$

$$\rho^{\mathrm{ps}}_p = \frac{m^2_\omega}{2g_{\omega N}}\omega_0 - \frac{g_{\omega\Lambda}}{g_{\phi\Lambda}}\frac{m^2_\phi}{2g_{\omega N}}\phi_0 + \frac{m^2_\rho}{g_{\rho N}}\rho_{03} \tag{3.54}$$

$$\rho^{\mathrm{ps}}_\Lambda = \frac{m^2_\phi}{g_{\phi\Lambda}}\phi_0 \tag{3.55}$$

The presence in the Lagrangian density of a binding energy shift that now depends on the ω, ρ and ϕ vector meson fields, will again modify the previously obtained equations of motion for these mesons (Eqs.(2.54),(2.55),(2.56)).

Solving the Euler-Lagrange equations results in the following modified equations of motion for the ω, ρ and ϕ vector meson fields, respectively:

$$\begin{aligned} m^2_{\omega,\mathrm{eff}}\omega_0 &= \sum_b g_{\omega b}\rho_b + \sum_\Delta g_{\omega\Delta}\rho_\Delta + \sum_i g_{\omega i}\rho_i + \sum_j g_{\omega j}\rho_j \\ &- \sum_{\substack{i={}^2\mathrm{H},{}^3\mathrm{H},{}^3\mathrm{He},\\ {}^4\mathrm{He},{}^6\mathrm{He}}} \rho_i^s \left[\frac{\partial(\delta B_i)}{\partial\rho_n^{\mathrm{ps}}}\frac{\partial\rho_n^{\mathrm{ps}}}{\omega_0} + \frac{\partial(\delta B_i)}{\partial\rho_p^{\mathrm{ps}}}\frac{\partial\rho_p^{\mathrm{ps}}}{\omega_0}\right] \\ &- \sum_{j={}^3_\Lambda\mathrm{H},{}^4_\Lambda\mathrm{H},{}^4_\Lambda\mathrm{He}} \rho_j^s \left[\frac{\partial(\delta B_j)}{\partial\rho_n^{\mathrm{ps}}}\frac{\partial\rho_n^{\mathrm{ps}}}{\omega_0} + \frac{\partial(\delta B_j)}{\partial\rho_p^{\mathrm{ps}}}\frac{\partial\rho_p^{\mathrm{ps}}}{\omega_0} + \frac{\partial(\delta B_j)}{\partial\rho_\Lambda^{\mathrm{ps}}}\frac{\partial\rho_\Lambda^{\mathrm{ps}}}{\omega_0}\right] \end{aligned} \tag{3.56}$$

$$\begin{aligned} m^2_{\rho,\mathrm{eff}}\rho_{03} &= g_{\rho N}\left[\sum_b I_{3b}\rho_b + \sum_\Delta I_{3\Delta}\rho_\Delta + \sum_i I_{3i}\rho_i + \sum_j I_{3j}\rho_j\right] \\ &- \sum_{\substack{i={}^2\mathrm{H},{}^3\mathrm{H},{}^3\mathrm{He},\\ {}^4\mathrm{He},{}^6\mathrm{He}}} \rho_i^s \left[\frac{\partial(\delta B_i)}{\partial\rho_n^{\mathrm{ps}}}\frac{\partial\rho_n^{\mathrm{ps}}}{\rho_{03}} + \frac{\partial(\delta B_i)}{\partial\rho_p^{\mathrm{ps}}}\frac{\partial\rho_p^{\mathrm{ps}}}{\rho_{03}}\right] \\ &- \sum_{j={}^3_\Lambda\mathrm{H},{}^4_\Lambda\mathrm{H},{}^4_\Lambda\mathrm{He}} \rho_j^s \left[\frac{\partial(\delta B_j)}{\partial\rho_n^{\mathrm{ps}}}\frac{\partial\rho_n^{\mathrm{ps}}}{\rho_{03}} + \frac{\partial(\delta B_j)}{\partial\rho_p^{\mathrm{ps}}}\frac{\partial\rho_p^{\mathrm{ps}}}{\rho_{03}} + \frac{\partial(\delta B_j)}{\partial\rho_\Lambda^{\mathrm{ps}}}\frac{\partial\rho_\Lambda^{\mathrm{ps}}}{\rho_{03}}\right] \end{aligned} \tag{3.57}$$

$$\begin{aligned} m^2_{\phi}\phi_0 &= \sum_b g_{\phi b}\rho_b + \sum_j g_{\phi j}\rho_j \\ &- \sum_{\substack{i={}^2\mathrm{H},{}^3\mathrm{H},{}^3\mathrm{He},\\ {}^4\mathrm{He},{}^6\mathrm{He}}} \rho_i^s \left[\frac{\partial(\delta B_i)}{\partial\rho_n^{\mathrm{ps}}}\frac{\partial\rho_n^{\mathrm{ps}}}{\phi_0} + \frac{\partial(\delta B_i)}{\partial\rho_p^{\mathrm{ps}}}\frac{\partial\rho_p^{\mathrm{ps}}}{\phi_0}\right] \\ &- \sum_{j={}^3_\Lambda\mathrm{H},{}^4_\Lambda\mathrm{H},{}^4_\Lambda\mathrm{He}} \rho_j^s \left[\frac{\partial(\delta B_j)}{\partial\rho_n^{\mathrm{ps}}}\frac{\partial\rho_n^{\mathrm{ps}}}{\phi_0} + \frac{\partial(\delta B_j)}{\partial\rho_p^{\mathrm{ps}}}\frac{\partial\rho_p^{\mathrm{ps}}}{\phi_0} + \frac{\partial(\delta B_j)}{\partial\rho_\Lambda^{\mathrm{ps}}}\frac{\partial\rho_\Lambda^{\mathrm{ps}}}{\phi_0}\right] \end{aligned} \tag{3.58}$$

Taking the results derived in Appendix A.1 and A.2, the equations of motion for the ω, ρ and ϕ mesons read:

$$\begin{aligned} m^2_{\omega,\mathrm{eff}}\omega_0 &= \sum_b g_{\omega b}\rho_b + \sum_\Delta g_{\omega\Delta}\rho_\Delta + \sum_i g_{\omega i}\rho_i + \sum_j g_{\omega j}\rho_j \\ &-\frac{1}{\rho_0}\left(\frac{m_\omega^2}{2g_{\omega N}}\right)\left(\rho^s_{{}^2\mathrm{H}} + \rho^s_{{}^3\mathrm{H}} + \rho^s_{{}^3\mathrm{He}} + 2\rho^s_{{}^4\mathrm{He}} + 2\rho^s_{{}^6\mathrm{He}}\right. \\ &\left.+\rho^s_{{}^3_\Lambda\mathrm{H}} + \rho^s_{{}^4_\Lambda\mathrm{H}} + \rho^s_{{}^4_\Lambda\mathrm{He}}\right)\left[\frac{\partial\epsilon_n^*}{\partial\rho_n^{\mathrm{ps}}} - \frac{m\partial\rho_n^*}{\partial\rho_n^{\mathrm{ps}}} + \frac{\partial\epsilon_p^*}{\partial\rho_p^{\mathrm{ps}}} - \frac{m\partial\rho_p^*}{\partial\rho_p^{\mathrm{ps}}}\right] \\ &-\frac{1}{\rho_0}\left(\frac{m_\omega^2}{2g_{\omega N}}\right)\left(\rho^s_{{}^3\mathrm{H}} + 2\rho^s_{{}^6\mathrm{He}} + \rho^s_{{}^4_\Lambda\mathrm{H}}\right)\left[\frac{\partial\epsilon_n^*}{\partial\rho_n^{\mathrm{ps}}} - \frac{m\partial\rho_n^*}{\partial\rho_n^{\mathrm{ps}}}\right] \end{aligned} \tag{3.59}$$

$$
\begin{aligned}
& -\frac{1}{\rho_0}\left(\frac{m_\omega^2}{2g_{\omega N}}\right)\left(\rho^s_{^3\mathrm{He}}+\rho^s_{^4_\Lambda\mathrm{He}}\right)\left[\frac{\partial\epsilon_p^*}{\partial\rho_p^{\mathrm{ps}}}-\frac{m\partial\rho_p^*}{\partial\rho_p^{\mathrm{ps}}}\right] \\
m^2_{\rho,\mathrm{eff}}\rho_{03} &= g_{\rho N}\left[\sum_b I_{3b}\rho_b+\sum_\Delta I_{3\Delta}\rho_\Delta+\sum_i I_{3i}\rho_i+\sum_j I_{3j}\rho_j\right] \\
& -\frac{1}{\rho_0}\left(\frac{m_\rho^2}{g_{\rho N}}\right)\left(\rho^s_{^2\mathrm{H}}+\rho^s_{^3\mathrm{H}}+\rho^s_{^3\mathrm{He}}+2\rho^s_{^4\mathrm{He}}+2\rho^s_{^6\mathrm{He}}\right. \\
& \left.+\rho^s_{^3_\Lambda\mathrm{H}}+\rho^s_{^4_\Lambda\mathrm{H}}+\rho^s_{^4_\Lambda\mathrm{He}}\right)\left[-\frac{\partial\epsilon_n^*}{\partial\rho_n^{\mathrm{ps}}}+\frac{m\partial\rho_n^*}{\partial\rho_n^{\mathrm{ps}}}+\frac{\partial\epsilon_p^*}{\partial\rho_p^{\mathrm{ps}}}-\frac{m\partial\rho_p^*}{\partial\rho_p^{\mathrm{ps}}}\right] \\
& -\frac{1}{\rho_0}\left(\frac{m_\rho^2}{g_{\rho N}}\right)\left(\rho^s_{^3\mathrm{H}}+2\rho^s_{^6\mathrm{He}}+\rho^s_{^4_\Lambda\mathrm{H}}\right)\left[-\frac{\partial\epsilon_n^*}{\partial\rho_n^{\mathrm{ps}}}+\frac{m\partial\rho_n^*}{\partial\rho_n^{\mathrm{ps}}}\right] \\
& -\frac{1}{\rho_0}\left(\frac{m_\rho^2}{g_{\rho N}}\right)\left(\rho^s_{^3\mathrm{He}}+\rho^s_{^4_\Lambda\mathrm{He}}\right)\left[\frac{\partial\epsilon_p^*}{\partial\rho_p^{\mathrm{ps}}}-\frac{m\partial\rho_p^*}{\partial\rho_p^{\mathrm{ps}}}\right]
\end{aligned}
\tag{3.60}
$$

$$
\begin{aligned}
m^2_\phi\phi_0 &= \sum_b g_{\phi b}\rho_b+\sum_j g_{\phi j}\rho_j \\
& +\frac{1}{\rho_0}\left(\frac{g_{\omega\Lambda}m_\phi^2}{2g_{\omega N}g_{\phi\Lambda}}\right)\left(\rho^s_{^2\mathrm{H}}+\rho^s_{^3\mathrm{H}}+\rho^s_{^3\mathrm{He}}+2\rho^s_{^4\mathrm{He}}+2\rho^s_{^6\mathrm{He}}\right. \\
& \left.+\rho^s_{^3_\Lambda\mathrm{H}}+\rho^s_{^4_\Lambda\mathrm{H}}+\rho^s_{^4_\Lambda\mathrm{He}}\right)\left[\frac{\partial\epsilon_n^*}{\partial\rho_n^{\mathrm{ps}}}-\frac{m\partial\rho_n^*}{\partial\rho_n^{\mathrm{ps}}}+\frac{\partial\epsilon_p^*}{\partial\rho_p^{\mathrm{ps}}}-\frac{m\partial\rho_p^*}{\partial\rho_p^{\mathrm{ps}}}\right] \\
& +\frac{1}{\rho_0}\left(\frac{g_{\omega\Lambda}m_\phi^2}{2g_{\omega N}g_{\phi\Lambda}}\right)\left(\rho^s_{^3\mathrm{H}}+2\rho^s_{^6\mathrm{He}}+\rho^s_{^4_\Lambda\mathrm{H}}\right)\left[\frac{\partial\epsilon_n^*}{\partial\rho_n^{\mathrm{ps}}}-\frac{m\partial\rho_n^*}{\partial\rho_n^{\mathrm{ps}}}\right] \\
& +\frac{1}{\rho_0}\left(\frac{g_{\omega\Lambda}m_\phi^2}{2g_{\omega N}g_{\phi\Lambda}}\right)\left(\rho^s_{^3\mathrm{He}}+\rho^s_{^4_\Lambda\mathrm{He}}\right)\left[\frac{\partial\epsilon_p^*}{\partial\rho_p^{\mathrm{ps}}}-\frac{m\partial\rho_p^*}{\partial\rho_p^{\mathrm{ps}}}\right] \\
& -\frac{1}{\rho_0}\left(\frac{m_\phi^2}{g_{\phi\Lambda}}\right)\left(\rho^s_{^3_\Lambda\mathrm{H}}+\rho^s_{^4_\Lambda\mathrm{H}}+\rho^s_{^4_\Lambda\mathrm{He}}\right)\left[\frac{\partial\epsilon_\Lambda^*}{\partial\rho_\Lambda^{\mathrm{ps}}}-\frac{m_\Lambda\partial\rho_\Lambda^*}{\partial\rho_\Lambda^{\mathrm{ps}}}\right]
\end{aligned}
\tag{3.61}
$$

Once again, the only modification in the equation of motion for the σ meson in relation to Eq.(2.53) will be an additional term for the light cluster and hypercluster scalar densities:

$$
m_\sigma^2\sigma+\frac{\kappa}{2}g_{\sigma N}^3\sigma^2+\frac{\lambda}{3!}g_{\sigma N}^4\sigma^3 = \sum_{c=b,\Delta,i,j} g_{\sigma c}\rho_c^s\ . \tag{3.62}
$$

The five purely nucleonic light clusters will have equations of motion equal to the ones derived in Section 3.1.3. Similarly, the equation of motion of the fermionic spin-1/2 hypercluster $j={}^3_\Lambda\mathrm{H}$ takes the form of a Dirac equation:

$$
\left[\gamma_\mu iD_j^\mu-M_j^*\right]\Psi_j=0\ ,\ j={}^3\mathrm{H},{}^3\mathrm{He} \tag{3.63}
$$

whereas for the bosonic spin-0 hyperclusters ($j={}^4_\Lambda\mathrm{H},\ {}^4_\Lambda\mathrm{He}$) the equation of motion corresponds to a Klein Gordon equation:

$$
\left[-iD_j^\mu iD_{\mu j}+M_j^{*2}\right]\Psi_j=0\ ,\ j={}^4_\Lambda\mathrm{H},{}^4_\Lambda\mathrm{He}\ . \tag{3.64}
$$

The baryonic ρ_c and scalar ρ_c^s densities ($c=b,\Delta,i,j$) for finite temperatures present in

Eqs.(3.56)-(3.62) are once again obtained through a similar process to the one derived in Section 2.1.5:

$$\rho_c = \frac{(2J_c+1)}{2\pi^2}\int_0^\infty k^2 dk[f_{k+} - f_{k-}] \tag{3.65}$$

$$\rho_c^s = \frac{(2J_c+1)}{2\pi^2}\int_0^\infty \frac{m_c^*}{\sqrt{k^2+m_c^{*2}}} k^2 dk[f_{k+} + f_{k-}] \ . \tag{3.66}$$

3.2.4 Charge Fraction with Hyperclusters

The hyperclusters will also contribute to the total charge fraction Y_Q of the system. Thus, Eq.(3.29) now reads

$$Y_Q = \sum_b q_b Y_b + \sum_\Delta q_\Delta Y_\Delta + \sum_i \frac{q_i}{A_i} Y_i + \sum_j \frac{q_j}{A_j} Y_j \tag{3.67}$$

where q_j is the electric charge (in units of $+e$) of light hypercluster j. The mass fraction Y_j of hypercluster j is given in a similar way to the light cluster mass fraction (Eq.(3.32)):

$$Y_j = A_j \frac{\rho_j}{n_B} \ . \tag{3.68}$$

3.2.5 Hyperclusters Chemical Potentials

The chemical potential of an hypercluster j can be defined in a similar way to what was done for the light clusters in Section 3.1.5. The only difference is that now we also need to consider the chemical potential of the Λ hyperon, μ_Λ. The hypercluster chemical potential is then written as:

$$\mu_j = N_j \mu_n + Z_j \mu_p + \Lambda_j \mu_\Lambda \ . \tag{3.69}$$

Their effective chemical potential μ_j^* follows

$$\mu_j^* = \mu_j - g_{\omega j}\omega_0 - g_{\rho j} I_{3j} \rho_{03} - g_{\phi c}\phi_0 \ . \tag{3.70}$$

3.2.6 Equation of State with Light Clusters and Hyperclusters

Following the same method used in Sections 2.1.7 and 3.1.6, the energy density of a system with the baryonic octet ($b = \Lambda, \Sigma^{-,0,+}, \Xi^{-,0}$), Δ isobars ($\Delta = \Delta^{-,0,+,++}$), the five purely nucleonic light clusters ($i = {}^2$H, ^{3}H, ^{3}He, ^{4}He, ^{6}He) and the three hyperclusters ($j = {}^3_\Lambda$H, ${}^4_\Lambda$H, ${}^4_\Lambda$He) reads

$$\epsilon = \sum_{c=b,\Delta,i,j} \left[\frac{2J_c+1}{2\pi^2}\int_0^{k_{F,c}} k^2\sqrt{k^2+m_c^{*2}}dk + g_{\omega c}\omega_0\rho_c \right. \tag{3.71}$$
$$\left. + g_{\rho c}\rho_{03} I_{3c}\rho_c + g_{\phi c}\phi_0\rho_c \right] - \mathcal{L}_{RMF}$$

whereas the pressure is

$$p = \frac{1}{3}\sum_{c=b,\Delta,i,j} \frac{2J_c+1}{2\pi^2}\int_0^{k_{F,c}} \frac{k^4 dk}{\sqrt{k^2+m_c^{*2}}} + \mathcal{L}_{RMF} \ . \tag{3.72}$$

3.3 Density Dependent RMF Models with Light Clusters and Hyperclusters

We will now take a look to the differences in the description of a system with light clusters and hyperclusters with a density-dependent RMF model when compared to a nonlinear one.

3.3.1 Lagrangian Density

The Lagrangian densities for the the mesonic fields, $\mathcal{L}_m$, the baryonic octet, $\mathcal{L}_b$, and the Δ isobars, $\mathcal{L}_\Delta$, are the same as Eqs.(2.85),(2.86),(2.87), respectively.

The Lagrangian densities of the light clusters and hyperclusters will also be the same as the ones derived in Eqs.(3.2),(3.3),(3.5) and Eqs.(3.37),(3.38), respectively. The only difference is that now their couplings will also depend on the density of the system, which means that they will be functionals of the operator ϱ: $g_{mi} = g_{mi}(\varrho)$; $g_{mj} = g_{mj}(\varrho)$. In practice, the density dependence of the cluster couplings will be considered to be the same as the nucleon density dependence defined in Eqs.(2.88) and (2.89), since the cluster couplings are written in function of the nucleons. Therefore, in the RMF approximation, the operator ϱ has the contribution of all particles included in the Lagrangian density and reduces to the total baryonic density:

$$\varrho = \sum_{c=b,\Delta,i,j} \rho_c \ . \tag{3.73}$$

The equations of motion for the meson fields will be similar to the ones in Section 3.2.3, except that now we no longer have the nonlinear terms and the couplings are density-dependent. Their expressions are given in Appendix A.3.

As for the baryonic octet, Δ isobars, light clusters and hyperclusters, their equations of motion will suffer modifications resulting from the fact that their couplings now depend on the total baryonic density ϱ. Then, following a similar process to Section 2.2.2, but now also for clusters and hyperclusters, their equations of motion will be modified by a rearrangement term that now takes the following form [41]:

$$\Sigma_0^R = \sum_{c=b,\Delta,i,j} \Big(\frac{\partial g_{\omega c}}{\partial \varrho} \omega_0 \rho_c + I_{3c} \frac{\partial g_{\rho c}}{\partial \varrho} \rho_{03} \rho_c + \frac{\partial g_{\phi c}}{\partial \varrho} \phi_0 \rho_c - \frac{\partial g_{\sigma c}}{\partial \varrho} \sigma \rho_c^s \Big) \ . \tag{3.74}$$

3.3.2 Chemical potentials

The chemical potentials for the baryonic octet and Δ isobars are equal to the ones presented in Section 2.2.4, except that now the rearrangement term is given by (3.74). As for the light clusters and hyperclusters, their chemical potentials are written in terms of the nucleons as discussed previously in Sections 3.1.5 and 3.2.5. Thus, the effective chemical potential μ_c^* of any particle $c = b, \Delta, i, j$ present in our system is written in terms of its chemical potential μ_c as:

$$\mu_c^* = \mu_c - g_{\omega c}\omega_0 - g_{\phi c}\phi_0 - g_{\rho c} I_{3c} \rho_{03} - A_c \Sigma_0^R \ . \tag{3.75}$$

3.3.3 Equation of State

The energy density is now given by:

$$\epsilon = \sum_{c=b,\Delta,i,j} \left[\frac{2J_c+1}{2\pi^2} \int_0^{k_{F,c}} k^2 \sqrt{k^2 + m_c^{*2}} dk + g_{\omega c}\omega_0\rho_c \right. \\ \left. + g_{\rho c}\rho_{03} I_{3c}\rho_c + g_{\phi c}\phi_0\rho_c + \Sigma_0^R \rho_c \right] - \mathcal{L}_{RMF} \tag{3.76}$$

whereas the pressure is

$$p = \frac{1}{3} \sum_{c=b,\Delta,i,j} \frac{2J_c+1}{2\pi^2} \int_0^{k_{F,c}} \frac{k^4 dk}{\sqrt{k^2 + m_c^{*2}}} + \mathcal{L}_{RMF} \ , \tag{3.77}$$

with $\mathcal{L}_{RFM}$ now being:

$$\mathcal{L}_{RMF} = -\frac{1}{2} m_\sigma^2 \sigma^2 + \frac{1}{2} m_\omega^2 \omega_0^2 + \frac{1}{2} m_\rho^2 \rho_{03}^2 + \frac{1}{2} m_\phi^2 \phi_0^2 + \sum_{c=b,\Delta,i,j} \Sigma_0^R \rho_c \ . \tag{3.78}$$

Chapter 4

Results and Discussion

In this chapter we discuss the results obtained, mainly focusing on how the presence of light clusters affects the abundances of heavy baryons, and vice-versa, at low densities and temperatures $T \lesssim 50$ MeV, and two different charge fractions, $Y_Q = 0.1$ and 0.3.

Above the critical temperature, $T_c \approx 15$ MeV, we do not expect the presence of heavy clusters, so we consider 5 purely nucleonic light nuclei, ^{2}H, ^{3}H, ^{3}He, ^{4}He and ^{6}He, which were measured by INDRA [13], and three light hypernuclei ${}^3_\Lambda$H, ${}^4_\Lambda$H, ${}^4_\Lambda$He.

This chapter is divided as follows: In the first section we present the RMF models (DD2 [37], DDME2 [42], FSU2H [43, 44] and TM1e [45, 46]) used in this work as well as the values of the couplings for the hyperons and Δ isobars. In the second section, we consider a system made up only of nuclear matter (unbound protons and neutrons) as well as the 5 purely nucleonic light clusters, ^{2}H, ^{3}H, ^{3}He, ^{4}He and ^{6}He. In the third section, we add six hyperons, Λ, $\Sigma^{-,0,+}$, $\Xi^{-,0}$ to the system considered in the second section. In the fourth section we include three hyperclusters, ${}^3_\Lambda$H, ${}^4_\Lambda$H, ${}^4_\Lambda$He, in the system considered in the third section. Finally, in the fifth section we introduce the Δ particles and study the Δ couplings values which correspond to valid EoSs, that is EoSs that are able to reproduce $\sim 2M_\odot$ stars. We analyze the effect of these particles in the systems considered in the second, third and fourth sections. In the second, third and fourth sections, the calculations are performed only for the DD2 model, whereas in the fifth section we also consider the DDME2, FSU2H and TM1e RMF models.

Model	n_0	B/A	K	$E_{\rm sym}$	L	m_N^*/m_N
DD2	0.149	−16.02	243	32.7	58	0.56
DDME2	0.152	−16.14	251	32.3	51	0.57
FSU2H	0.1505	−16.28	238	30.5	44.5	0.593
TM1e	0.145	−16.26	281.16	31.38	40	0.63

Table 4.1: A few symmetric nuclear matter properties for the models used in this work, calculated at saturation density, n_0: the binding energy per particle B/A, the incompressibility K , the symmetry energy $E_{\rm sym}$, the slope of the symmetry energy L, and the nucleon effective mass m_N^*. All quantities are in MeV, except for n_0 that is given in fm^{-3}, and for the effective nucleon mass that is normalized to the nucleon mass m_N.

4.1 EoS RMF Models

In this work, we will use four different relativistic effective interactions. Two of them belong to the class of density-dependent models (DD2 [37] and DDME2 [42]) whereas the other two correspond to nonlinear models (FSU2H [43, 44] and TM1e [45, 46]). These models have been calibrated to properties of nuclei and nuclear matter. In Table 4.1 we show some symmetric nuclear matter properties for the four models, calculated at saturation density, n_0.

All four models used in this work were chosen because they satisfy a set of up to date experimental constraints regarding both astronomical measurements (e.g NS mass) as well as microscopic measurements (e.g. properties of nuclei and nuclear matter). In fact, as explained in Ref. [47], DD2 [37] was built as a result of a fitting to nuclei properties. Similarly, properties of symmetric and asymmetric nuclear matter, binding energies, charge radii, and neutron radii of spherical nuclei are reproduced by DDME2 [42]. In the case of FSU2H [43, 44] it reproduces properties of finite nuclei, satisfies constraints from kaon production and collective flow in HIC and is able to predict pressures of neutron star matter consistent with effective chiral forces. Moreover, its symmetry energy and slope are in good accordance with experimental predictions as well as its neutron skin thickness which is in line with experiments for ^{208}Pb and ^{48}Ca and for the electric dipole polarizability of nuclei. Finally the TM1e [45, 46], is also able to describe finite nuclei and provides radii in the range of those defined by NICER latest observations [48]. Furthermore, its symmetry energy and slope are compatible with astrophysical measurements and terrestrial nuclear experiments [49–51]. All four models are able to reproduce $2M_\odot$ stars.

The values of the parameters used to define the Lagrangian densities of the previous chapters can be found in Table 4.2 for all models.

The coupling constants g_{mN} of the nucleons ($N = n, p$) to the σ, ω and ρ mesons are given in Table 4.2. In the case of density-dependent models, these couplings are yet modified to include the density dependence as defined in Eqs.(2.88) and (2.89).

The values of the couplings of the hyperons and Δ particles to the mesons are not shown in Table 4.2. We will take a closer look at them in the next subsections.

4.1.1 Hyperon Coupling Constants

When it comes to the hyperons ($\Lambda, \Sigma^-, \Sigma^0, \Sigma^+, \Xi^-, \Xi^0$), their coupling parameters g_{mb} can be defined in terms of the nucleon couplings as

$$g_{mb} \;=\; R_{mb} g_{mN} \;,\; m = \sigma, \omega, \rho \tag{4.1}$$

	DD2	DDME2	FSU2H	TM1e
m_σ(MeV)	546.212459	550.1238	497.479	511.198
m_ω(MeV)	783.000	783.000	782.500	783.000
m_ϕ(MeV)	1020.000	1020.000	1020.000	1020.000
m_ρ(MeV)	763.000	763.000	763.000	770.000
$g_{\sigma N}$	10.686681	10.5396	10.135087567	10.0289
$g_{\omega N}$	13.342362	13.0189	13.02042626	12.6139
$g_{\rho N}$	7.25388	7.3672	14.045255427	13.9714
κ(MeV)	–	–	4.0014	2.829729793
λ	–	–	−0.013298	0.000366722
ζ	–	–	0.008	0.016900086
Λ_ω	–	–	0.045	0.0429
a_σ	1.357630	1.3881	–	–
b_σ	0.634442	1.0943	–	–
c_σ	1.005358	1.7057	–	–
d_σ	0.575810	0.4421	–	–
a_ω	1.369718	1.3892	–	–
b_ω	0.496475	0.9240	–	–
c_ω	0.817753	1.4620	–	–
d_ω	0.638452	0.4775	–	–
a_ρ	0.518903	0.5647	–	–

Table 4.2: Parameter sets for the four models considered in this work.

b	$R_{\omega b}$	$R_{\phi b}$	$R_{\rho b}$
Λ	2/3	$-\sqrt{2}/3$	1
Σ	2/3	$-\sqrt{2}/3$	1
Ξ	1/3	$-2\sqrt{2}/3$	1

Table 4.3: Coupling constants of the ω, ϕ and ρ to the different hyperons, normalized to the respective meson nucleon coupling, i.e. $R_{mb} = g_{mb}/g_{mN}$, except for the $\phi-$meson where $g_{\omega N}$ is used for normalisation. These couplings were fixed using the SU(6) quark model as described in Ref. [52] and are common to all four models considered in this work.

$$g_{mb} \;=\; R_{mb} g_{\omega N} \;,\; m = \phi \;. \tag{4.2}$$

The factors R_{mb} correspond to the ratio between the coupling of hyperon b to meson m and the coupling of the nucleons to meson m. To fix the values of these ratios for the ω and ϕ mesons, we will use the SU(6) quark model described in Ref. [52]. We will consider the "ideal mixing" scenario in which the nucleons do not couple to the ϕ meson ($g_{\phi N} = 0$). That is why in Eq.(4.2) the couplings to the ϕ meson were defined in terms of the nucleon coupling to the ω meson. The couplings of the hyperons to the ρ meson are taken to be equal to the nucleons. Concerning this coupling, what differentiates each hyperon is simply their isospin projection. The values for the ratios R_{mb} for $m = \omega, \phi, \rho$ can be found in Table 4.3 and are the same for the four models considered here.

Once the couplings of the vector mesons to the hyperons are fixed by the SU(6) symmetry, the couplings of the σ meson to the hyperons are usually obtained by defining the value of the

$R_{\sigma b}$	DD2	DDME2	FSU2H	TM1e
$R_{\sigma\Lambda}$	0.621	0.621	0.620	0.621
$R_{\sigma\Sigma}$	0.474	0.468	0.452	0.446
$R_{\sigma\Xi}$	0.320	0.320	0.310	0.310

Table 4.4: Coupling constants of the σ meson to the different hyperons, normalized to the σ meson nucleon coupling, i.e. $R_{\sigma b} = g_{\sigma b}/g_{\sigma N}$, for the four models considered in this work.

hyperon potential in symmetric nuclear matter, U_b^N, at saturation density (n_0) as [29]

$$U_b^N(n_0) = -(g_{\sigma b} + g_{\sigma b}^{'}\rho_s)\sigma + (g_{\omega b} + g_{\omega b}^{'}n_0)\omega_0 \ , \tag{4.3}$$

where ρ_s is the scalar density and $g_{mb}^{'}$ ($m = \sigma, \omega$) is the derivative of $g_{\omega b}$ with respect to the density ($g_{mb}^{'}$ are zero for the nonlinear models).

This was the method followed do derive the couplings of the Σ hyperon to the σ meson. In fact, according to Ref. [53] the Σ potential in symmetric nuclear matter lies in the range $U_\Sigma^{(N)}(n_0) \approx 30 \pm 20$ MeV. We then chose to fix $U_\Sigma^{(N)}(n_0) = 30$ MeV as an intermediate value and calculate the couplings for the four models using Eq.(4.3). The values of the couplings can be found in Table 4.4.

As for the σ couplings to the Λ and Ξ hyperons, the approach followed was different from the one just described for the Σ hyperon. Instead of imposing a symmetric nuclear matter potential, the couplings were calibrated by fitting the experimental binding energy of Λ and Ξ hypernuclei as in Refs. [29, 54]. For the DD2 and DDME2 models, the couplings of the Λ and Ξ hyperons were taken to be the same as the DDME2D-a model in Ref. [29] and the DDME2 model in [54], respectively. For the FSU2H model, the coupling of the Λ was taken from the FSU2H-a model in Ref. [55] and the Ξ coupling from Ref. [54]. Finally for the TM1e model, the coupling of the Λ was taken to be the same as TM1-a from Ref. [29] whereas the Ξ coupling was taken as the TM1 coupling from Ref. [54]. All couplings of the σ meson to the hyperons can be found in Table 4.4.

4.1.2 Δ Coupling Constants

Similarly to what we have done for the hyperons, we can write the couplings of the Δ isobars to the mesons, $g_{m\Delta}$, in terms of the nucleon couplings as:

$$g_{m\Delta} = x_{m\Delta}\ g_{mN} \ , \ m = \sigma, \omega, \rho \ , \tag{4.4}$$

with $x_{m\Delta}$ being the ratio between the Δ and nucleon couplings to the mesons.

Unfortunately, due to limited experimental observations, the couplings of the Δs to the mesons are still poorly constrained. However, some phenomenological analyses from pion-nucleus scattering [56], electron scattering on nuclei [57] and electromagnetic excitations of the Δ isobars [58] have set the following constraints on the values of the couplings, as summarized in Ref. [59]:

- the Δ potential in nuclear matter is a little more attractive than the nucleon potential which means that the ratio $x_{\sigma\Delta}$ should be slightly above 1;
- $x_{\sigma\Delta}$ is never less than $x_{\omega\Delta}$:

$$0 \lesssim x_{\sigma\Delta} - x_{\omega\Delta} \lesssim 0.2 \ ; \tag{4.5}$$

- there is no experimental constraints on $x_{\rho\Delta}$.

As we can see from these three points, even though it is possible to derive some constraints on the Δ couplings, there are still large uncertainties to be accounted for.

In previous works from other authors [28, 59–61], these uncertainties were accounted for by allowing the couplings to vary within a large interval of values. For example, in [28], the couplings used were: $0.8 \leq x_{\sigma\Delta},\ x_{\omega\Delta} \leq 1.2$ and $0 \leq x_{\rho\Delta} \leq 2$. Here we will adopt the following intervals that will be discuss later:

$$0.9 \leq \quad x_{\sigma\Delta} \quad \leq 1.2 \tag{4.6}$$

$$0.9 \leq \quad x_{\omega\Delta} \quad \leq 1.2 \tag{4.7}$$

$$0.8 \leq \quad x_{\rho\Delta} \quad \leq 2\ . \tag{4.8}$$

Instead of starting at 0.8, we start the intervals of $x_{\sigma\Delta}$ and $x_{\omega\Delta}$ at 0.9, since as we will see in Section 4.5.1 at $x_{\sigma\Delta},\ x_{\omega\Delta} = 0.9$ we already have some problems related to the nucleon effective mass, which only become worse at lower values of $x_{\sigma\Delta}$ and $x_{\omega\Delta}$. In the case of $x_{\rho\Delta}$, we start at 0.8 because the interaction is definitely dependent on the isospin so it cannot be zero. It is worth mentioning that these intervals are somewhat exploratory in the sense that we do not really know which values are correct and so we will choose several combinations within the above intervals and will analyze what differences arise in the description of NS EoSs.

4.2 Nuclear Matter with Light Clusters

In Eq.(3.10) we have introduced the fraction x_s of the scalar meson-cluster coupling whose purpose was to account for the correlations in the σ-cluster coupling. In Ref. [26], this x_s fraction was calibrated to the equilibrium constants obtained in [13] for different RMF models. For the density-dependent DD2 RMF model, the value obtained was $x_s = 0.93 \pm 0.02$. This range of values is going to be used throughout this work for the DD2 RMF model.

We consider the system described in Sections 3.1 and 3.3 but now only for unbound protons and neutrons and the five purely nucleonic light clusters, ^{2}H, ^{3}H, ^{3}He, ^{4}He and ^{6}He.

In Fig. 4.1, we plot the mass fractions of light clusters (^{2}H, ^{3}H, ^{3}He, ^{4}He and ^{6}He) and unbound protons and neutrons in equilibrium as a function of density for two temperatures $T = 10$ MeV (top) and 30 MeV (bottom) and two different values of the charge fraction $Y_Q = 0.3$ (left) and 0.1 (right). The bands take into account the uncertainty on x_s, and mainly affect the maximum of the fractions and the dissolution density. For the low densities and high temperatures, it is the mass that determines the most abundant light cluster, and the smaller the mass the larger the abundance. For $T = 10$ MeV, the most abundant cluster at the maximum fraction is ^{3}H, reflecting the isospin asymmetry. In particular, ^{6}He becomes more abundant than ^{3}He for the two charge fractions considered. For this temperature, it is also interesting to observe that even though ^{3}He is less abundant than ^{3}H, ^{4}He or ^{6}He, it dissolves at larger densities than those three (of the five clusters, ^{2}H is the one that dissolves at larger densities). This is an effect of the binding energy shift (δB_i) that depends on the density of unbound neutrons and protons separately. The neutrons, being more abundant, have a stronger effect, and, in particular, affect more the clusters with a larger neutron fraction. At $T = 30$ MeV, it is the mass that defines the largest abundances. In this case, it is ^{2}H that becomes the most abundant light cluster for all densities due to its smaller mass. Moreover, at the maximum of the cluster fractions, their mass

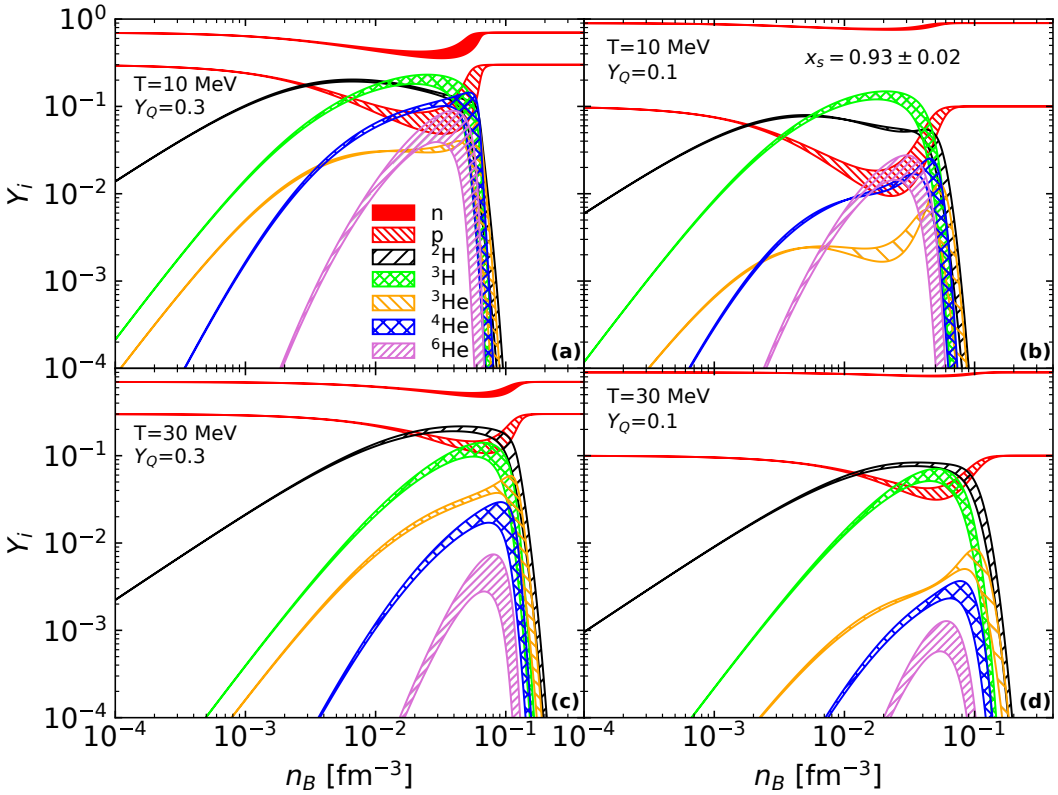

Figure 4.1: Mass fractions of light clusters (^{2}H, ^{3}H, ^{3}He, ^{4}He and ^{6}He) and unbound protons and neutrons in equilibrium are plotted versus the density for $T = 10$ MeV (top) and 30 MeV (bottom) with charge fraction of $Y_Q = 0.3$ (left) and 0.1 (right). The bands take into account the uncertainty on the x_s coupling fraction of the clusters to the σ-meson. The calculation is performed for the DD2 RMF model.

fractions are larger than the proton fraction.

In Fig. 4.2, the mass fractions are again plotted against the density, but this time for two larger temperatures, $T = 50$ and 100 MeV, the last one represented by grey lines to be well distinguished from the $T = 50$ MeV case. As already discussed for $T = 30$ MeV, the relative abundances of the light nuclei are dictated by their masses, the deuteron being the most abundant and ^{6}He the least. The superposition of the distribution for both temperatures shows clearly that an increase of the temperature pushes the light nuclei maxima to larger densities and reduces the abundances of the heavier clusters: only ^{2}H keeps a similar fraction at the maximum. The cluster dissolution shifts to much larger densities for the larger temperature. A reduction of the charge fraction reduces the cluster fractions, such that for $T = 100$ MeV, $Y_Q = 0.1$ the fraction of ^{6}He is always below 10^{-4}.

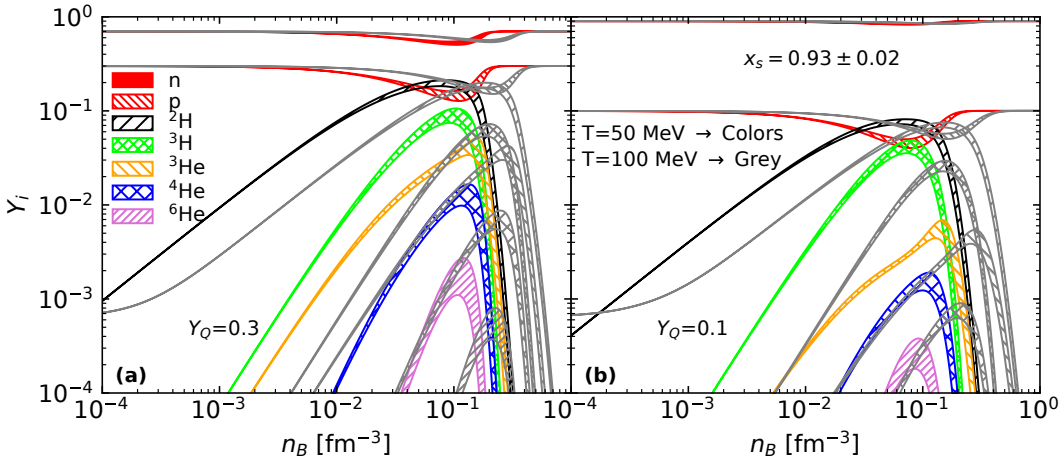

Figure 4.2: Mass fractions of light clusters (^{2}H, ^{3}H, ^{3}He, ^{4}He and ^{6}He) and unbound protons and neutrons in equilibrium are plotted versus the density for $T = 50$ MeV (colored lines) and 100 MeV (grey lines), with a charge fraction of $Y_Q = 0.3$ (left) and 0.1 (right). The bands take into account the uncertainty on the x_s coupling fraction of the clusters to the σ-meson. The calculation is performed for the DD2 RMF model.

4.3 Nuclear Matter with Light Clusters and Hyperons

We now add the six hyperons, Λ, $\Sigma^{-,0,+}$ and $\Xi^{-,0}$, to the system of the previous section, and analyze the impact they have on the abundances of the unbound nucleons (n, p) and nucleonic light clusters.

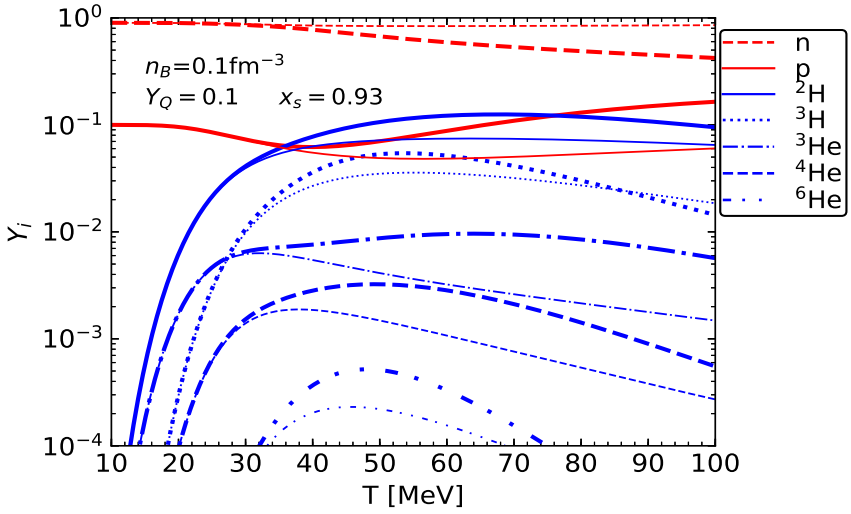

Figure 4.3: Unbound nucleon and light cluster fractions in a calculation with (thick lines) and without (thin lines) hyperons as a function of the temperature for a charge fraction of $Y_Q = 0.1$, and a density of $n_B = 0.1$ fm^{-3}. The scalar cluster-meson coupling is fixed to $x_s = 0.93$ for the DD2 RMF model.

In Fig. 4.3 we show the unbound nucleon and cluster abundances as a function of the temperature for a charge fraction $Y_Q = 0.1$ and a density $n_B = 0.1$ fm^{-3}. This density value was chosen because it is where the fraction of the clusters is close to a maximum in the range of temperatures considered. We also analyze the impact of hyperons by comparing the abundances

in a system with (thick lines) or without (thin lines) hyperons. It is seen that the abundance of the ^{2}H surpasses the one of protons for $25 \lesssim T \lesssim 70$ MeV. It is also above $T = 25$ MeV that the cluster fractions obtained with and without hyperons start differing, and they start being more abundant in the presence of hyperons.

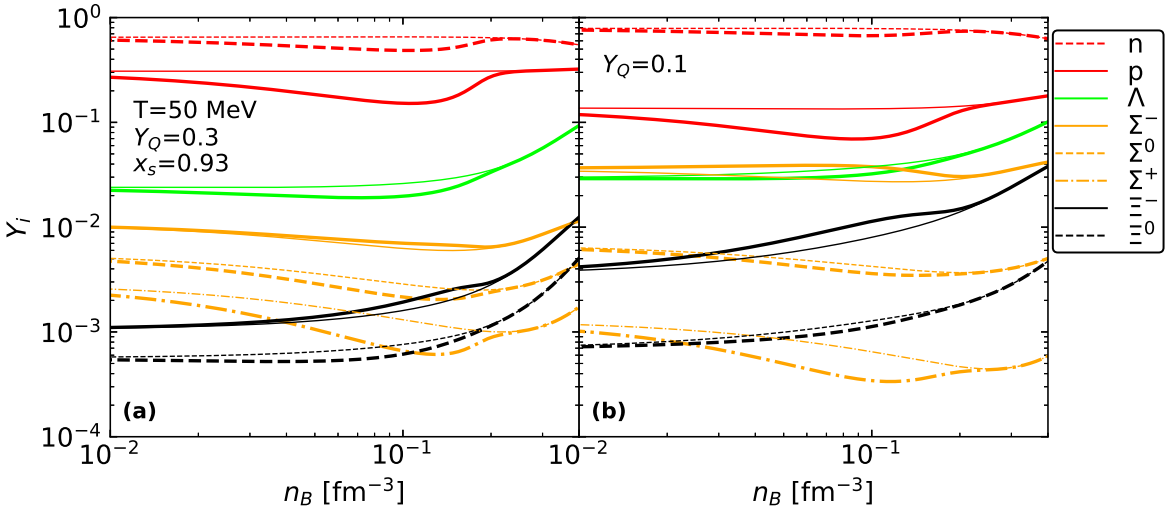

Figure 4.4: Unbound nucleon and hyperon fractions as a function of the density in a calculation with (thick lines) and without (thin lines) light clusters, for a charge fraction of $Y_Q = 0.3$ (left) and 0.1 (right) and $T = 50$ MeV. The scalar cluster-meson coupling fraction is set to $x_s = 0.93$ for the DD2 RMF model.

The effect of the inclusion of light clusters on the hyperon fractions is clearly seen in Fig. 4.4, where the thick lines were obtained including light clusters, while the calculation without clusters is represented by thin lines. The main effect of introducing clusters is a reduction of the unbound nucleons and of the electrically neutral or positive hyperons, while the fraction of the negatively charged hyperons increases. The formation of clusters is energetically favored but these clusters are positively charged, so its formation is compensated by a reduction of the unbound nucleons, together with a reduction (increase) of positively (negatively) charged baryons. A decrease of the neutron fraction also induces a reduction of the other neutral baryons. Moreover, a smaller charge fraction favors the formation of negatively charged baryons, and for $Y_Q = 0.1$, it is seen a clear competition between Σ^- and Λ for the smaller densities. At smaller densities, for a fixed temperature, the hyperon mass defines the abundance, but for larger densities, the magnitude and sign of the hyperonic potential is reflected on the hyperon abundances. In this case, the more attractive interaction between Ξ hyperons and nucleons ($U_\Xi^N = -18.78$ MeV) gives rise to a larger fraction of Ξ hyperons than Σ hyperons ($U_\Sigma^N = +30$ MeV).

The effect of the hyperons on the cluster abundances, which was already seen in Fig. 4.3, and on the dissolution densities is clearly seen in Fig. 4.5. In the left panel, we show the total mass fraction of all the light clusters, defined as

$$Y_{tot} = \sum_i Y_i \ , \ i = {}^2\mathrm{H}, {}^3\mathrm{H}, {}^3\mathrm{He}, {}^4\mathrm{He}, {}^6\mathrm{He} \ , \tag{4.9}$$

with the mass fraction Y_i defined in Eq.(3.32), at $T = 50$ MeV (notice the linear scale on the x-axis contrary to the log-scale used in the previous figures), and in the right panel, the dissolution density of the light clusters, n_d, which was defined as the density for which the light cluster fraction has dropped to 10^{-4}, is displayed. The charge fraction is set to $Y_Q = 0.3$ and 0.1, and

the scalar cluster-meson coupling fraction to $x_s = 0.93$. Two different calculations are compared: a calculation with the full baryonic octet (solid lines); and one excluding hyperons (dashed lines). We can see that when we include hyperons there is an increase in the cluster fraction above the maximum of the cluster distribution, shifting the dissolution density to larger densities. This effect gets stronger as the temperature increases. In fact, the increase of the dissolution density starts to be non-negligible for $T \gtrsim 25 - 30$ MeV. We can also see that the smaller the charge fraction, the stronger the effect. In fact, for $T = 50$ MeV, the main effect is an increase of the dissolution density of the order of 10% if $Y_Q = 0.3$, and 20% for $Y_Q = 0.1$. Since the presence of the hyperons reduces the nucleon fraction, this is reflected on the medium effects felt by the clusters through the binding energy shift that is smaller. This explains why the effect of the hyperons on the clusters is larger for $Y_Q = 0.1$, since, as we saw in Fig. 4.4, a smaller charge fraction corresponds to an overall larger hyperon fraction.

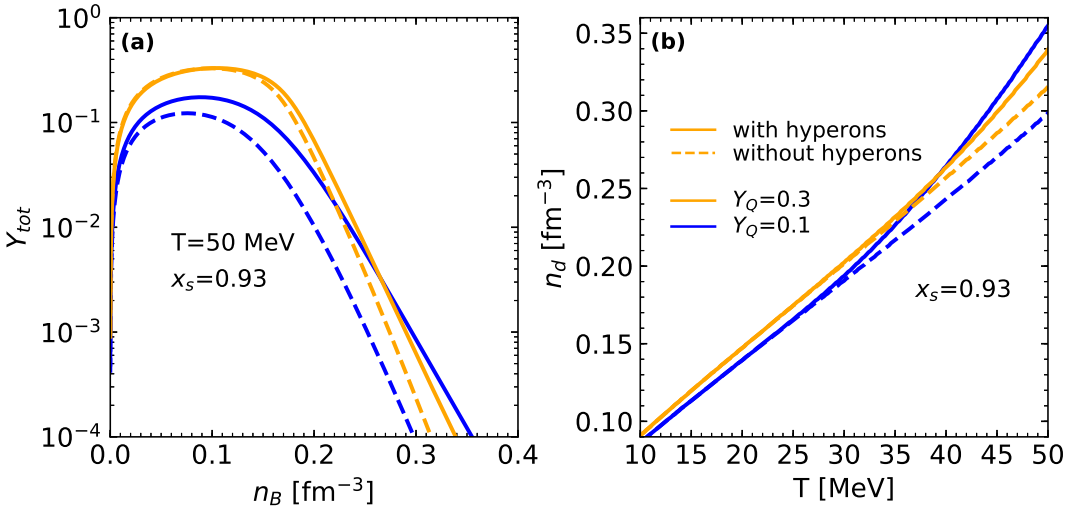

Figure 4.5: Total mass fraction of the light clusters as a function of the density at $T = 50$ MeV (left) and the dissolution density of the clusters, n_d, as a function of the temperature (right) for a calculation with (solid) and without (dashed) hyperons and a charge fraction of $Y_Q = 0.3$ (orange) and 0.1 (blue). The scalar cluster-meson coupling fraction is set to $x_s = 0.93$ for the DD2 RMF model.

4.4 Nuclear Matter with Light Clusters, Hyperons and Hyperclusters

We are now going to study the effect of considering hyperclusters in the system analyzed in the previous section. We will consider the three hyperclusters mentioned before: ${}^{3}_{\Lambda}\mathrm{H}$, known as hypertriton, ${}^{4}_{\Lambda}\mathrm{H}$ (hyperhydrogen 4), and ${}^{4}_{\Lambda}\mathrm{He}$ (hyperhelium 4).

A fraction of hypernuclei above 10^{-4} is only obtained for big enough temperatures, i.e. $T \gtrsim 25$ MeV. For lower temperatures, the abundance of Λ hyperons is still too small to give rise to significant hypercluster fractions. Therefore, in the next two Figures, we consider $T = 50$ MeV.

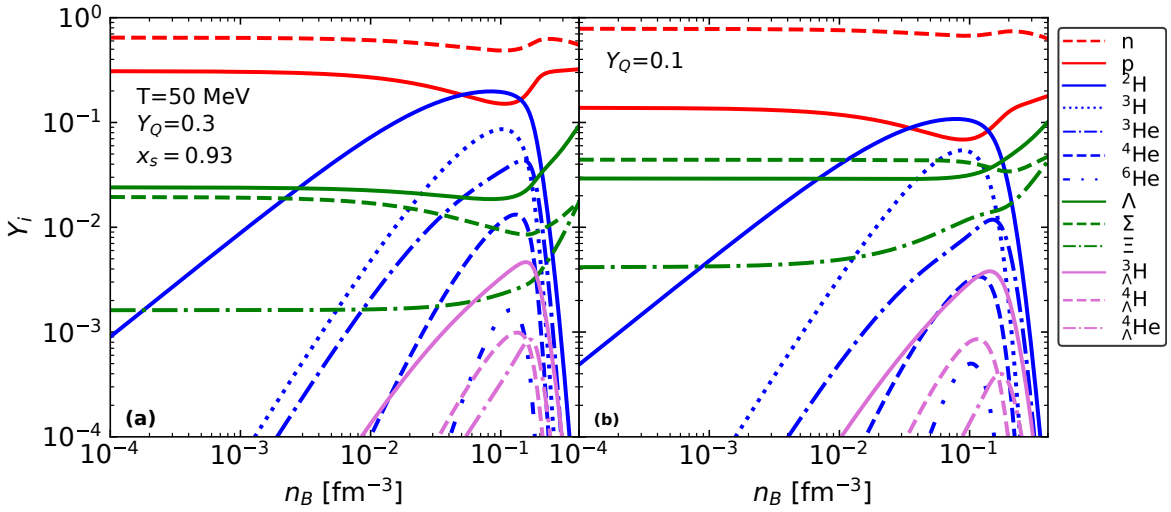

Figure 4.6: Mass fractions of the unbound protons and neutrons (red lines), Λ, Σ and Ξ (green lines), light clusters (blue lines) and light hypernuclei (pink lines) as a function of the density for $T = 50$ MeV and $x_s = 0.93$, with $Y_Q = 0.3$ (left) and 0.1 (right). The calculation is performed for the DD2 RMF model.

In Fig. 4.6, the light nuclei and hypernuclei mass fractions are plotted together with the unbound proton and neutron fractions, the Λ fraction, the total Σ fraction corresponding to the sum of the $\Sigma^{+,0,-}$ fractions, and the total Ξ fraction corresponding to the sum of the $\Xi^{0,-}$ fractions, for a charge fraction of $Y_Q = 0.3$ (left) and 0.1 (right). There is a clear competition between the hypernuclei and the ^{4}He and ^{6}He light clusters, i.e. the light clusters with a larger mass: for $Y_Q = 0.1$, the hypernuclei have larger abundances, but even for the larger charge fraction, the dissolution density occurs at larger densities for the hypernuclei. The behavior of the hyperclusters in the medium is defined by their couplings to the mesons. The difference in relation to the light clusters may be attributed to the fact that hypernuclei are interacting more weakly with the medium, which is clearly seen considering the hypercluster couplings defined in Eqs. (3.40) and (3.51). Since the coupling of the hyperclusters to the ω-meson is strongly correlated with the dissolution density, a smaller ω-coupling implies larger dissolution densities. On the other hand, a weaker coupling to the σ-meson gives rise to smaller mass fractions, since a smaller binding occurs. Furthermore, the binding energy shift is weaker for the hypernuclei: this binding shift is introduced to take into account Pauli blocking, but hypernuclei have less nucleons and therefore experience smaller shifts.

It is also interesting to notice that the isospin pair formed by the hyperclusters ${}^{4}_{\Lambda}\mathrm{H}$ and ${}^{4}_{\Lambda}\mathrm{He}$ behaves in a similar way to the analogous isospin pair formed by the purely nucleonic clusters

^{3}H and ^{3}He. In fact, since the Λ-hyperon present at the hyperclusters has isospin zero, the interactions of these two pairs of clusters with the medium is similar, the only difference being their masses and binding energies, resulting in smaller fractions for the hyperclusters.

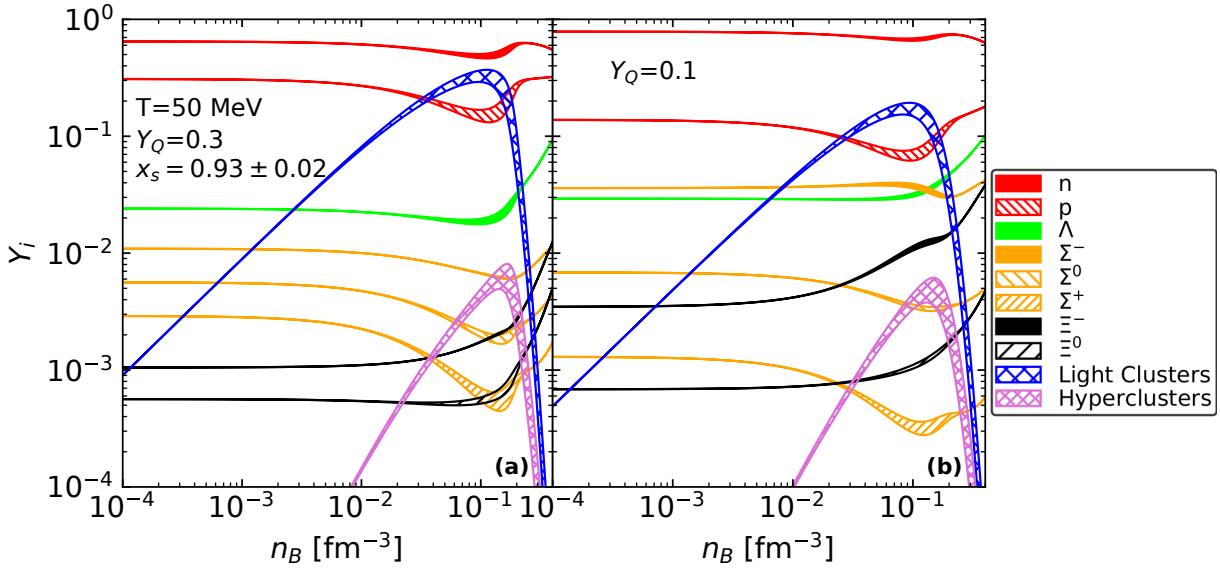

Figure 4.7: Mass fractions of the unbound protons and neutrons (red), Λ (green), $\Sigma^{-,0,+}$ (orange) and $\Xi^{-,0}$ (black), total light clusters (blue) and light hypernuclei (pink) as a function of the density for $T = 50$ MeV and $x_s = 0.93 \pm 0.02$, with $Y_Q = 0.3$ (left) and 0.1 (right). The calculation is performed for the DD2 RMF model.

In Fig. 4.7, the total light cluster fraction and the total light hypercluster fraction are compared with the baryonic octet fractions for the two charge fractions, 0.3 and 0.1. We take $T = 50$ MeV, and calculate the effect of the uncertainty on the x_s coupling of the particle fractions, shown by the bands. The abundances of the hypernuclei are small compared to the light nuclei, and even taking $T = 100$ MeV (not shown), there is not a big difference whether the hypernuclei are included or not in the calculation, only slightly affecting the abundances of the heavier clusters and their dissolution density.

In order to understand how the charge fraction affects the light cluster abundances, and under which conditions the hyperclusters are more abundant, in Fig. 4.8, we plot for a fixed density (0.01, 0.1 and 0.2 fm^{-3}), and temperatures 10, 30 and 50 MeV, the cluster fractions as a function of the charge fraction. The densities chosen are below, close and above the cluster fraction maxima. Depending on the temperature, the last two density values may be above the dissolution density, taken as the density for which the cluster fraction is below 10^{-4}. Considering the lowest density (0.01 fm^{-3}), we can see that for the lowest temperature, the most abundant clusters are not only determined by their mass, but also by their isospin and binding energy, contrary to the other two temperatures, for which the mass essentially determines their abundances, and only in a second order, the isospin. When it comes to the hyperons, they are only present at $T = 30$ and 50 MeV, whereas the hypernuclei appear with an abundance above 10^{-4} at $T = 30$ MeV for $n_B = 0.1$ fm^{-3} and at $T = 50$ MeV for all densities considered. As for the protons, they may be less abundant than some light clusters, as for instance ^{2}H and ^{3}H, below $Y_Q < 0.5$ for $T = 10$ MeV, and $T = 50$ MeV and $n_B = 0.1$ fm^{-3}. Only for $T = 50$ MeV do hyperons become more abundant than most of the light clusters (only ^{2}H are more abundant). For $T = 10$ MeV

and the highest density, only nucleons are present, since the clusters have already dissolved and hyperons did not yet set in. For $T = 30$ MeV, at $n_B = 0.2$ fm^{-3}, only ^{2}H did not dissolve and hypernuclei are only present for 0.1 fm^{-3}. For $T = 50$ MeV, hypernuclei are present in the three densities considered being the lowest density the one showing the smallest abundance. Once again, a similar behaviour is observed for the pairs ${}^4_\Lambda$H, ${}^4_\Lambda$He and ^{3}H, ^{3}He. Hypernuclei seem to be most abundant for charge fractions of the order of $Y_Q = 0.3$ in all situations studied.

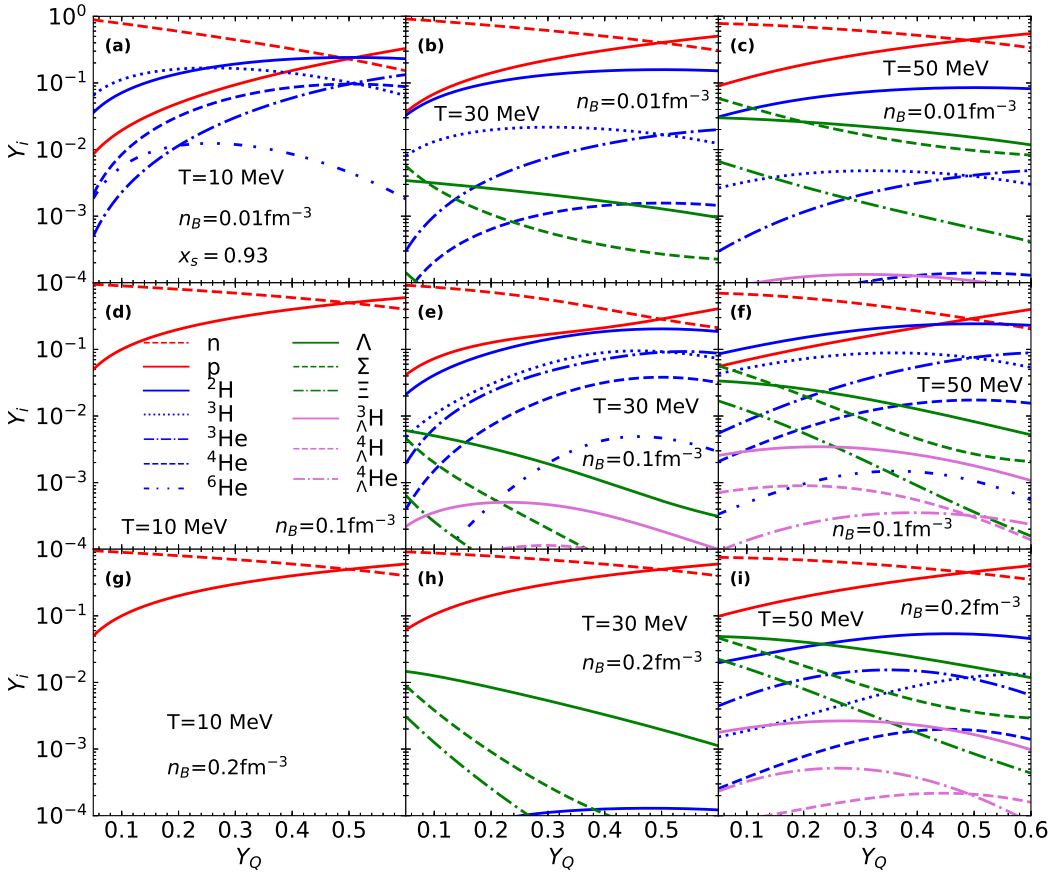

Figure 4.8: Mass fractions of the unbound protons and neutrons (red), unbound hyperons: Λ (solid green), sum of $\Sigma^{+,0,-}$ (dashed green) and sum of $\Xi^{-,0}$ (dash-dotted green), light clusters (blue), and light hypernuclei (pink) as a function of the charge fraction for $T = 10$ MeV (left), $T = 30$ MeV (middle) and $T = 50$ MeV (right). The fractions were determined at $n_B = 0.01$ fm^{-3}(top), 0.1 fm^{-3} (middle) and 0.2 fm^{-3}(bottom). The scalar cluster-meson coupling is set to $x_s = 0.93$ for the DD2 RMF model.

4.5 Adding Δ isobars

We now want to include the four Delta isobars, $\Delta^{-,0,+,++}$, in the systems studied in sections 4.3 and 4.4. However, before we can do that, we need to define some values for the Δ couplings to the mesons.

4.5.1 Appropriate Δ couplings for describing Neutron Stars

As we mentioned in Section 4.1.2, the uncertainty on the Δ couplings can be accounted by allowing them to vary within a large interval of values. We chose to adopt the following intervals

$$\begin{aligned} 0.9 \leq \quad & x_{\sigma\Delta} \quad \leq 1.2 \\ 0.9 \leq \quad & x_{\omega\Delta} \quad \leq 1.2 \\ 0.8 \leq \quad & x_{\rho\Delta} \quad \leq 2 \ . \end{aligned} \tag{4.10}$$

So before including the Δ isobars, we first want to select a few representative sets of these parameters $x_{m\Delta}$ ($m = \sigma, \omega, \rho$) and check if their corresponding EoSs are valid (appropriate to describe NSs). For example, a valid EoS needs to be able to describe observations of NSs masses of around $\sim 2M_\odot$. To guarantee that a given EoS is able to achieve such values for the mass, we have to obtain their corresponding mass-radius relation through the integration of the Tolman-Oppenheimer-Volkoff equations given by [1, 62, 63]:

$$\frac{dp(r)}{dr} = -\frac{G}{r^2}\left[\epsilon(r) + p(r)\right]\left[M(r) + 4\pi r^3 p(r)\right]\left[1 - \frac{2GM(r)}{r}\right]^{-1} \tag{4.11}$$

$$\frac{dM(r)}{dr} = 4\pi r^2 \epsilon(r), \tag{4.12}$$

where r is the distance to the center of the star and $M(r)$ is the mass enclosed in a sphere of radius r. We will do this for the four RMF models mentioned above: DD2, DDME2, FSU2H and TM1e. To that purpose, we need as an input a complete EoS (energy density ϵ and pressure p) from the outer crust until the core of the star. These EoSs are built matching the three different EoSs that correspond to each layer of the star: outer crust, inner crust and core. For the outer crust we use the BPS EoS [64] for all four models. For the inner crust, we use EoSs obtained through Thomas-Fermi calculations where non-spherical heavy clusters are included [65, 66]. For the DD2, DDME2 and FSU2H models, we will use their Thomas-Fermi EoS published in Refs. [67], [68] and [69], respectively. For the TM1e we will use the Thomas-Fermi calculation corresponding to the TM1$\omega\rho$ model calculated in Ref. [66]. The TM1$\omega\rho$ is one of the most similar models to TM1e, since both share the same isoscalar parameters, differing only in their isovector sectors. Finally, for the core, we consider a system made up of the full spin-1/2 baryonic octet, the four Δ isobars, electrons and muons in β-equilibrium and $T = 0$ MeV. Using the results obtained in Sections 2.1.7 and 2.2.5, we calculate the energy density and pressure as a function of the density (EoS) for the core of the star, for each EoS corresponding to a different set of Δ couplings.

In the left panels of Fig. 4.9 we plot, for the four RMF models, the Mass-Radius relations of the EoSs corresponding to a few representative sets of the Δ couplings, fixing $x_{\rho\Delta} = 1$: $x_{\sigma\Delta} = x_{\omega\Delta} = 0.9$; $x_{\sigma\Delta} = x_{\omega\Delta} = 1$; $x_{\sigma\Delta} = 1.1,\ x_{\omega\Delta} = 1$; $x_{\sigma\Delta} = 1.2,\ x_{\omega\Delta} = 1.05$; $x_{\sigma\Delta} = 1.2,\ x_{\omega\Delta} = 1.1$; $x_{\sigma\Delta} = x_{\omega\Delta} = 1.2$. For comparison, we also show (black) the curve corresponding to the case

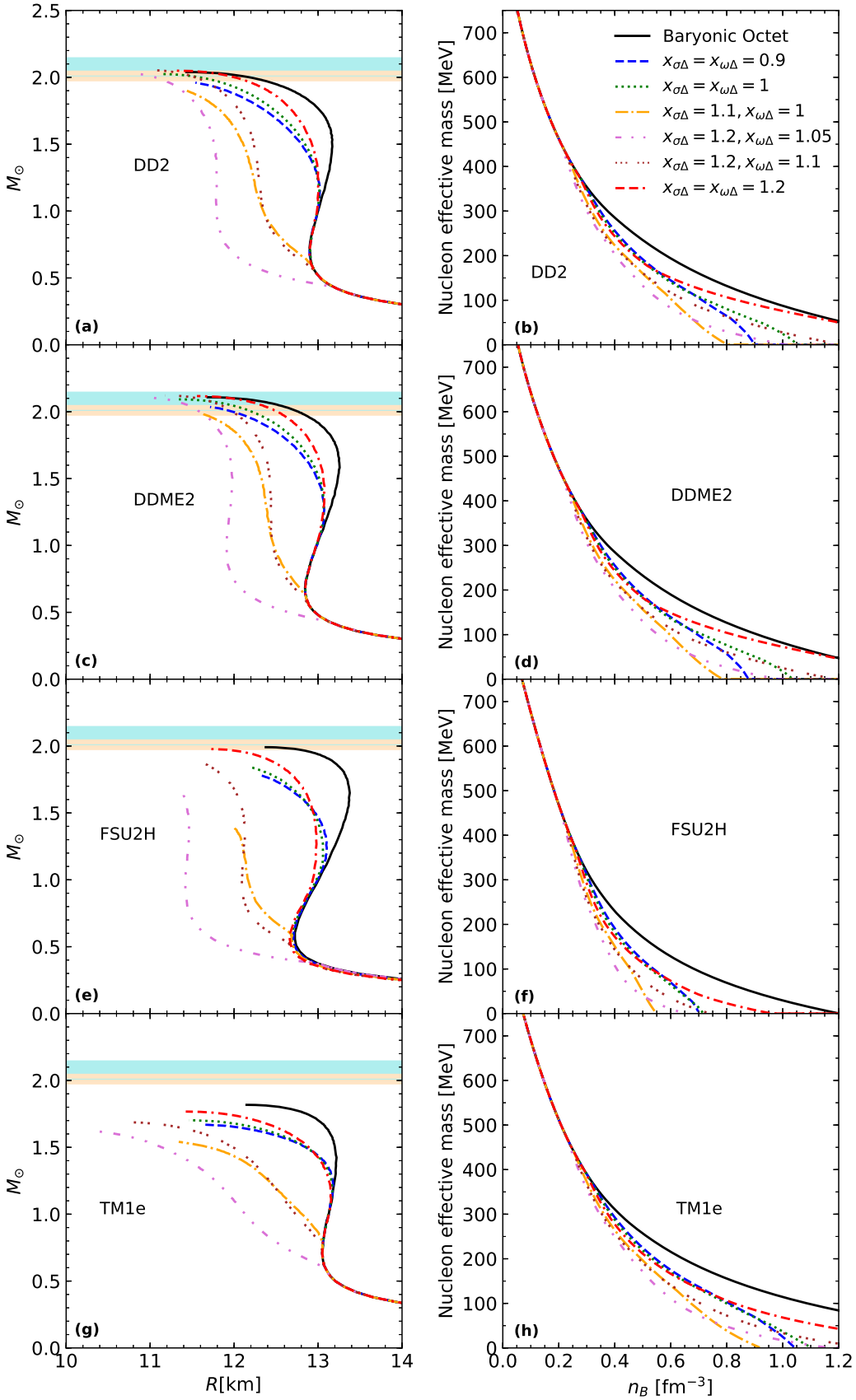

Figure 4.9: Left panels: Mass-Radius relations for several sets of values for the $x_{\sigma\Delta}$, $x_{\omega\Delta}$ couplings, fixing $x_{\rho\Delta} = 1$. The calculation was done for four different RMF models: DD2 (a); DDME2 (c); FSU2H (e); TM1e (g). The Mass-Radius relation for the case when Δ isobars are absent is represented by the Baryonic Octet curve (black). The blue band corresponds to the mass $M = 2.08 \pm 0.07 M_\odot$ of pulsar PSR J0740+6620 [70]; the brownish band to the mass $M = 2.01 \pm 0.04 M_\odot$ of PSR J0348+0432 [71] (the bands correspond to the 1σ uncertainty interval). Right panels: Nucleon effective mass as a function of the density for the EoSs showed in the left panels: DD2 (b); DDME2 (d); FSU2H (f); TM1e (h).

when the Δ isobars are absent from the system made up of the full baryonic octet, electrons and muons. We also plot two horizontal bands corresponding to two of the most massive pulsars ever observed, PSR J0740+6620 [70] and PSR J0348+0432 [71], with masses $M = 2.08 \pm 0.07 M_\odot$ and $M = 2.01 \pm 0.04 M_\odot$, respectively.

It is interesting to see that, for all models alike, the EoSs for which the Δ isobars are present show a significant decrease in the radius of the stars with intermediate masses ($\sim 1.4 M_\odot$) compared to when Δs are absent. This is explained by the fact that the appearance of the Δs softens the EoS, compressing the star even further and consequently reducing its radius, as discussed in Ref. [28]. On the other hand, the presence of the Δs does not seem to significantly affect the maximum masses.

There is also a visible difference in the intermediate mass radius between the EoSs with different values of the Δ couplings. It can be noticed that the EoSs with the same difference between the σ and ω couplings ($x_{\sigma\Delta} - x_{\omega\Delta}$) have similar intermediate mass radius. This is easily understood if we consider the Δ potential in nuclear matter, which takes a similar form to the one presented in Eq.(4.3) for the hyperons:

$$U_\Delta^N(n_0) = -g_{\sigma b}\sigma + g_{\omega b}\omega_0 + g_{\rho b} I_{3\Delta} \rho_{03} \ . \tag{4.13}$$

If $g_{\sigma b}$ increases, the Δ potential decreases and becomes more attractive, which leads to an increase in the abundances of the Δs. On the other hand, if $g_{\omega b}$ increases, the potential becomes less attractive and the Δs are less favored. Therefore, the larger the difference between $x_{\sigma\Delta}$ and $x_{\omega\Delta}$, the higher the abundances of the Δs and the earlier their onset (see Table 4.5), which leads to a more significant softening of the EoS and a larger reduction of its intermediate mass radius. Looking at Eq.(4.13), it is also reasonable to conclude that different EoSs with the same difference between $x_{\sigma\Delta}$ and $x_{\omega\Delta}$ (e.g. $x_{\sigma\Delta} = x_{\omega\Delta} = 0.9$ and $x_{\sigma\Delta} = x_{\omega\Delta} = 1$) will have similar potentials and therefore similar intermediate mass radius since the increase in $x_{\sigma\Delta}$ is more or less compensated by a similar increase in $x_{\omega\Delta}$.

If we now look more carefully at the Mass-Radius relations in the left panels of Fig. 4.9, we notice that there are some EoS that do not reach the maximum mass star. The maximum mass star is reached when the derivative of the mass with respect to the radius is zero. The reason why some of these EoSs cannot reach the maximum mass star, becomes clear if we take a look at the right panels of Fig. 4.9 where we plot the nucleon effective mass ($m_N^* = m_N - g_{\sigma N}\sigma$) as a function of the density. We can see that the nucleon effective mass corresponding to the EoSs that include Δs decrease much faster than the ones where Δs are absent and eventually become zero. For some of them the drop is so fast and at such low densities that they cannot reach the maximum mass star. As a result, the EoSs that reach zero nucleon effective mass before reaching the maximum mass star are not fit to describe NSs and therefore must be discarded from our analysis. The only scenario where these EoSs would be valid was if a phase transition to quark matter had occurred at a density below the one at which the nucleon effective mass becomes zero. Otherwise, the EoSs are not valid for densities above the one at which the nucleon effective mass becomes zero. Considering the couplings we have tested satisfying (4.10), for the DD2 and DDME2 models, the following set of Δ couplings are not valid: $x_{\sigma\Delta} = x_{\omega\Delta} = 0.9$; $x_{\sigma\Delta} = 1.1,\ x_{\omega\Delta} = 1$; $x_{\sigma\Delta} = 1.2,\ x_{\omega\Delta} = 1.05$. For the FSU2H model only the pair $x_{\sigma\Delta} = x_{\omega\Delta} = 1.2$ corresponds to a valid EoS. Finally, for the TM1e model, the invalid Δ couplings are: $x_{\sigma\Delta} = 1.1,\ x_{\omega\Delta} = 1$; $x_{\sigma\Delta} = 1.2,\ x_{\omega\Delta} = 1.05$. The valid Δ couplings are shown in Table 4.5.

In Fig. 4.10 we plot the mass of the star as a function of its central density for the remaining valid EoSs. We can clearly see a deviation from the EoS where Δs are absent, which suggests

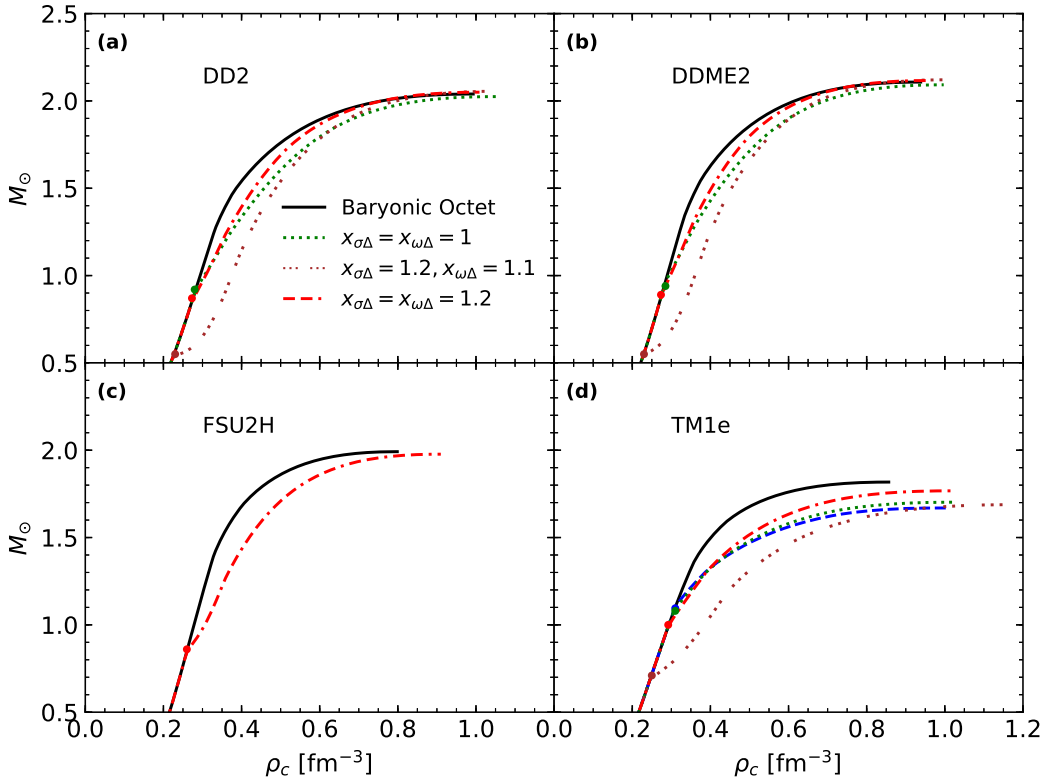

Figure 4.10: Mass of the star as a function of the central density for the four model's EoSs corresponding to values of Δ couplings that are able to reach the maximum mass before the nucleon effective mass becomes zero. $x_{\rho\Delta} = 1$ for all EoSs. The dots correspond to the onset of Δ^-.

that this deviation is caused by the onset of Δ isobars. This is confirmed by the values of the Δ onset densities showed in Table 4.5. In fact, the tiny dots in Fig. 4.10 mark the onset of Δ^- for each valid EoS, showing that the deviations start at the precise density corresponding to the onset of Δ^-, which is the first Δ isobar to appear[1]. Another piece of information that we can extract from Fig. 4.10 is that roughly above $1M_\odot$, all EoSs contain Δ isobars.

So far we have fixed the couplings of the Δs to the ρ meson and varied the σ and ω couplings. In order to test the impact of changing $x_{\rho\Delta}$, in Fig. 4.11 we fix $x_{\sigma\Delta} = x_{\omega\Delta} = 1.2$ and plot the EoSs for three different values of $x_{\rho\Delta}$: 0.8; 1; 2. Since our system is made up of highly asymmetric matter, the sign of the ρ_{03} will be the same as the sign of the isospin of the neutron [1], which is negative, see Table 2.1. If we add to this the fact that the isospin projection of the Δ^- is also negative ($I_{3\Delta^-} = -3/2$, see Table 2.1), we conclude that the term in ρ_{03} from Eq.(4.13) will be positive for the Δ^-, which is the first Δ isobar to appear. Then, the larger the $x_{\rho\Delta}$, the less attractive the Δ^- potential, delaying the appearance of Δ^- to larger densities. As a result, larger values of the coupling $x_{\rho\Delta}$ result in a smaller softening of the EoS producing larger intermediate mass radius, whereas low values of $x_{\rho\Delta}$ have the opposite effect (see also Table 4.5). However, even for the largest $x_{\rho\Delta}$, there is still a decrease in the intermediate mass radius compared to the EoS with absent Δs.

To check if the appearance of Δ isobars has any impact on the stability of the EoSs, in Fig. 4.12 we plot the baryon chemical potential μ_n as a function of the density for both valid and invalid EoSs. We find out that all EoSs that were previously validated do not present any instabilities, with their baryon chemical potential behaving as a monotonically increasing

[1]Since the Δ^- is negatively charged, it can replace a neutron and an electron from their highest Fermi levels, which is energetically favourable. For this reason, the Δ^- is the first of the four Δ isobars to appear, as discussed in Ref. [28].

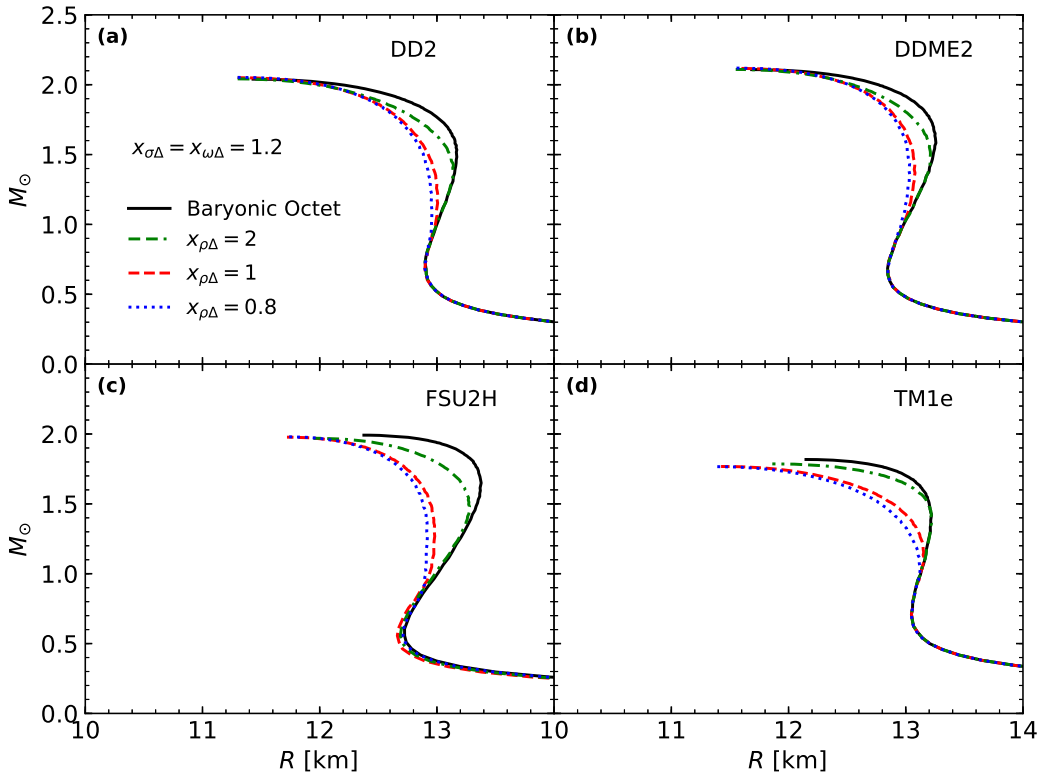

Figure 4.11: Mass-Radius relations for the EoSs with fixed $x_{\sigma\Delta} = x_{\omega\Delta} = 1.2$ for several values of $x_{\rho\Delta}$: 0.8; 1; 2.

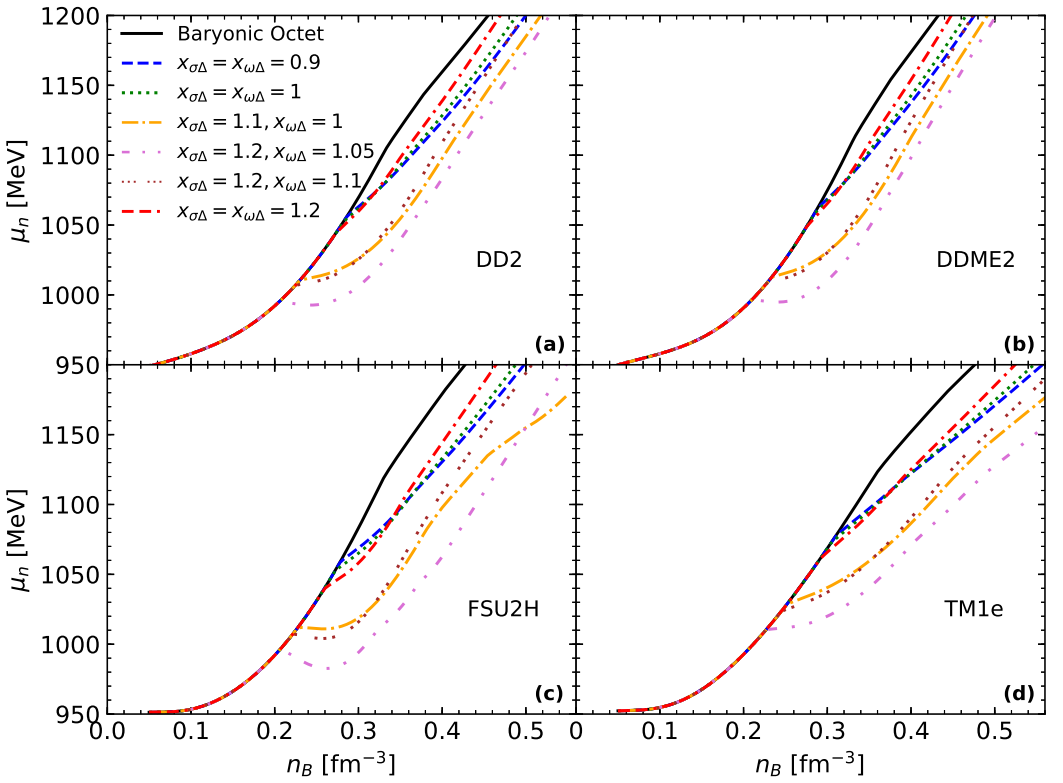

Figure 4.12: Baryon chemical potential, μ_n, as a function of the density for both valid and invalid EoS, fixing $x_{\rho\Delta} = 1$.

function. On the other hand, there are some invalid EoSs that show a drop in the baryon chemical potential for densities below the point at which they were invalidated (that is the density at which the nucleon effective mass becomes zero). As the models considered adequate to describe NSs do not show any instabilities, we do not need to worry about instabilities in this work.

In Ref. [59], the author argues that for some values of the σ and ω couplings to Δ, the appearance of Δs leads to instabilities in the EoSs. However, those EoSs also see their nucleon effective mass dropping to zero at too low densities, which means that we should not consider them to describe NSs.

As we have already mentioned, in Table 4.5 we gathered the values of several NS properties for the valid EoSs considered so far. It is interesting to see how the inclusion of Δs delays the onset of the Λ hyperon[2] to larger densities compared with the EoS with no Δs. Something that can also be easily noticed by looking at Table 4.5 is that, despite the fact that the intermediate mass radius $R(1.4M_\odot)$ suffers a significant drop with the presence of Δs, the maximum masses $M_{\max}$ are roughly the same as they were in the absence of Δs.

DD2	$M_{\max}/M_\odot$	$R(M_{\max})$(km)	ρ_c(fm^{-3})	$R(1.4M_\odot)$(km)	Onset ρ_{Δ^-}(fm^{-3})	Onset ρ_Λ(fm^{-3})
Baryonic Octet	2.04	11.45	0.99	13.91	-	0.33
$x_{\sigma\Delta} = x_{\omega\Delta} = 1, x_{\rho\Delta} = 1$	2.02	11.11	1.05	12.93	0.28	0.36
$x_{\sigma\Delta} = 1.2, x_{\omega\Delta} = 1.1, x_{\rho\Delta} = 1$	2.06	10.95	1.05	12.26	0.23	0.39
$x_{\sigma\Delta} = x_{\omega\Delta} = 1.2, x_{\rho\Delta} = 1$	2.05	11.31	1.01	12.97	0.27	0.35
$x_{\sigma\Delta} = x_{\omega\Delta} = 1.2, x_{\rho\Delta} = 2$	2.04	11.32	1.01	13.13	0.32	0.34
$x_{\sigma\Delta} = x_{\omega\Delta} = 1.2, x_{\rho\Delta} = 0.8$	2.05	11.31	1.00	12.92	0.26	0.36
DDME2	$M_{\max}/M_\odot$	$R(M_{\max})$(km)	ρ_c(fm^{-3})	$R(1.4M_\odot)$(km)	Onset ρ_{Δ^-}(fm^{-3})	Onset ρ_Λ(fm^{-3})
Baryonic Octet	2.11	11.70	0.93	13.20	-	0.33
$x_{\sigma\Delta} = x_{\omega\Delta} = 1, x_{\rho\Delta} = 1$	2.09	11.35	0.99	13.05	0.29	0.36
$x_{\sigma\Delta} = 1.2, x_{\omega\Delta} = 1.1, x_{\rho\Delta} = 1$	2.12	11.19	1.00	12.43	0.23	0.39
$x_{\sigma\Delta} = x_{\omega\Delta} = 1.2, x_{\rho\Delta} = 1$	2.12	11.57	0.95	13.07	0.28	0.35
$x_{\sigma\Delta} = x_{\omega\Delta} = 1.2, x_{\rho\Delta} = 2$	2.11	11.56	0.95	13.20	0.32	0.34
$x_{\sigma\Delta} = x_{\omega\Delta} = 1.2, x_{\rho\Delta} = 0.8$	2.12	11.57	0.95	13.03	0.26	0.36
FSU2H	$M_{\max}/M_\odot$	$R(M_{\max})$(km)	ρ_c(fm^{-3})	$R(1.4M_\odot)$(km)	Onset ρ_{Δ^-}(fm^{-3})	Onset ρ_Λ(fm^{-3})
Baryonic Octet	1.99	12.39	0.79	13.29	-	0.33
$x_{\sigma\Delta} = x_{\omega\Delta} = 1.2, x_{\rho\Delta} = 1$	1.98	11.73	0.91	12.97	0.26	0.35
$x_{\sigma\Delta} = x_{\omega\Delta} = 1.2, x_{\rho\Delta} = 2$	1.97	11.97	0.87	13.26	0.30	0.34
$x_{\sigma\Delta} = x_{\omega\Delta} = 1.2, x_{\rho\Delta} = 0.8$	1.98	11.72	0.91	12.90	0.25	0.36
TM1e	$M_{\max}/M_\odot$	$R(M_{\max})$(km)	ρ_c(fm^{-3})	$R(1.4M_\odot)$(km)	Onset ρ_{Δ^-}(fm^{-3})	Onset ρ_Λ(fm^{-3})
Baryonic Octet	1.82	12.16	0.85	13.22	-	0.36
$x_{\sigma\Delta} = x_{\omega\Delta} = 0.9, x_{\rho\Delta} = 1$	1.67	11.64	1.00	13.07	0.31	0.39
$x_{\sigma\Delta} = x_{\omega\Delta} = 1, x_{\rho\Delta} = 1$	1.70	11.48	1.02	13.04	0.31	0.39
$x_{\sigma\Delta} = 1.2, x_{\omega\Delta} = 1.1, x_{\rho\Delta} = 1$	1.69	10.69	1.18	12.20	0.25	0.44
$x_{\sigma\Delta} = x_{\omega\Delta} = 1.2, x_{\rho\Delta} = 1$	1.77	11.44	1.01	13.03	0.29	0.39
$x_{\sigma\Delta} = x_{\omega\Delta} = 1.2, x_{\rho\Delta} = 2$	1.79	11.89	0.91	13.22	0.36	0.36
$x_{\sigma\Delta} = x_{\omega\Delta} = 1.2, x_{\rho\Delta} = 0.8$	1.77	11.38	1.02	12.93	0.28	0.40

Table 4.5: Maximum mass, $M_{\max}$, maximum mass star's radius, $R(M_{\max})$, central density, ρ_c, radius of the star with 1.4 solar masses, $R(1.4M_\odot)$, onset density of Δ^-, ρ_{Δ^-}, onset density of the Λ hyperon, ρ_Λ, for the four model's EoSs corresponding to values of Δ couplings that are able to reach the maximum mass before the nucleon effective mass becomes zero.

[2] As discussed in Ref. [28], the Λ is the first hyperon to appear due to its lowest mass and the repulsive potential of the Σ^-.

4.5.2 Nuclear Matter with Light Clusters, Hyperons, Hyperclusters and Δ isobars

If we look again at Fig. 4.9, we can see that for all the EoSs previously validated, the TM1e EoSs are the only ones that do not reach any of the horizontal bands corresponding to two of the most massive pulsars ever detected, which means that they are not able to describe the observed massive NSs. For this reason, we will also discard the remaining TM1e EoSs. Furthermore, the DD2 and DDME2 models (both density-dependent) produce very similar results, as can be seen by comparing their data from Table 4.5 and Figs. 4.9-4.12. Then, to simplify our analysis, we won't make any further calculations with the DDME2, since the results would be very similar to the DD2's.

It must be mentioned that we are now going to study systems with a finite temperature and a fixed charge fraction in opposition to the ones considered in Section 4.5.1 where we had β-equilibrium at $T = 0$ MeV, since, as we mentioned before, we are interested in studying light clusters in warm matter that still did not converge to cold catalyzed matter (e.g. CCS and BNSM).

In order to study the general features of the effect of including Δs in the systems of Sections 4.3 and 4.4 without having to care about the differences between different models and Δ couplings, let us for the time being use the DD2 RMF model fixing $x_{\sigma\Delta} = x_{\omega\Delta} = x_{\rho\Delta} = 1$.

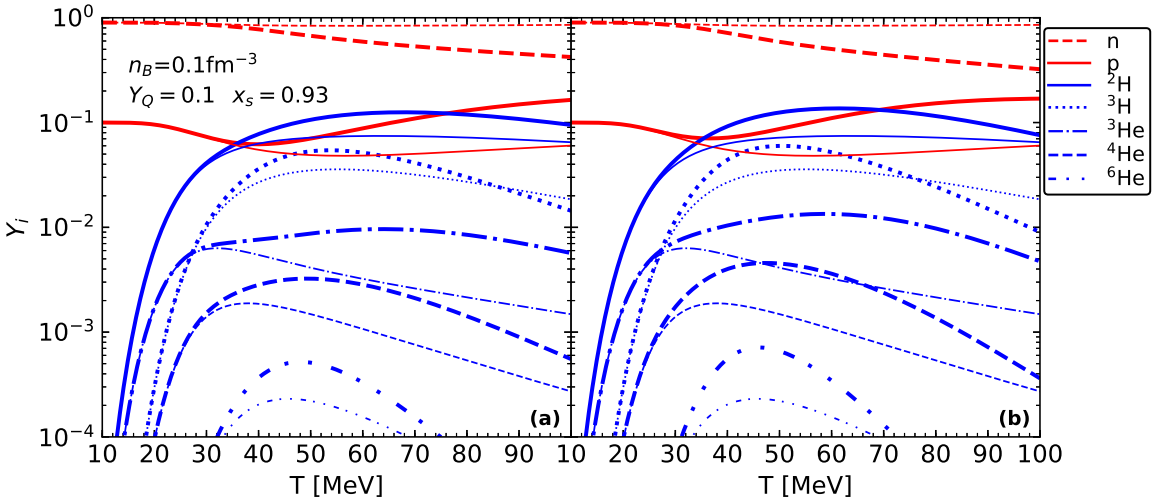

Figure 4.13: Left panel: Unbound nucleon and light cluster fractions in a calculation with (thick lines) and without (thin lines): hyperons (a), hyperons and Δ isobars (b); as a function of the temperature for a charge fraction of $Y_Q = 0.1$, and a density of $n_B = 0.1$ fm^{-3}. The scalar cluster-meson coupling is fixed to $x_s = 0.93$ for the DD2 RMF model.

In the left panel of Fig. 4.13 we show the exact same calculation of Fig. 4.3, consisting of unbound nucleon and purely nucleonic light cluster abundances in the presence (thick lines) and absence (thin lines) of hyperons as a function of the temperature for a charge fraction of $Y_Q = 0.1$ and a density $n_B = 0.1$ fm^{-3}. In the right panel, the thin lines correspond to the same calculation of the thin lines of the left panel whereas the thick lines now show the abundances for a calculation where hyperons and Δs are present in the system. In Fig. 4.3 we had seen that the inclusion of hyperons increased the fraction of light clusters above $T = 25$ MeV. From Fig. 4.13 we conclude that the presence of both hyperons and Δs increases even further the abundances

of light clusters. Again, the reason is a smaller nucleon density in the presence of hyperons and Δs therefore leading to smaller binding energy shifts.

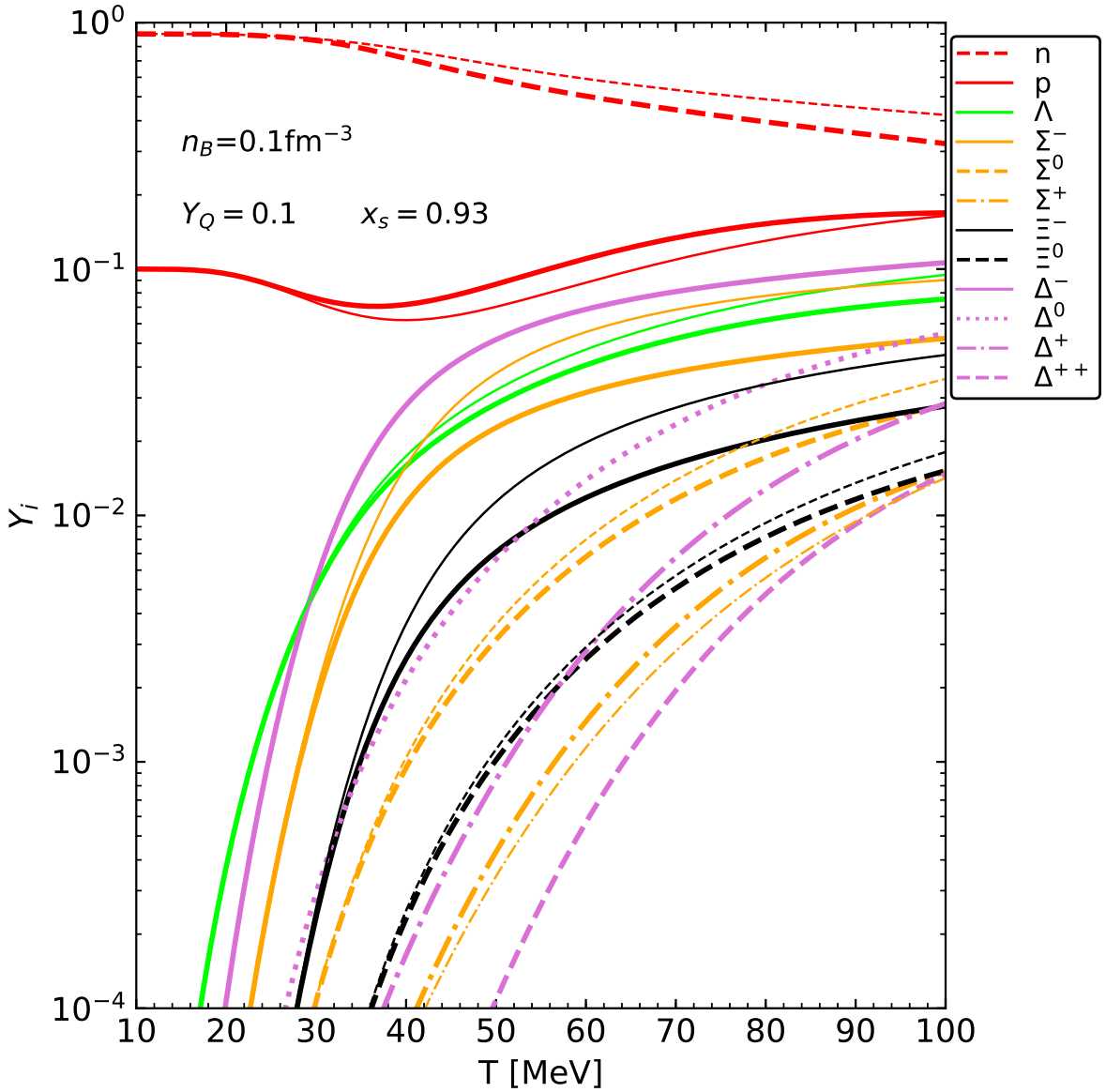

Figure 4.14: Unbound nucleon and hyperon fractions as a function of the temperature in a calculation with (thick lines) and without (thin lines) Δ isobars, for a charge fraction of $Y_Q = 0.1$ and density $n_B = 0.1$ fm^{-3}. The scalar cluster-meson coupling fraction is set to $x_s = 0.93$. The Δ abundances are also displayed with thick lines. Light clusters are present in the calculation but their fractions are not shown. The calculation is performed for the DD2 RMF model.

To study how the hyperon abundances are affected by the inclusion of Δ isobars, in Fig. 4.14 we plot the unbound nucleon and hyperon fractions as a function of the temperature in the presence (thick lines) and absence (thin lines) of Δs for a charge fraction of $Y_Q = 0.1$ and density $n_B = 0.1$ fm^{-3}. The Δ abundances are also displayed with thick pink lines. The main effect of introducing Δs is a reduction of the neutrons as well as the neutral and negatively charged

hyperons, whereas the abundances of protons and the positively charged Σ^+ hyperon increase. The most abundant Δ isobar is clearly the Δ^- which is negatively charged, so its appearance is compensated by a reduction of the neutral and negatively charged particles and an increase of the positively charged ones. Except for the neutrons, all particles increase their abundances with the temperature. At finite temperature new channels are opened and the interaction, the mass and the charge define the abundances. It is energetically favorable to convert highly energetic neutrons into other particles. The more attractive couplings of the Δs compared to the hyperons explains why they are more abundant than their equally charged hyperon counterparts.

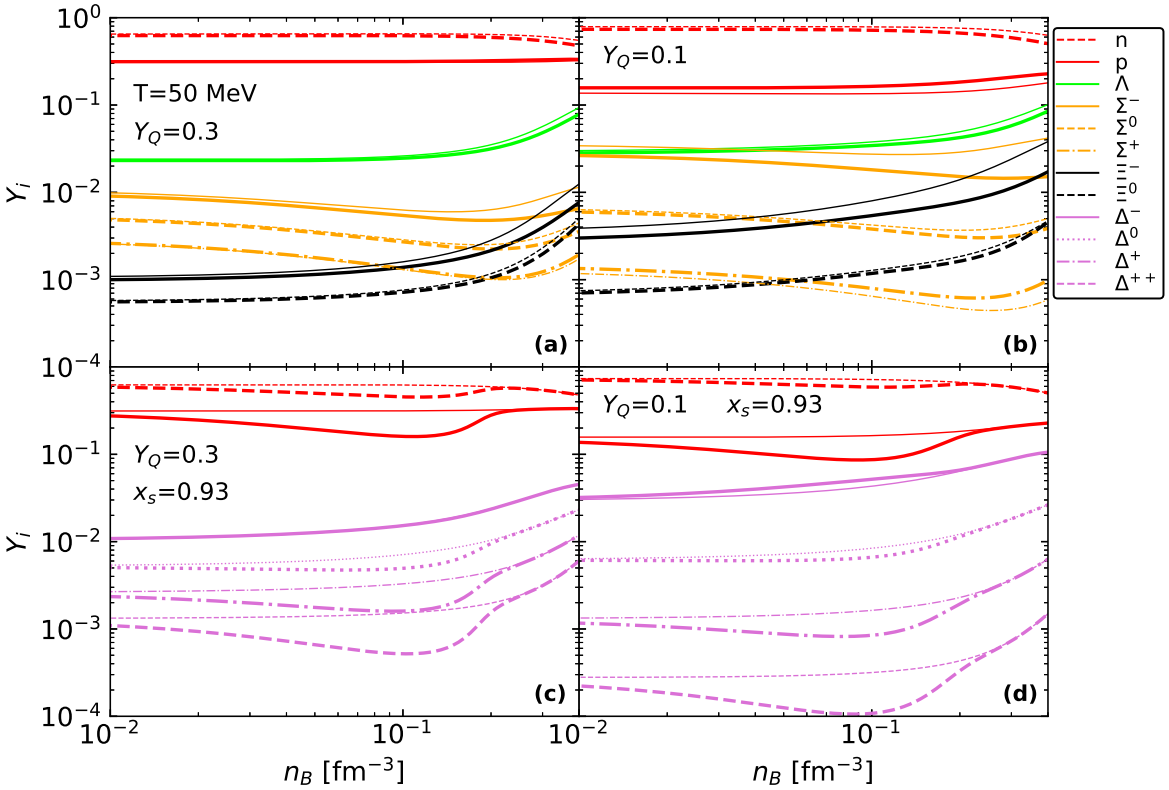

Figure 4.15: Top panels: Unbound nucleon and hyperon fractions as a function of the density in a calculation with (thick lines) and without (thin lines) Δ isobars, for a charge fraction of $Y_Q = 0.3$ (left) and 0.1 (right) and temperature $T = 50$ MeV. Light clusters are not included in this calculation. Bottom panels: Unbound nucleon and Δ fractions as a function of the density in a calculation with (thick lines) and without (thin lines) the five light clusters ^{2}H, ^{3}H, ^{3}He, ^{4}He, ^{6}He, for a charge fraction of $Y_Q = 0.3$ (left) and 0.1 (right) and temperature $T = 50$ MeV. Hyperons are also included in the calculation but the impact of clusters on them was already displayed in Fig. 4.4. The calculation is performed for the DD2 RMF model.

To further confirm the effect the appearance of Δs has on hyperons, the top panels of Fig. 4.15 show the unbound nucleon and hyperon fractions as a function of the density in a calculation with (thick lines) and without (thin lines) Δ isobars, for a charge fraction of $Y_Q = 0.3$ (left) and 0.1 (right) and temperature $T = 50$ MeV. Light clusters are not included in this calculation. We can see that the dynamics of the relative fractions between the different hyperons as a function of the density are essentially the same as in Fig. 4.4, since the introduction of Δs does not considerably affect this dynamics, only slightly reducing or increasing the hyperon fractions according to their electric charge as discussed in Fig. 4.14.

In the bottom panels of Fig. 4.15 we plot the unbound nucleon and Δ fractions as a function of the density in a calculation with (thick lines) and without (thin lines) the five light clusters ^{2}H, ^{3}H, ^{3}He, ^{4}He, ^{6}He, for a charge fraction of $Y_Q = 0.3$ (left) and 0.1 (right) and temperature $T = 50$ MeV. Hyperons are also included in the calculation but the way clusters influence their abundances was already displayed in Fig. 4.4. The effect of clusters on the fractions of Δs is similar to the one felt by hyperons in Fig. 4.4: since the clusters are positively charged, the negatively charged Δ^- is favored whereas the neutral and positively charged Δs see their abundances decrease. Once again, a smaller charge fraction, Y_Q, favours the formation of negatively charged particles (Δ^- in this case).

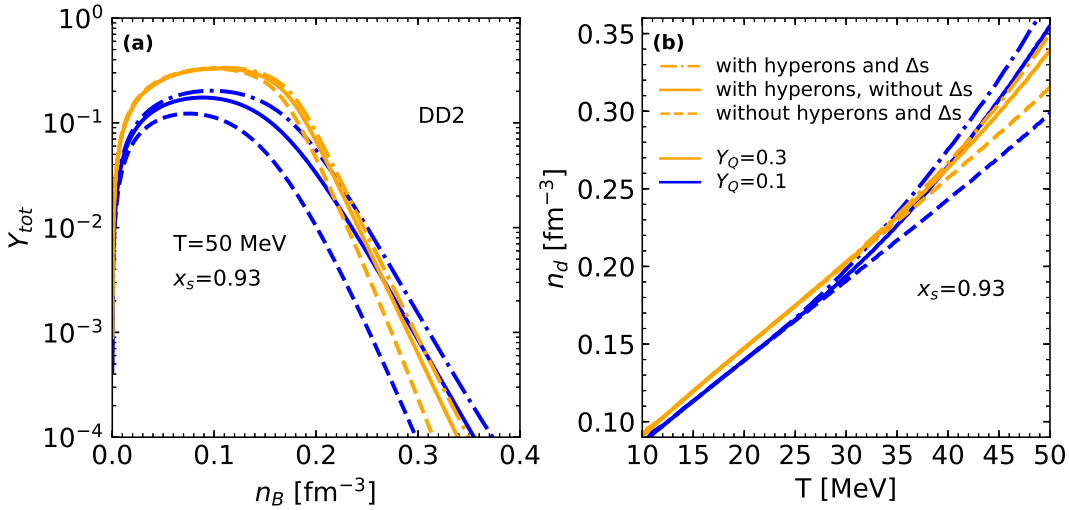

Figure 4.16: Total mass fraction of the light clusters as a function of the density at $T = 50$ MeV (left) and the dissolution density of the clusters, n_d, as a function of the temperature (right) for a calculation without hyperons and Δs (dashed), with hyperons but no Δs (solid) and with hyperons and Δs (dashdot), and a charge fraction of $Y_Q = 0.3$ (orange) and 0.1 (blue). The scalar cluster-meson coupling fraction is set to $x_s = 0.93$ for the DD2 RMF model.

In Fig. 4.5 we showed the impact on the total mass fractions and dissolution densities of the clusters caused by the inclusion of hyperons. To see the added effect of including Δs, in Fig. 4.16, we replot the curves of Fig. 4.5 together with the curves corresponding to the inclusion of Δs (dashdot). The presence of Δs increases even further the cluster fraction above the maximum of the cluster distribution and shifts the dissolution density to larger densities. Once again, this is explained by the fact that the presence of Δs reduces the nucleon fraction, which is reflected on the medium effects felt by the clusters through a smaller binding energy shift.

So far we have not showed any calculation that includes both Δs and hypernuclei at the same time. In Fig. 4.17 we do so by plotting together the fractions of unbound protons and neutrons, light clusters, light hypernuclei, the Λ fraction, the total Σ fraction corresponding to the sum of the $\Sigma^{+,0,-}$ fractions, the total Ξ fraction corresponding to the sum of the $\Xi^{0,-}$ fractions, with (thick lines) and without (thin lines) the total Δ fraction corresponding to the sum of $\Delta^{-,0,+,++}$, for a charge fraction of $Y_Q = 0.3$ (left) and 0.1 (right). The thin lines are the same as the ones in Fig. 4.6, except that now we removed the log scale in the x axis to better see the effect of introducing Δs. As we have discussed, the inclusion of Δs increases the abundances of the purely nucleonic light clusters above their maxima through the reduction of the binding energy shift of the clusters, so we would expect a similar increase for the hyperclusters. In

fact, that is exactly what Fig. 4.17 shows. Once again, the effect is higher for a charge fraction $Y_Q = 0.1$, since a smaller charge fraction favours negatively charged particles, which is the case of the Δ^- (the most abundant of the Δs). Therefore, if the Δs are more abundant for $Y_Q = 0.1$, the reduction of the binding energy shifts of the hyperclusters after their maxima will be larger, resulting in higher dissolution densities and fractions. On the other hand, for densities below the hyperclusters maxima, the introduction of Δs actually slightly reduces the abundances of hyperclusters, which may be due to a drop in the Λs, which are essential to build hyperclusters.

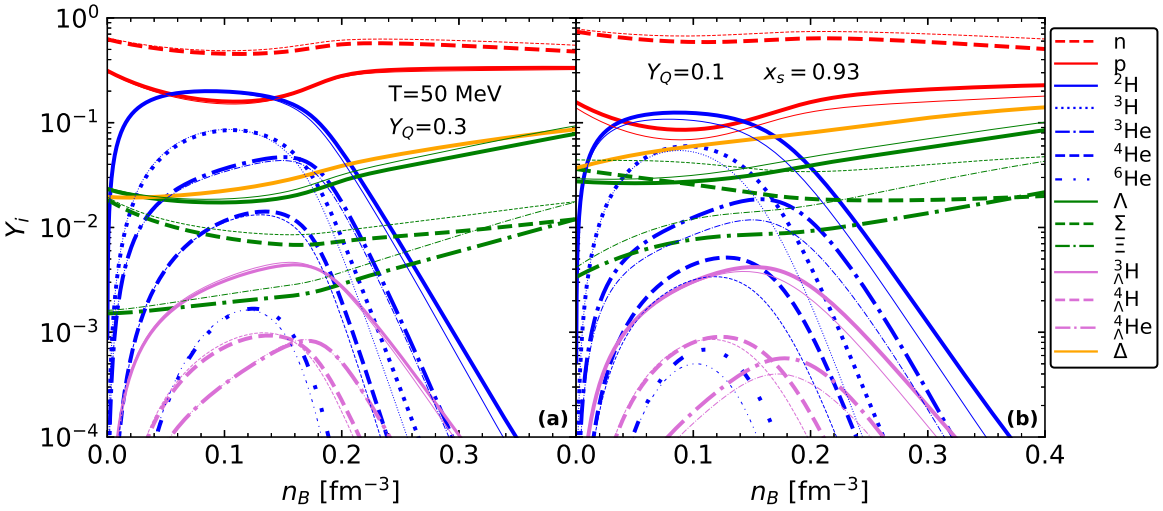

Figure 4.17: Mass fractions of the unbound protons and neutrons (red lines), Λ, Σ and Ξ (green lines), Δ (orange line), light clusters (blue lines) and light hypernuclei (pink lines), with (thick lines) and without (thin lines) Δ particles as a function of the density for $T = 50$ MeV and $x_s = 0.93$, with $Y_Q = 0.3$ (left) and 0.1 (right). The calculation is performed for the DD2 RMF model.

So far we have been performing calculations for the DD2 model with fixed Δ couplings $x_{\sigma\Delta} = x_{\omega\Delta} = x_{\rho\Delta} = 1$. Let us now compare the total fraction of Δ isobars, Y_Δ, corresponding to the sum of $\Delta^{-,0,+,++}$ fractions, as a function of the density for a temperature $T = 50$ MeV and a charge fraction of $Y_Q = 0.3$, in a calculation consisting also of unbound nucleons, hyperons, light clusters and hyperclusters for different values of the Δ couplings using the DD2 and FSU2H models. The FSU2H σ-cluster coupling fraction is set to be $x_s = 0.91$, the same as FSU2R calibrated in [26]. In the left panel, we fix $x_{\rho\Delta} = 1$ and perform the calculation for the three previously validated DD2 EoSs and the only valid FSU2H EoS. As we have mentioned before, the larger the difference between $x_{\sigma\Delta}$ and $x_{\omega\Delta}$, the higher the abundances of Δ isobars. On the other hand, DD2 parameterizations for which the difference is zero, show similar abundances of Δs as a function of the density, with the one with a higher σ and ω couplings producing slightly higher abundances at smaller densities (where the σ coupling is dominant [28]) and lower abundances at higher densities (where the repulsion associated with the ω coupling dominates [28]). As for the difference between the DD2 and FSU2H models with $x_{\sigma\Delta} = x_{\omega\Delta} = 1.2$, we can see that for small densities they show a similar fraction of Δs, whereas for higher densities the FSU2H starts yielding an higher fraction of Δs. Finally, in the right panel we fix $x_{\sigma\Delta} = x_{\omega\Delta} = 1.2$ and perform the calculation for two values of $x_{\rho\Delta} = 1; 2$ for DD2 and FSU2H. As we have discussed before, the larger the value of $x_{\rho\Delta}$, the less attractive the Δ^- potential is, making its presence less favorable, which is observed for both models. All these different parameterizations will affect the fractions of the various particles, since a parameterization with more Δs than the one presented

in Fig. 4.17 accentuates the effects mentioned back then whereas a smaller abundance reduces the impact of the Δs.

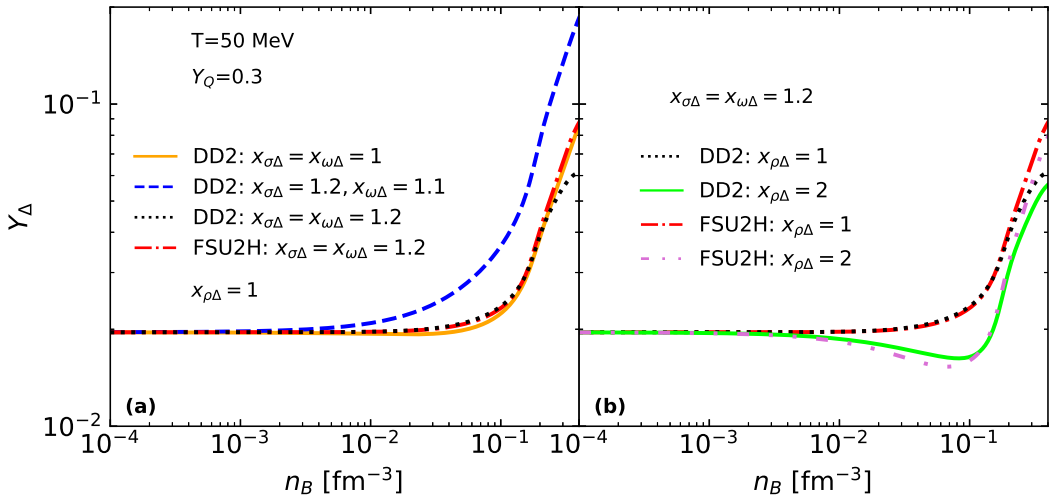

Figure 4.18: Total fraction of Δ isobars, Y_Δ, corresponding to the sum of $\Delta^{-,0,+,++}$, as a function of the density for a temperature $T = 50$ MeV and a charge fraction of $Y_Q = 0.3$, in a calculation consisting also of unbound nucleons, hyperons, light clusters and hyperclusters. The σ-cluster meson fractions are $x_s = 0.93$ (DD2) and $x_s = 0.91$ (FSU2H). Left panel: we fix $x_{\rho\Delta} = 1$ and perform the calculation for different values of the Δ couplings to the σ and ω mesons for the DD2 and FSU2H models. Right panel: we fix $x_{\sigma\Delta} = x_{\omega\Delta} = 1.2$ and perform the calculation for $x_{\rho\Delta} = 1$ and 2 for the DD2 and FSU2H models.

The effect of heavy baryons on the presence of light clusters at low densities has also been discussed in Ref. [22]. In that study the author includes besides nucleons and the classical light clusters (^{2}H, ^{3}H, ^{3}He, ^{4}He) also pions, the Δ-quadruplet and Λ hyperons. The calculation is performed in the dilute limit within a Green's function formalism. Medium effects on the distribution of particles are included through the definition of the particles self-energies. For the nucleons the self-energies are approximated by the nucleon effective masses and are calculated within a Skyrme nuclear matter model. A similar approach is introduced for the light clusters whose self-energies are defined in terms of the nucleons effective masses. Besides, a binding energy that is temperature and density dependent and that is based on results from many-body calculations was also included for the clusters. The Λ hyperon and the Δ isobars are taken with their vacuum masses and for the pions the leading contribution to the self-energy within a chiral perturbation theory was considered. With the simplified description of the heavy baryons the effect of the clusters on the heavy cluster fractions is not seen. In particular the heavy baryon fractions are insensitive to the cluster formations. Another effect is the fact that in Ref. [22] the Λ fraction is larger than the Δ fraction because they are defined by the baryon mass and the interaction with the medium is not considered. On the other hand, in our system all particles interact with the medium in a self-consistent way, therefore the introduction of the heavy baryons such as hyperons and Δs does have an effect on the clusters abundance. Besides that, since our heavy baryons interact with the medium, their abundances do not depend only on their masses, which allows the Δ isobars to be more abundant than the Λ hyperon for certain conditions.

In our study we did not include pions. Since the Δ isobars decay into a nucleon and pion through the strong force if there are available states, the presence of pions is expected in a finite temperature scenario. This will be analyzed in a future study.

Chapter 5

Conclusions

The first goal of this work was to introduce hyperonic degrees of freedom (hyperons and light hyperclusters) on the low-density EoS of warm matter that already included unbound nucleons and purely nucleonic light clusters. The calculations were performed at a fixed charge fraction and temperatures until 100 MeV were considered within the density-dependent DD2 RMF model. The introduction of the clusters was done following the formalism first described in Ref. [23], where clusters couple to the mesonic fields and the Pauli blocking effects are accounted for by including a binding energy shift which basically contributes to the dissolution of the clusters.

We saw that, for a system with only unbound nucleons and nucleonic light clusters, at low densities the abundances are determined by the cluster binding energy and isospin, and for charge fractions below $Y_Q = 0.3$, light clusters like ^{6}He may be at some densities more abundant than ^{3}He or ^{4}He. However, neutron-rich clusters dissolve at lower densities due to stronger binding energy shifts, which take into account Pauli blocking effects. For high temperatures, cluster fraction maxima and dissolution densities are shifted to larger densities, while their abundances, determined by their masses, decrease.

We have then showed that the introduction of hyperons shifts the dissolution of clusters to larger densities and increases the cluster abundances for temperatures $T \gtrsim 25$ MeV. This effect is larger the smaller the charge fraction, and the higher the temperature. This increase of clusters is attributed to a weaker effect of the Pauli-blocking implemented in the model via the binding energy shifts since the overall nucleon density is lower. On the other hand, clusters also have an impact on the hyperon fractions: while neutral and positively charged baryons decrease when clusters are included, the fractions of negatively charged hyperons increase.

After that, we included light hyperclusters in the system and found out that they only set in at temperatures above 25 MeV, competing with ^{4}He and ^{6}He for $T \gtrsim 50$ MeV. Despite that, the introduction of hyperclusters does not have a significant impact on the other particle abundances. We also saw that the larger abundances for the total fraction of hyperclusters occurs for a charge fraction close to $Y_Q \sim 0.3$.

The other main goal of this work was to introduce Δ isobars to the systems discussed above and see what kind of impact they would have on the other particles abundances. However, before we could do that, the large uncertainties regarding the Δ couplings forced us to check which couplings were adequate to describe NSs. For that, we performed a calculation for β-equilibrium matter at $T = 0$ MeV for the core and matched them with a crust EoS. We found out that some of the EoSs corresponding to couplings that a priori were consistent with the existing poorly constraining experimental results for the Δ couplings could not reach the maximum mass star,

therefore not being adequate to describe a NS. This was due to the fact that the nucleon effective mass for these EoSs became zero at too low densities.

After reducing the number of possible values for the Δ couplings, we finally introduced the Δ isobars to the systems previously studied. We found out that the presence of Δs reduced the abundances of neutral and negatively charged particles while increasing positively charged ones. This was due to the fact that the Δ^- is the most abundant of the Δs. We also saw that the presence of Δs increases the fractions of both light nucleonic clusters and hyperclusters through a reduction of the binding energy shifts, as well as shifting their dissolution densities to larger values.

It is crucial to know the effects of introducing all these kinds of particles since any change in the abundances of unbound nucleons, hyperons or light clusters and hyperclusters will affect the weak reaction rates that determine the CCS evolution [14, 15] or the BNSM [16–18].

It is important to notice that in the model presented in this work, both light nucleonic clusters and hyperclusters survive up to quite large densities if the temperature considered is large. This should be investigated more thoroughly in the future to find out if it is necessary to include a temperature dependence on the binding energy shifts in order to dissolve the clusters at lower densities, since it is reasonable to think that at higher densities clusters should already be melted. On the other hand, in Ref. [11] clusters are described as surviving up to temperatures as high as 150 MeV.

Finally, our study did not take into account all hadrons that are produced in heavy ion collisions and that could also appear in CCS or BNSM, such as the pseudoscalar mesons pions and kaons. In fact, since Δ isobars decay into a nucleon and a pion, pions are expected to be formed and have been included in a study of hot low-density EoS of nuclear matter [22], together with Δ isobars. On the other hand, several studies seem to indicate that kaons will appear as a new degree of freedom in stellar matter only if their potential in symmetric nuclear matter is more attractive than chiral models seem to indicate [72–75]. The introduction of these degrees of freedom should be considered in a future work.

Appendix A

Vector Mesons Equations of Motion with Binding Energy Shift

A.1 Light Clusters

As we have seen, Eqs.(3.17) and (3.18) have an extra term as a result of the dependence of the binding energy shift on the ω and ρ mesons through the pseudo-densities $\rho_n^{\rm ps}$ and $\rho_p^{\rm ps}$ (Eqs.(3.15),(3.16)).

Taking into account the definition of the binding energy shift (Eq.(3.11)), the extra terms are given by:

$$
\begin{aligned}
\bullet \quad & -\sum_{i={}^2\mathrm{H},{}^3\mathrm{H},{}^3\mathrm{He},{}^4\mathrm{He},{}^6\mathrm{He}} \rho_i^s \left[\frac{\partial(\delta B_i)}{\partial\rho_n^{\rm ps}}\frac{\partial\rho_n^{\rm ps}}{\omega_0}+\frac{\partial(\delta B_i)}{\partial\rho_p^{\rm ps}}\frac{\partial\rho_p^{\rm ps}}{\omega_0}\right] \qquad (A.1)\\
= \quad & -\frac{\rho_{^2\mathrm{H}}^s}{\rho_0}\left[\frac{\partial\left(1\cdot\left(\epsilon_p^*-m\rho_p^*\right)+1\cdot\left(\epsilon_n^*-m\rho_n^*\right)\right)}{\partial\rho_n^{\rm ps}}\left(\frac{m_\omega^2}{2g_{\omega N}}\right)+\frac{\partial\left(1\cdot\left(\epsilon_p^*-m\rho_p^*\right)+1\cdot\left(\epsilon_n^*-m\rho_n^*\right)\right)}{\partial\rho_p^{\rm ps}}\left(\frac{m_\omega^2}{2g_{\omega N}}\right)\right]\\
& -\frac{\rho_{^3\mathrm{H}}^s}{\rho_0}\left[\frac{\partial\left(1\cdot\left(\epsilon_p^*-m\rho_p^*\right)+2\cdot\left(\epsilon_n^*-m\rho_n^*\right)\right)}{\partial\rho_n^{\rm ps}}\left(\frac{m_\omega^2}{2g_{\omega N}}\right)+\frac{\partial\left(1\cdot\left(\epsilon_p^*-m\rho_p^*\right)+2\cdot\left(\epsilon_n^*-m\rho_n^*\right)\right)}{\partial\rho_p^{\rm ps}}\left(\frac{m_\omega^2}{2g_{\omega N}}\right)\right]\\
& -\frac{\rho_{^3\mathrm{He}}^s}{\rho_0}\left[\frac{\partial\left(2\cdot\left(\epsilon_p^*-m\rho_p^*\right)+1\cdot\left(\epsilon_n^*-m\rho_n^*\right)\right)}{\partial\rho_n^{\rm ps}}\left(\frac{m_\omega^2}{2g_{\omega N}}\right)+\frac{\partial\left(2\cdot\left(\epsilon_p^*-m\rho_p^*\right)+1\cdot\left(\epsilon_n^*-m\rho_n^*\right)\right)}{\partial\rho_p^{\rm ps}}\left(\frac{m_\omega^2}{2g_{\omega N}}\right)\right]\\
& -\frac{\rho_{^4\mathrm{He}}^s}{\rho_0}\left[\frac{\partial\left(2\cdot\left(\epsilon_p^*-m\rho_p^*\right)+2\cdot\left(\epsilon_n^*-m\rho_n^*\right)\right)}{\partial\rho_n^{\rm ps}}\left(\frac{m_\omega^2}{2g_{\omega N}}\right)+\frac{\partial\left(2\cdot\left(\epsilon_p^*-m\rho_p^*\right)+2\cdot\left(\epsilon_n^*-m\rho_n^*\right)\right)}{\partial\rho_p^{\rm ps}}\left(\frac{m_\omega^2}{2g_{\omega N}}\right)\right]\\
& -\frac{\rho_{^6\mathrm{He}}^s}{\rho_0}\left[\frac{\partial\left(2\cdot\left(\epsilon_p^*-m\rho_p^*\right)+4\cdot\left(\epsilon_n^*-m\rho_n^*\right)\right)}{\partial\rho_n^{\rm ps}}\left(\frac{m_\omega^2}{2g_{\omega N}}\right)+\frac{\partial\left(2\cdot\left(\epsilon_p^*-m\rho_p^*\right)+4\cdot\left(\epsilon_n^*-m\rho_n^*\right)\right)}{\partial\rho_p^{\rm ps}}\left(\frac{m_\omega^2}{2g_{\omega N}}\right)\right]\\
= \quad & -\frac{\rho_{^2\mathrm{H}}^s}{\rho_0}\left(\frac{m_\omega^2}{2g_{\omega N}}\right)\left[\frac{\partial\epsilon_n^*}{\partial\rho_n^{\rm ps}}-\frac{m\partial\rho_n^*}{\partial\rho_n^{\rm ps}}+\frac{\partial\epsilon_p^*}{\partial\rho_p^{\rm ps}}-\frac{m\partial\rho_p^*}{\partial\rho_p^{\rm ps}}\right]\\
& -\frac{\rho_{^3\mathrm{H}}^s}{\rho_0}\left(\frac{m_\omega^2}{2g_{\omega N}}\right)\left[2\frac{\partial\epsilon_n^*}{\partial\rho_n^{\rm ps}}-2\frac{m\partial\rho_n^*}{\partial\rho_n^{\rm ps}}+\frac{\partial\epsilon_p^*}{\partial\rho_p^{\rm ps}}-\frac{m\partial\rho_p^*}{\partial\rho_p^{\rm ps}}\right]\\
& -\frac{\rho_{^3\mathrm{He}}^s}{\rho_0}\left(\frac{m_\omega^2}{2g_{\omega N}}\right)\left[\frac{\partial\epsilon_n^*}{\partial\rho_n^{\rm ps}}-\frac{m\partial\rho_n^*}{\partial\rho_n^{\rm ps}}+2\frac{\partial\epsilon_p^*}{\partial\rho_p^{\rm ps}}-2\frac{m\partial\rho_p^*}{\partial\rho_p^{\rm ps}}\right]\\
& -\frac{\rho_{^4\mathrm{He}}^s}{\rho_0}\left(\frac{m_\omega^2}{2g_{\omega N}}\right)\left[2\frac{\partial\epsilon_n^*}{\partial\rho_n^{\rm ps}}-2\frac{m\partial\rho_n^*}{\partial\rho_n^{\rm ps}}+2\frac{\partial\epsilon_p^*}{\partial\rho_p^{\rm ps}}-2\frac{m\partial\rho_p^*}{\partial\rho_p^{\rm ps}}\right]\\
& -\frac{\rho_{^6\mathrm{He}}^s}{\rho_0}\left(\frac{m_\omega^2}{2g_{\omega N}}\right)\left[4\frac{\partial\epsilon_n^*}{\partial\rho_n^{\rm ps}}-4\frac{m\partial\rho_n^*}{\partial\rho_n^{\rm ps}}+2\frac{\partial\epsilon_p^*}{\partial\rho_p^{\rm ps}}-2\frac{m\partial\rho_p^*}{\partial\rho_p^{\rm ps}}\right]
\end{aligned}
$$

$$
\begin{aligned}
&= -\frac{1}{\rho_0}\left(\frac{m_\omega^2}{2g_{\omega N}}\right)\left(\rho^s_{^2\mathrm{H}}+\rho^s_{^3\mathrm{H}}+\rho^s_{^3\mathrm{He}}+2\rho^s_{^4\mathrm{He}}+2\rho^s_{^6\mathrm{He}}\right)\left[\frac{\partial\epsilon_n^*}{\partial\rho_n^{\mathrm{ps}}}-\frac{m\partial\rho_n^*}{\partial\rho_n^{\mathrm{ps}}}+\frac{\partial\epsilon_p^*}{\partial\rho_p^{\mathrm{ps}}}-\frac{m\partial\rho_p^*}{\partial\rho_p^{\mathrm{ps}}}\right]\\
&\quad -\frac{1}{\rho_0}\left(\frac{m_\omega^2}{2g_{\omega N}}\right)\left(\rho^s_{^3\mathrm{H}}+2\rho^s_{^6\mathrm{He}}\right)\left[\frac{\partial\epsilon_n^*}{\partial\rho_n^{\mathrm{ps}}}-\frac{m\partial\rho_n^*}{\partial\rho_n^{\mathrm{ps}}}\right]\\
&\quad -\frac{1}{\rho_0}\left(\frac{m_\omega^2}{2g_{\omega N}}\right)\rho^s_{^3\mathrm{He}}\left[\frac{\partial\epsilon_p^*}{\partial\rho_p^{\mathrm{ps}}}-\frac{m\partial\rho_p^*}{\partial\rho_p^{\mathrm{ps}}}\right]
\end{aligned}
$$

and

$$
\bullet \quad -\sum_{\substack{i=^2\mathrm{H},^3\mathrm{H},^3\mathrm{He},\\ ^4\mathrm{He},^6\mathrm{He}}}\rho_i^s\left[\frac{\partial(\delta B_i)}{\partial\rho_n^{\mathrm{ps}}}\frac{\partial\rho_n^{\mathrm{ps}}}{\rho_{03}}+\frac{\partial(\delta B_i)}{\partial\rho_p^{\mathrm{ps}}}\frac{\partial\rho_p^{\mathrm{ps}}}{\rho_{03}}\right] \tag{A.2}
$$

$$
\begin{aligned}
&= -\frac{\rho^s_{^2\mathrm{H}}}{\rho_0}\left[\frac{\partial\left(1\cdot\left(\epsilon_p^*-m\rho_p^*\right)+1\cdot\left(\epsilon_n^*-m\rho_n^*\right)\right)}{\partial\rho_n^{\mathrm{ps}}}\left(-\frac{m_\rho^2}{g_{\rho N}}\right)+\frac{\partial\left(1\cdot\left(\epsilon_p^*-m\rho_p^*\right)+1\cdot\left(\epsilon_n^*-m\rho_n^*\right)\right)}{\partial\rho_p^{\mathrm{ps}}}\left(\frac{m_\rho^2}{g_{\rho N}}\right)\right]\\
&\quad -\frac{\rho^s_{^3\mathrm{H}}}{\rho_0}\left[\frac{\partial\left(1\cdot\left(\epsilon_p^*-m\rho_p^*\right)+2\cdot\left(\epsilon_n^*-m\rho_n^*\right)\right)}{\partial\rho_n^{\mathrm{ps}}}\left(-\frac{m_\rho^2}{g_{\rho N}}\right)+\frac{\partial\left(1\cdot\left(\epsilon_p^*-m\rho_p^*\right)+2\cdot\left(\epsilon_n^*-m\rho_n^*\right)\right)}{\partial\rho_p^{\mathrm{ps}}}\left(\frac{m_\rho^2}{g_{\rho N}}\right)\right]\\
&\quad -\frac{\rho^s_{^3\mathrm{He}}}{\rho_0}\left[\frac{\partial\left(2\cdot\left(\epsilon_p^*-m\rho_p^*\right)+1\cdot\left(\epsilon_n^*-m\rho_n^*\right)\right)}{\partial\rho_n^{\mathrm{ps}}}\left(-\frac{m_\rho^2}{g_{\rho N}}\right)+\frac{\partial\left(2\cdot\left(\epsilon_p^*-m\rho_p^*\right)+1\cdot\left(\epsilon_n^*-m\rho_n^*\right)\right)}{\partial\rho_p^{\mathrm{ps}}}\left(\frac{m_\rho^2}{g_{\rho N}}\right)\right]\\
&\quad -\frac{\rho^s_{^4\mathrm{He}}}{\rho_0}\left[\frac{\partial\left(2\cdot\left(\epsilon_p^*-m\rho_p^*\right)+2\cdot\left(\epsilon_n^*-m\rho_n^*\right)\right)}{\partial\rho_n^{\mathrm{ps}}}\left(-\frac{m_\rho^2}{g_{\rho N}}\right)+\frac{\partial\left(2\cdot\left(\epsilon_p^*-m\rho_p^*\right)+2\cdot\left(\epsilon_n^*-m\rho_n^*\right)\right)}{\partial\rho_p^{\mathrm{ps}}}\left(\frac{m_\rho^2}{g_{\rho N}}\right)\right]\\
&\quad -\frac{\rho^s_{^6\mathrm{He}}}{\rho_0}\left[\frac{\partial\left(2\cdot\left(\epsilon_p^*-m\rho_p^*\right)+4\cdot\left(\epsilon_n^*-m\rho_n^*\right)\right)}{\partial\rho_n^{\mathrm{ps}}}\left(-\frac{m_\rho^2}{g_{\rho N}}\right)+\frac{\partial\left(2\cdot\left(\epsilon_p^*-m\rho_p^*\right)+4\cdot\left(\epsilon_n^*-m\rho_n^*\right)\right)}{\partial\rho_p^{\mathrm{ps}}}\left(\frac{m_\rho^2}{g_{\rho N}}\right)\right]\\
&= -\frac{\rho^s_{^2\mathrm{H}}}{\rho_0}\left(\frac{m_\rho^2}{g_{\rho N}}\right)\left[-\frac{\partial\epsilon_n^*}{\partial\rho_n^{\mathrm{ps}}}+\frac{m\partial\rho_n^*}{\partial\rho_n^{\mathrm{ps}}}+\frac{\partial\epsilon_p^*}{\partial\rho_p^{\mathrm{ps}}}-\frac{m\partial\rho_p^*}{\partial\rho_p^{\mathrm{ps}}}\right]\\
&\quad -\frac{\rho^s_{^3\mathrm{H}}}{\rho_0}\left(\frac{m_\rho^2}{g_{\rho N}}\right)\left[-2\frac{\partial\epsilon_n^*}{\partial\rho_n^{\mathrm{ps}}}+2\frac{m\partial\rho_n^*}{\partial\rho_n^{\mathrm{ps}}}+\frac{\partial\epsilon_p^*}{\partial\rho_p^{\mathrm{ps}}}-\frac{m\partial\rho_p^*}{\partial\rho_p^{\mathrm{ps}}}\right]\\
&\quad -\frac{\rho^s_{^3\mathrm{He}}}{\rho_0}\left(\frac{m_\rho^2}{g_{\rho N}}\right)\left[-\frac{\partial\epsilon_n^*}{\partial\rho_n^{\mathrm{ps}}}+\frac{m\partial\rho_n^*}{\partial\rho_n^{\mathrm{ps}}}+2\frac{\partial\epsilon_p^*}{\partial\rho_p^{\mathrm{ps}}}-2\frac{m\partial\rho_p^*}{\partial\rho_p^{\mathrm{ps}}}\right]\\
&\quad -\frac{\rho^s_{^4\mathrm{He}}}{\rho_0}\left(\frac{m_\rho^2}{g_{\rho N}}\right)\left[-2\frac{\partial\epsilon_n^*}{\partial\rho_n^{\mathrm{ps}}}+2\frac{m\partial\rho_n^*}{\partial\rho_n^{\mathrm{ps}}}+2\frac{\partial\epsilon_p^*}{\partial\rho_p^{\mathrm{ps}}}-2\frac{m\partial\rho_p^*}{\partial\rho_p^{\mathrm{ps}}}\right]\\
&\quad -\frac{\rho^s_{^6\mathrm{He}}}{\rho_0}\left(\frac{m_\rho^2}{g_{\rho N}}\right)\left[-4\frac{\partial\epsilon_n^*}{\partial\rho_n^{\mathrm{ps}}}+4\frac{m\partial\rho_n^*}{\partial\rho_n^{\mathrm{ps}}}+2\frac{\partial\epsilon_p^*}{\partial\rho_p^{\mathrm{ps}}}-2\frac{m\partial\rho_p^*}{\partial\rho_p^{\mathrm{ps}}}\right]\\
&= -\frac{1}{\rho_0}\left(\frac{m_\rho^2}{g_{\rho N}}\right)\left(\rho^s_{^2\mathrm{H}}+\rho^s_{^3\mathrm{H}}+\rho^s_{^3\mathrm{He}}+2\rho^s_{^4\mathrm{He}}+2\rho^s_{^6\mathrm{He}}\right)\left[-\frac{\partial\epsilon_n^*}{\partial\rho_n^{\mathrm{ps}}}+\frac{m\partial\rho_n^*}{\partial\rho_n^{\mathrm{ps}}}+\frac{\partial\epsilon_p^*}{\partial\rho_p^{\mathrm{ps}}}-\frac{m\partial\rho_p^*}{\partial\rho_p^{\mathrm{ps}}}\right]\\
&\quad -\frac{1}{\rho_0}\left(\frac{m_\rho^2}{g_{\rho N}}\right)\left(\rho^s_{^3\mathrm{H}}+2\rho^s_{^6\mathrm{He}}\right)\left[-\frac{\partial\epsilon_n^*}{\partial\rho_n^{\mathrm{ps}}}+\frac{m\partial\rho_n^*}{\partial\rho_n^{\mathrm{ps}}}\right]\\
&\quad -\frac{1}{\rho_0}\left(\frac{m_\rho^2}{g_{\rho N}}\right)\rho^s_{^3\mathrm{He}}\left[\frac{\partial\epsilon_p^*}{\partial\rho_p^{\mathrm{ps}}}-\frac{m\partial\rho_p^*}{\partial\rho_p^{\mathrm{ps}}}\right]
\end{aligned}
$$

A.2 Light Clusters and Hyperclusters

The extra terms on the light clusters in Eqs.(3.56),(3.57), will be the same as Eqs.(A.1),(A.2), respectively.

The remaining extra terms in Eqs.(3.56),(3.57),(3.58) are:

$$\bullet \quad -\sum_{j={}^{3}_{\Lambda}\mathrm{H},{}^{4}_{\Lambda}\mathrm{H},{}^{4}_{\Lambda}\mathrm{He}} \rho_j^s \left[\frac{\partial(\delta B_j)}{\partial \rho_n^{\mathrm{ps}}} \frac{\partial \rho_n^{\mathrm{ps}}}{\omega_0} + \frac{\partial(\delta B_j)}{\partial \rho_p^{\mathrm{ps}}} \frac{\partial \rho_p^{\mathrm{ps}}}{\omega_0} + \frac{\partial(\delta B_j)}{\partial \rho_\Lambda^{\mathrm{ps}}} \frac{\partial \rho_\Lambda^{\mathrm{ps}}}{\omega_0} \right] \tag{A.3}$$

$$\begin{aligned}
&= -\frac{\rho^s_{{}^{3}_{\Lambda}\mathrm{H}}}{\rho_0} \left[\frac{\partial \left(1 \cdot \left(\epsilon_p^* - m\rho_p^*\right) + 1 \cdot \left(\epsilon_n^* - m\rho_n^*\right) + 1 \cdot \left(\epsilon_\Lambda^* - m_\Lambda \rho_\Lambda^*\right)\right)}{\partial \rho_n^{\mathrm{ps}}} \left(\frac{m_\omega^2}{2g_{\omega N}} \right) \right. \\
&\left. + \frac{\partial \left(1 \cdot \left(\epsilon_p^* - m\rho_p^*\right) + 1 \cdot \left(\epsilon_n^* - m\rho_n^*\right) + 1 \cdot \left(\epsilon_\Lambda^* - m_\Lambda \rho_\Lambda^*\right)\right)}{\partial \rho_p^{\mathrm{ps}}} \left(\frac{m_\omega^2}{2g_{\omega N}} \right) \right] \\
&\quad -\frac{\rho^s_{{}^{4}_{\Lambda}\mathrm{H}}}{\rho_0} \left[\frac{\partial \left(1 \cdot \left(\epsilon_p^* - m\rho_p^*\right) + 2 \cdot \left(\epsilon_n^* - m\rho_n^*\right) + 1 \cdot \left(\epsilon_\Lambda^* - m_\Lambda \rho_\Lambda^*\right)\right)}{\partial \rho_n^{\mathrm{ps}}} \left(\frac{m_\omega^2}{2g_{\omega N}} \right) \right. \\
&\left. + \frac{\partial \left(1 \cdot \left(\epsilon_p^* - m\rho_p^*\right) + 2 \cdot \left(\epsilon_n^* - m\rho_n^*\right) + 1 \cdot \left(\epsilon_\Lambda^* - m_\Lambda \rho_\Lambda^*\right)\right)}{\partial \rho_p^{\mathrm{ps}}} \left(\frac{m_\omega^2}{2g_{\omega N}} \right) \right] \\
&\quad -\frac{\rho^s_{{}^{4}_{\Lambda}\mathrm{He}}}{\rho_0} \left[\frac{\partial \left(2 \cdot \left(\epsilon_p^* - m\rho_p^*\right) + 1 \cdot \left(\epsilon_n^* - m\rho_n^*\right) + 1 \cdot \left(\epsilon_\Lambda^* - m_\Lambda \rho_\Lambda^*\right)\right)}{\partial \rho_n^{\mathrm{ps}}} \left(\frac{m_\omega^2}{2g_{\omega N}} \right) \right. \\
&\left. + \frac{\partial \left(2 \cdot \left(\epsilon_p^* - m\rho_p^*\right) + 1 \cdot \left(\epsilon_n^* - m\rho_n^*\right) + 1 \cdot \left(\epsilon_\Lambda^* - m_\Lambda \rho_\Lambda^*\right)\right)}{\partial \rho_p^{\mathrm{ps}}} \left(\frac{m_\omega^2}{2g_{\omega N}} \right) \right] \\
&= -\frac{\rho^s_{{}^{3}_{\Lambda}\mathrm{H}}}{\rho_0} \left(\frac{m_\omega^2}{2g_{\omega N}} \right) \left[\frac{\partial \epsilon_n^*}{\partial \rho_n^{\mathrm{ps}}} - \frac{m\partial \rho_n^*}{\partial \rho_n^{\mathrm{ps}}} + \frac{\partial \epsilon_p^*}{\partial \rho_p^{\mathrm{ps}}} - \frac{m\partial \rho_p^*}{\partial \rho_p^{\mathrm{ps}}} \right] \\
&\quad -\frac{\rho^s_{{}^{4}_{\Lambda}\mathrm{H}}}{\rho_0} \left(\frac{m_\omega^2}{2g_{\omega N}} \right) \left[2\frac{\partial \epsilon_n^*}{\partial \rho_n^{\mathrm{ps}}} - 2\frac{m\partial \rho_n^*}{\partial \rho_n^{\mathrm{ps}}} + \frac{\partial \epsilon_p^*}{\partial \rho_p^{\mathrm{ps}}} - \frac{m\partial \rho_p^*}{\partial \rho_p^{\mathrm{ps}}} \right] \\
&\quad -\frac{\rho^s_{{}^{4}_{\Lambda}\mathrm{He}}}{\rho_0} \left(\frac{m_\omega^2}{2g_{\omega N}} \right) \left[\frac{\partial \epsilon_n^*}{\partial \rho_n^{\mathrm{ps}}} - \frac{m\partial \rho_n^*}{\partial \rho_n^{\mathrm{ps}}} + 2\frac{\partial \epsilon_p^*}{\partial \rho_p^{\mathrm{ps}}} - 2\frac{m\partial \rho_p^*}{\partial \rho_p^{\mathrm{ps}}} \right] \\
&= -\frac{1}{\rho_0} \left(\frac{m_\omega^2}{2g_{\omega N}} \right) \left(\rho^s_{{}^{3}_{\Lambda}\mathrm{H}} + \rho^s_{{}^{4}_{\Lambda}\mathrm{H}} + \rho^s_{{}^{4}_{\Lambda}\mathrm{He}} \right) \left[\frac{\partial \epsilon_n^*}{\partial \rho_n^{\mathrm{ps}}} - \frac{m\partial \rho_n^*}{\partial \rho_n^{\mathrm{ps}}} + \frac{\partial \epsilon_p^*}{\partial \rho_p^{\mathrm{ps}}} - \frac{m\partial \rho_p^*}{\partial \rho_p^{\mathrm{ps}}} \right] \\
&\quad -\frac{1}{\rho_0} \left(\frac{m_\omega^2}{2g_{\omega N}} \right) \rho^s_{{}^{4}_{\Lambda}\mathrm{H}} \left[\frac{\partial \epsilon_n^*}{\partial \rho_n^{\mathrm{ps}}} - \frac{m\partial \rho_n^*}{\partial \rho_n^{\mathrm{ps}}} \right] - \frac{1}{\rho_0} \left(\frac{m_\omega^2}{2g_{\omega N}} \right) \rho^s_{{}^{4}_{\Lambda}\mathrm{He}} \left[\frac{\partial \epsilon_p^*}{\partial \rho_p^{\mathrm{ps}}} - \frac{m\partial \rho_p^*}{\partial \rho_p^{\mathrm{ps}}} \right]
\end{aligned}$$

$$\bullet \quad -\sum_{j={}^{3}_{\Lambda}\mathrm{H},{}^{4}_{\Lambda}\mathrm{H},{}^{4}_{\Lambda}\mathrm{He}} \rho_j^s \left[\frac{\partial(\delta B_j)}{\partial \rho_n^{\mathrm{ps}}} \frac{\partial \rho_n^{\mathrm{ps}}}{\rho_{03}} + \frac{\partial(\delta B_j)}{\partial \rho_p^{\mathrm{ps}}} \frac{\partial \rho_p^{\mathrm{ps}}}{\rho_{03}} + \frac{\partial(\delta B_j)}{\partial \rho_\Lambda^{\mathrm{ps}}} \frac{\partial \rho_\Lambda^{\mathrm{ps}}}{\rho_{03}} \right] \tag{A.4}$$

$$\begin{aligned}
&= -\frac{\rho^s_{{}^{3}_{\Lambda}\mathrm{H}}}{\rho_0} \left[\frac{\partial \left(1 \cdot \left(\epsilon_p^* - m\rho_p^*\right) + 1 \cdot \left(\epsilon_n^* - m\rho_n^*\right) + 1 \cdot \left(\epsilon_\Lambda^* - m_\Lambda \rho_\Lambda^*\right)\right)}{\partial \rho_n^{\mathrm{ps}}} \left(-\frac{m_\rho^2}{g_{\rho N}} \right) \right. \\
&\left. + \frac{\partial \left(1 \cdot \left(\epsilon_p^* - m\rho_p^*\right) + 1 \cdot \left(\epsilon_n^* - m\rho_n^*\right) + 1 \cdot \left(\epsilon_\Lambda^* - m_\Lambda \rho_\Lambda^*\right)\right)}{\partial \rho_p^{\mathrm{ps}}} \left(\frac{m_\rho^2}{g_{\rho N}} \right) \right] \\
&\quad -\frac{\rho^s_{{}^{4}_{\Lambda}\mathrm{H}}}{\rho_0} \left[\frac{\partial \left(1 \cdot \left(\epsilon_p^* - m\rho_p^*\right) + 2 \cdot \left(\epsilon_n^* - m\rho_n^*\right) + 1 \cdot \left(\epsilon_\Lambda^* - m_\Lambda \rho_\Lambda^*\right)\right)}{\partial \rho_n^{\mathrm{ps}}} \left(-\frac{m_\rho^2}{g_{\rho N}} \right) \right. \\
&\left. + \frac{\partial \left(1 \cdot \left(\epsilon_p^* - m\rho_p^*\right) + 2 \cdot \left(\epsilon_n^* - m\rho_n^*\right) + 1 \cdot \left(\epsilon_\Lambda^* - m_\Lambda \rho_\Lambda^*\right)\right)}{\partial \rho_p^{\mathrm{ps}}} \left(\frac{m_\rho^2}{g_{\rho N}} \right) \right] \\
&\quad -\frac{\rho^s_{{}^{4}_{\Lambda}\mathrm{He}}}{\rho_0} \left[\frac{\partial \left(2 \cdot \left(\epsilon_p^* - m\rho_p^*\right) + 1 \cdot \left(\epsilon_n^* - m\rho_n^*\right) + 1 \cdot \left(\epsilon_\Lambda^* - m_\Lambda \rho_\Lambda^*\right)\right)}{\partial \rho_n^{\mathrm{ps}}} \left(-\frac{m_\rho^2}{g_{\rho N}} \right) \right. \\
&\left. + \frac{\partial \left(2 \cdot \left(\epsilon_p^* - m\rho_p^*\right) + 1 \cdot \left(\epsilon_n^* - m\rho_n^*\right) + 1 \cdot \left(\epsilon_\Lambda^* - m_\Lambda \rho_\Lambda^*\right)\right)}{\partial \rho_p^{\mathrm{ps}}} \left(\frac{m_\rho^2}{g_{\rho N}} \right) \right]
\end{aligned}$$

$$
\begin{aligned}
&= -\frac{\rho^s_{{}^3_\Lambda\mathrm{H}}}{\rho_0}\left(\frac{m_\rho^2}{g_{\rho N}}\right)\left[-\frac{\partial\epsilon_n^*}{\partial\rho_n^{\mathrm{ps}}}+\frac{m\partial\rho_n^*}{\partial\rho_n^{\mathrm{ps}}}+\frac{\partial\epsilon_p^*}{\partial\rho_p^{\mathrm{ps}}}-\frac{m\partial\rho_p^*}{\partial\rho_p^{\mathrm{ps}}}\right]\\
&\quad -\frac{\rho^s_{{}^4_\Lambda\mathrm{H}}}{\rho_0}\left(\frac{m_\rho^2}{g_{\rho N}}\right)\left[-2\frac{\partial\epsilon_n^*}{\partial\rho_n^{\mathrm{ps}}}+2\frac{m\partial\rho_n^*}{\partial\rho_n^{\mathrm{ps}}}+\frac{\partial\epsilon_p^*}{\partial\rho_p^{\mathrm{ps}}}-\frac{m\partial\rho_p^*}{\partial\rho_p^{\mathrm{ps}}}\right]\\
&\quad -\frac{\rho^s_{{}^4_\Lambda\mathrm{He}}}{\rho_0}\left(\frac{m_\rho^2}{g_{\rho N}}\right)\left[-\frac{\partial\epsilon_n^*}{\partial\rho_n^{\mathrm{ps}}}+\frac{m\partial\rho_n^*}{\partial\rho_n^{\mathrm{ps}}}+2\frac{\partial\epsilon_p^*}{\partial\rho_p^{\mathrm{ps}}}-2\frac{m\partial\rho_p^*}{\partial\rho_p^{\mathrm{ps}}}\right]\\
&= -\frac{1}{\rho_0}\left(\frac{m_\rho^2}{g_{\rho N}}\right)\left(\rho^s_{{}^3_\Lambda\mathrm{H}}+\rho^s_{{}^4_\Lambda\mathrm{H}}+\rho^s_{{}^4_\Lambda\mathrm{He}}\right)\left[-\frac{\partial\epsilon_n^*}{\partial\rho_n^{\mathrm{ps}}}+\frac{m\partial\rho_n^*}{\partial\rho_n^{\mathrm{ps}}}+\frac{\partial\epsilon_p^*}{\partial\rho_p^{\mathrm{ps}}}-\frac{m\partial\rho_p^*}{\partial\rho_p^{\mathrm{ps}}}\right]\\
&\quad -\frac{1}{\rho_0}\left(\frac{m_\rho^2}{g_{\rho N}}\right)\rho^s_{{}^4_\Lambda\mathrm{H}}\left[-\frac{\partial\epsilon_n^*}{\partial\rho_n^{\mathrm{ps}}}+\frac{m\partial\rho_n^*}{\partial\rho_n^{\mathrm{ps}}}\right]\\
&\quad -\frac{1}{\rho_0}\left(\frac{m_\rho^2}{g_{\rho N}}\right)\rho^s_{{}^4_\Lambda\mathrm{He}}\left[\frac{\partial\epsilon_p^*}{\partial\rho_p^{\mathrm{ps}}}-\frac{m\partial\rho_p^*}{\partial\rho_p^{\mathrm{ps}}}\right]
\end{aligned}
$$

- $$-\sum_{\substack{i={}^2\mathrm{H},{}^3\mathrm{H},{}^3\mathrm{He},\\ {}^4\mathrm{He},{}^6\mathrm{He}}}\rho_i^s\left[\frac{\partial(\delta B_i)}{\partial\rho_n^{\mathrm{ps}}}\frac{\partial\rho_n^{\mathrm{ps}}}{\phi_0}+\frac{\partial(\delta B_i)}{\partial\rho_p^{\mathrm{ps}}}\frac{\partial\rho_p^{\mathrm{ps}}}{\phi_0}\right] \tag{A.5}$$

$$
\begin{aligned}
&= -\frac{\rho^s_{{}^2\mathrm{H}}}{\rho_0}\left[\frac{\partial\left(1\cdot\left(\epsilon_p^*-m\rho_p^*\right)+1\cdot\left(\epsilon_n^*-m\rho_n^*\right)\right)}{\partial\rho_n^{\mathrm{ps}}}\left(\frac{-g_{\omega\Lambda}m_\phi^2}{2g_{\omega N}g_{\phi\Lambda}}\right)+\frac{\partial\left(1\cdot\left(\epsilon_p^*-m\rho_p^*\right)+1\cdot\left(\epsilon_n^*-m\rho_n^*\right)\right)}{\partial\rho_p^{\mathrm{ps}}}\left(\frac{-g_{\omega\Lambda}m_\phi^2}{2g_{\omega N}g_{\phi\Lambda}}\right)\right]\\
&\quad -\frac{\rho^s_{{}^3\mathrm{H}}}{\rho_0}\left[\frac{\partial\left(1\cdot\left(\epsilon_p^*-m\rho_p^*\right)+2\cdot\left(\epsilon_n^*-m\rho_n^*\right)\right)}{\partial\rho_n^{\mathrm{ps}}}\left(\frac{-g_{\omega\Lambda}m_\phi^2}{2g_{\omega N}g_{\phi\Lambda}}\right)+\frac{\partial\left(1\cdot\left(\epsilon_p^*-m\rho_p^*\right)+2\cdot\left(\epsilon_n^*-m\rho_n^*\right)\right)}{\partial\rho_p^{\mathrm{ps}}}\left(\frac{-g_{\omega\Lambda}m_\phi^2}{2g_{\omega N}g_{\phi\Lambda}}\right)\right]\\
&\quad -\frac{\rho^s_{{}^3\mathrm{He}}}{\rho_0}\left[\frac{\partial\left(2\cdot\left(\epsilon_p^*-m\rho_p^*\right)+1\cdot\left(\epsilon_n^*-m\rho_n^*\right)\right)}{\partial\rho_n^{\mathrm{ps}}}\left(\frac{-g_{\omega\Lambda}m_\phi^2}{2g_{\omega N}g_{\phi\Lambda}}\right)+\frac{\partial\left(2\cdot\left(\epsilon_p^*-m\rho_p^*\right)+1\cdot\left(\epsilon_n^*-m\rho_n^*\right)\right)}{\partial\rho_p^{\mathrm{ps}}}\left(\frac{-g_{\omega\Lambda}m_\phi^2}{2g_{\omega N}g_{\phi\Lambda}}\right)\right]\\
&\quad -\frac{\rho^s_{{}^4\mathrm{He}}}{\rho_0}\left[\frac{\partial\left(2\cdot\left(\epsilon_p^*-m\rho_p^*\right)+2\cdot\left(\epsilon_n^*-m\rho_n^*\right)\right)}{\partial\rho_n^{\mathrm{ps}}}\left(\frac{-g_{\omega\Lambda}m_\phi^2}{2g_{\omega N}g_{\phi\Lambda}}\right)+\frac{\partial\left(2\cdot\left(\epsilon_p^*-m\rho_p^*\right)+2\cdot\left(\epsilon_n^*-m\rho_n^*\right)\right)}{\partial\rho_p^{\mathrm{ps}}}\left(\frac{-g_{\omega\Lambda}m_\phi^2}{2g_{\omega N}g_{\phi\Lambda}}\right)\right]\\
&\quad -\frac{\rho^s_{{}^6\mathrm{He}}}{\rho_0}\left[\frac{\partial\left(2\cdot\left(\epsilon_p^*-m\rho_p^*\right)+4\cdot\left(\epsilon_n^*-m\rho_n^*\right)\right)}{\partial\rho_n^{\mathrm{ps}}}\left(\frac{-g_{\omega\Lambda}m_\phi^2}{2g_{\omega N}g_{\phi\Lambda}}\right)+\frac{\partial\left(2\cdot\left(\epsilon_p^*-m\rho_p^*\right)+4\cdot\left(\epsilon_n^*-m\rho_n^*\right)\right)}{\partial\rho_p^{\mathrm{ps}}}\left(\frac{-g_{\omega\Lambda}m_\phi^2}{2g_{\omega N}g_{\phi\Lambda}}\right)\right]\\
&= -\frac{\rho^s_{{}^2\mathrm{H}}}{\rho_0}\left(\frac{-g_{\omega\Lambda}m_\phi^2}{2g_{\omega N}g_{\phi\Lambda}}\right)\left[\frac{\partial\epsilon_n^*}{\partial\rho_n^{\mathrm{ps}}}-\frac{m\partial\rho_n^*}{\partial\rho_n^{\mathrm{ps}}}+\frac{\partial\epsilon_p^*}{\partial\rho_p^{\mathrm{ps}}}-\frac{m\partial\rho_p^*}{\partial\rho_p^{\mathrm{ps}}}\right]\\
&\quad -\frac{\rho^s_{{}^3\mathrm{H}}}{\rho_0}\left(\frac{-g_{\omega\Lambda}m_\phi^2}{2g_{\omega N}g_{\phi\Lambda}}\right)\left[2\frac{\partial\epsilon_n^*}{\partial\rho_n^{\mathrm{ps}}}-2\frac{m\partial\rho_n^*}{\partial\rho_n^{\mathrm{ps}}}+\frac{\partial\epsilon_p^*}{\partial\rho_p^{\mathrm{ps}}}-\frac{m\partial\rho_p^*}{\partial\rho_p^{\mathrm{ps}}}\right]\\
&\quad -\frac{\rho^s_{{}^3\mathrm{He}}}{\rho_0}\left(\frac{-g_{\omega\Lambda}m_\phi^2}{2g_{\omega N}g_{\phi\Lambda}}\right)\left[\frac{\partial\epsilon_n^*}{\partial\rho_n^{\mathrm{ps}}}-\frac{m\partial\rho_n^*}{\partial\rho_n^{\mathrm{ps}}}+2\frac{\partial\epsilon_p^*}{\partial\rho_p^{\mathrm{ps}}}-2\frac{m\partial\rho_p^*}{\partial\rho_p^{\mathrm{ps}}}\right]\\
&\quad -\frac{\rho^s_{{}^4\mathrm{He}}}{\rho_0}\left(\frac{-g_{\omega\Lambda}m_\phi^2}{2g_{\omega N}g_{\phi\Lambda}}\right)\left[2\frac{\partial\epsilon_n^*}{\partial\rho_n^{\mathrm{ps}}}-2\frac{m\partial\rho_n^*}{\partial\rho_n^{\mathrm{ps}}}+2\frac{\partial\epsilon_p^*}{\partial\rho_p^{\mathrm{ps}}}-2\frac{m\partial\rho_p^*}{\partial\rho_p^{\mathrm{ps}}}\right]\\
&\quad -\frac{\rho^s_{{}^6\mathrm{He}}}{\rho_0}\left(\frac{-g_{\omega\Lambda}m_\phi^2}{2g_{\omega N}g_{\phi\Lambda}}\right)\left[4\frac{\partial\epsilon_n^*}{\partial\rho_n^{\mathrm{ps}}}-4\frac{m\partial\rho_n^*}{\partial\rho_n^{\mathrm{ps}}}+2\frac{\partial\epsilon_p^*}{\partial\rho_p^{\mathrm{ps}}}-2\frac{m\partial\rho_p^*}{\partial\rho_p^{\mathrm{ps}}}\right]\\
&= +\frac{1}{\rho_0}\left(\frac{g_{\omega\Lambda}m_\phi^2}{2g_{\omega N}g_{\phi\Lambda}}\right)\left(\rho^s_{{}^2\mathrm{H}}+\rho^s_{{}^3\mathrm{H}}+\rho^s_{{}^3\mathrm{He}}+2\rho^s_{{}^4\mathrm{He}}+2\rho^s_{{}^6\mathrm{He}}\right)\left[\frac{\partial\epsilon_n^*}{\partial\rho_n^{\mathrm{ps}}}-\frac{m\partial\rho_n^*}{\partial\rho_n^{\mathrm{ps}}}+\frac{\partial\epsilon_p^*}{\partial\rho_p^{\mathrm{ps}}}-\frac{m\partial\rho_p^*}{\partial\rho_p^{\mathrm{ps}}}\right]\\
&\quad +\frac{1}{\rho_0}\left(\frac{g_{\omega\Lambda}m_\phi^2}{2g_{\omega N}g_{\phi\Lambda}}\right)\left(\rho^s_{{}^3\mathrm{H}}+2\rho^s_{{}^6\mathrm{He}}\right)\left[\frac{\partial\epsilon_n^*}{\partial\rho_n^{\mathrm{ps}}}-\frac{m\partial\rho_n^*}{\partial\rho_n^{\mathrm{ps}}}\right]\\
&\quad +\frac{1}{\rho_0}\left(\frac{g_{\omega\Lambda}m_\phi^2}{2g_{\omega N}g_{\phi\Lambda}}\right)\rho^s_{{}^3\mathrm{He}}\left[\frac{\partial\epsilon_p^*}{\partial\rho_p^{\mathrm{ps}}}-\frac{m\partial\rho_p^*}{\partial\rho_p^{\mathrm{ps}}}\right]
\end{aligned}
$$

$$
\begin{aligned}
\bullet \quad & -\sum_{j={}^{3}_{\Lambda}\mathrm{H},{}^{4}_{\Lambda}\mathrm{H},{}^{4}_{\Lambda}\mathrm{He}} \rho_j^s \left[\frac{\partial(\delta B_j)}{\partial \rho_n^{\mathrm{ps}}} \frac{\partial \rho_n^{\mathrm{ps}}}{\phi_0} + \frac{\partial(\delta B_j)}{\partial \rho_p^{\mathrm{ps}}} \frac{\partial \rho_p^{\mathrm{ps}}}{\phi_0} + \frac{\partial(\delta B_j)}{\partial \rho_\Lambda^{\mathrm{ps}}} \frac{\partial \rho_\Lambda^{\mathrm{ps}}}{\phi_0} \right] \qquad \text{(A.6)} \\
= \quad & -\frac{\rho^s_{{}^{3}_{\Lambda}\mathrm{H}}}{\rho_0} \left[\frac{\partial \left(1 \cdot \left(\epsilon_p^* - m\rho_p^*\right) + 1 \cdot (\epsilon_n^* - m\rho_n^*) + 1 \cdot (\epsilon_\Lambda^* - m_\Lambda \rho_\Lambda^*)\right)}{\partial \rho_n^{\mathrm{ps}}} \left(\frac{-g_{\omega\Lambda} m_\phi^2}{2 g_{\omega N} g_{\phi\Lambda}} \right) \right. \\
& + \frac{\partial \left(1 \cdot \left(\epsilon_p^* - m\rho_p^*\right) + 1 \cdot (\epsilon_n^* - m\rho_n^*) + 1 \cdot (\epsilon_\Lambda^* - m_\Lambda \rho_\Lambda^*)\right)}{\partial \rho_p^{\mathrm{ps}}} \left(\frac{-g_{\omega\Lambda} m_\phi^2}{2 g_{\omega N} g_{\phi\Lambda}} \right) \\
& \left. + \frac{\partial \left(1 \cdot \left(\epsilon_p^* - m\rho_p^*\right) + 1 \cdot (\epsilon_n^* - m\rho_n^*) + 1 \cdot (\epsilon_\Lambda^* - m_\Lambda \rho_\Lambda^*)\right)}{\partial \rho_\Lambda^{\mathrm{ps}}} \left(\frac{m_\phi^2}{g_{\phi\Lambda}} \right) \right] \\
& -\frac{\rho^s_{{}^{4}_{\Lambda}\mathrm{H}}}{\rho_0} \left[\frac{\partial \left(1 \cdot \left(\epsilon_p^* - m\rho_p^*\right) + 2 \cdot (\epsilon_n^* - m\rho_n^*) + 1 \cdot (\epsilon_\Lambda^* - m_\Lambda \rho_\Lambda^*)\right)}{\partial \rho_n^{\mathrm{ps}}} \left(\frac{-g_{\omega\Lambda} m_\phi^2}{2 g_{\omega N} g_{\phi\Lambda}} \right) \right. \\
& + \frac{\partial \left(1 \cdot \left(\epsilon_p^* - m\rho_p^*\right) + 2 \cdot (\epsilon_n^* - m\rho_n^*) + 1 \cdot (\epsilon_\Lambda^* - m_\Lambda \rho_\Lambda^*)\right)}{\partial \rho_p^{\mathrm{ps}}} \left(\frac{-g_{\omega\Lambda} m_\phi^2}{2 g_{\omega N} g_{\phi\Lambda}} \right) \\
& \left. + \frac{\partial \left(1 \cdot \left(\epsilon_p^* - m\rho_p^*\right) + 2 \cdot (\epsilon_n^* - m\rho_n^*) + 1 \cdot (\epsilon_\Lambda^* - m_\Lambda \rho_\Lambda^*)\right)}{\partial \rho_\Lambda^{\mathrm{ps}}} \left(\frac{m_\phi^2}{g_{\phi\Lambda}} \right) \right] \\
& -\frac{\rho^s_{{}^{4}_{\Lambda}\mathrm{He}}}{\rho_0} \left[\frac{\partial \left(2 \cdot \left(\epsilon_p^* - m\rho_p^*\right) + 1 \cdot (\epsilon_n^* - m\rho_n^*) + 1 \cdot (\epsilon_\Lambda^* - m_\Lambda \rho_\Lambda^*)\right)}{\partial \rho_n^{\mathrm{ps}}} \left(\frac{-g_{\omega\Lambda} m_\phi^2}{2 g_{\omega N} g_{\phi\Lambda}} \right) \right. \\
& + \frac{\partial \left(2 \cdot \left(\epsilon_p^* - m\rho_p^*\right) + 1 \cdot (\epsilon_n^* - m\rho_n^*) + 1 \cdot (\epsilon_\Lambda^* - m_\Lambda \rho_\Lambda^*)\right)}{\partial \rho_p^{\mathrm{ps}}} \left(\frac{-g_{\omega\Lambda} m_\phi^2}{2 g_{\omega N} g_{\phi\Lambda}} \right) \\
& \left. + \frac{\partial \left(2 \cdot \left(\epsilon_p^* - m\rho_p^*\right) + 1 \cdot (\epsilon_n^* - m\rho_n^*) + 1 \cdot (\epsilon_\Lambda^* - m_\Lambda \rho_\Lambda^*)\right)}{\partial \rho_\Lambda^{\mathrm{ps}}} \left(\frac{m_\phi^2}{g_{\phi\Lambda}} \right) \right] \\
= \quad & -\frac{\rho^s_{{}^{3}_{\Lambda}\mathrm{H}}}{\rho_0} \left(\frac{-g_{\omega\Lambda} m_\phi^2}{2 g_{\omega N} g_{\phi\Lambda}} \right) \left[\frac{\partial \epsilon_n^*}{\partial \rho_n^{\mathrm{ps}}} - \frac{m \partial \rho_n^*}{\partial \rho_n^{\mathrm{ps}}} + \frac{\partial \epsilon_p^*}{\partial \rho_p^{\mathrm{ps}}} - \frac{m \partial \rho_p^*}{\partial \rho_p^{\mathrm{ps}}} \right] \\
& -\frac{\rho^s_{{}^{4}_{\Lambda}\mathrm{H}}}{\rho_0} \left(\frac{-g_{\omega\Lambda} m_\phi^2}{2 g_{\omega N} g_{\phi\Lambda}} \right) \left[2\frac{\partial \epsilon_n^*}{\partial \rho_n^{\mathrm{ps}}} - 2\frac{m \partial \rho_n^*}{\partial \rho_n^{\mathrm{ps}}} + \frac{\partial \epsilon_p^*}{\partial \rho_p^{\mathrm{ps}}} - \frac{m \partial \rho_p^*}{\partial \rho_p^{\mathrm{ps}}} \right] \\
& -\frac{\rho^s_{{}^{4}_{\Lambda}\mathrm{He}}}{\rho_0} \left(\frac{-g_{\omega\Lambda} m_\phi^2}{2 g_{\omega N} g_{\phi\Lambda}} \right) \left[\frac{\partial \epsilon_n^*}{\partial \rho_n^{\mathrm{ps}}} - \frac{m \partial \rho_n^*}{\partial \rho_n^{\mathrm{ps}}} + 2\frac{\partial \epsilon_p^*}{\partial \rho_p^{\mathrm{ps}}} - 2\frac{m \partial \rho_p^*}{\partial \rho_p^{\mathrm{ps}}} \right] \\
& -\frac{\rho^s_{{}^{3}_{\Lambda}\mathrm{H}}}{\rho_0} \left(\frac{m_\phi^2}{g_{\phi\Lambda}} \right) \left[\frac{\partial \epsilon_\Lambda^*}{\partial \rho_\Lambda^{\mathrm{ps}}} - \frac{m_\Lambda \partial \rho_\Lambda^*}{\partial \rho_\Lambda^{\mathrm{ps}}} \right] \\
& -\frac{\rho^s_{{}^{4}_{\Lambda}\mathrm{H}}}{\rho_0} \left(\frac{m_\phi^2}{g_{\phi\Lambda}} \right) \left[\frac{\partial \epsilon_\Lambda^*}{\partial \rho_\Lambda^{\mathrm{ps}}} - \frac{m_\Lambda \partial \rho_\Lambda^*}{\partial \rho_\Lambda^{\mathrm{ps}}} \right] \\
& -\frac{\rho^s_{{}^{4}_{\Lambda}\mathrm{He}}}{\rho_0} \left(\frac{m_\phi^2}{g_{\phi\Lambda}} \right) \left[\frac{\partial \epsilon_\Lambda^*}{\partial \rho_\Lambda^{\mathrm{ps}}} - \frac{m_\Lambda \partial \rho_\Lambda^*}{\partial \rho_\Lambda^{\mathrm{ps}}} \right] \\
= \quad & +\frac{1}{\rho_0} \left(\frac{g_{\omega\Lambda} m_\phi^2}{2 g_{\omega N} g_{\phi\Lambda}} \right) \left(\rho^s_{{}^{3}_{\Lambda}\mathrm{H}} + \rho^s_{{}^{4}_{\Lambda}\mathrm{H}} + \rho^s_{{}^{4}_{\Lambda}\mathrm{He}} \right) \left[\frac{\partial \epsilon_n^*}{\partial \rho_n^{\mathrm{ps}}} - \frac{m \partial \rho_n^*}{\partial \rho_n^{\mathrm{ps}}} + \frac{\partial \epsilon_p^*}{\partial \rho_p^{\mathrm{ps}}} - \frac{m \partial \rho_p^*}{\partial \rho_p^{\mathrm{ps}}} \right] \\
& +\frac{1}{\rho_0} \left(\frac{g_{\omega\Lambda} m_\phi^2}{2 g_{\omega N} g_{\phi\Lambda}} \right) \rho^s_{{}^{4}_{\Lambda}\mathrm{H}} \left[\frac{\partial \epsilon_n^*}{\partial \rho_n^{\mathrm{ps}}} - \frac{m \partial \rho_n^*}{\partial \rho_n^{\mathrm{ps}}} \right] + \frac{1}{\rho_0} \left(\frac{g_{\omega\Lambda} m_\phi^2}{2 g_{\omega N} g_{\phi\Lambda}} \right) \rho^s_{{}^{4}_{\Lambda}\mathrm{He}} \left[\frac{\partial \epsilon_p^*}{\partial \rho_p^{\mathrm{ps}}} - \frac{m \partial \rho_p^*}{\partial \rho_p^{\mathrm{ps}}} \right] \\
& -\frac{1}{\rho_0} \left(\frac{m_\phi^2}{g_{\phi\Lambda}} \right) \left(\rho^s_{{}^{3}_{\Lambda}\mathrm{H}} + \rho^s_{{}^{4}_{\Lambda}\mathrm{H}} + \rho^s_{{}^{4}_{\Lambda}\mathrm{He}} \right) \left[\frac{\partial \epsilon_\Lambda^*}{\partial \rho_\Lambda^{\mathrm{ps}}} - \frac{m_\Lambda \partial \rho_\Lambda^*}{\partial \rho_\Lambda^{\mathrm{ps}}} \right]
\end{aligned}
$$

A.3 Meson Equations of Motion for Density-Dependent RMF Models

$$m_\sigma^2 \sigma = \sum_{c=b,\Delta,i,j} g_{\sigma c} \rho_c^s \tag{A.7}$$

$$\begin{aligned} m_\omega^2 \omega_0 &= \sum_b g_{\omega b}\rho_b + \sum_\Delta g_{\omega\Delta}\rho_\Delta + \sum_i g_{\omega i}\rho_i + \sum_j g_{\omega j}\rho_j \\ &\quad -\frac{1}{\rho_0}\left(\frac{m_\omega^2}{2g_{\omega N}}\right)\left(\rho_{^2\mathrm{H}}^s + \rho_{^3\mathrm{H}}^s + \rho_{^3\mathrm{He}}^s + 2\rho_{^4\mathrm{He}}^s + 2\rho_{^6\mathrm{He}}^s\right. \\ &\quad \left. +\rho_{^3_\Lambda\mathrm{H}}^s + \rho_{^4_\Lambda\mathrm{H}}^s + \rho_{^4_\Lambda\mathrm{He}}^s\right)\left[\frac{\partial\epsilon_n^*}{\partial\rho_n^{\mathrm{ps}}} - \frac{m\partial\rho_n^*}{\partial\rho_n^{\mathrm{ps}}} + \frac{\partial\epsilon_p^*}{\partial\rho_p^{\mathrm{ps}}} - \frac{m\partial\rho_p^*}{\partial\rho_p^{\mathrm{ps}}}\right] \\ &\quad -\frac{1}{\rho_0}\left(\frac{m_\omega^2}{2g_{\omega N}}\right)\left(\rho_{^3\mathrm{H}}^s + 2\rho_{^6\mathrm{He}}^s + \rho_{^4_\Lambda\mathrm{H}}^s\right)\left[\frac{\partial\epsilon_n^*}{\partial\rho_n^{\mathrm{ps}}} - \frac{m\partial\rho_n^*}{\partial\rho_n^{\mathrm{ps}}}\right] \\ &\quad -\frac{1}{\rho_0}\left(\frac{m_\omega^2}{2g_{\omega N}}\right)\left(\rho_{^3\mathrm{He}}^s + \rho_{^4_\Lambda\mathrm{He}}^s\right)\left[\frac{\partial\epsilon_p^*}{\partial\rho_p^{\mathrm{ps}}} - \frac{m\partial\rho_p^*}{\partial\rho_p^{\mathrm{ps}}}\right] \end{aligned} \tag{A.8}$$

$$\begin{aligned} m_\rho^2 \rho_{03} &= g_{\rho N}\left[\sum_b I_{3b}\rho_b + \sum_\Delta I_{3\Delta}\rho_\Delta + \sum_i I_{3i}\rho_i + \sum_j I_{3j}\rho_j\right] \\ &\quad -\frac{1}{\rho_0}\left(\frac{m_\rho^2}{g_{\rho N}}\right)\left(\rho_{^2\mathrm{H}}^s + \rho_{^3\mathrm{H}}^s + \rho_{^3\mathrm{He}}^s + 2\rho_{^4\mathrm{He}}^s + 2\rho_{^6\mathrm{He}}^s\right. \\ &\quad \left. +\rho_{^3_\Lambda\mathrm{H}}^s + \rho_{^4_\Lambda\mathrm{H}}^s + \rho_{^4_\Lambda\mathrm{He}}^s\right)\left[-\frac{\partial\epsilon_n^*}{\partial\rho_n^{\mathrm{ps}}} + \frac{m\partial\rho_n^*}{\partial\rho_n^{\mathrm{ps}}} + \frac{\partial\epsilon_p^*}{\partial\rho_p^{\mathrm{ps}}} - \frac{m\partial\rho_p^*}{\partial\rho_p^{\mathrm{ps}}}\right] \\ &\quad -\frac{1}{\rho_0}\left(\frac{m_\rho^2}{g_{\rho N}}\right)\left(\rho_{^3\mathrm{H}}^s + 2\rho_{^6\mathrm{He}}^s + \rho_{^4_\Lambda\mathrm{H}}^s\right)\left[-\frac{\partial\epsilon_n^*}{\partial\rho_n^{\mathrm{ps}}} + \frac{m\partial\rho_n^*}{\partial\rho_n^{\mathrm{ps}}}\right] \\ &\quad -\frac{1}{\rho_0}\left(\frac{m_\rho^2}{g_{\rho N}}\right)\left(\rho_{^3\mathrm{He}}^s + \rho_{^4_\Lambda\mathrm{He}}^s\right)\left[\frac{\partial\epsilon_p^*}{\partial\rho_p^{\mathrm{ps}}} - \frac{m\partial\rho_p^*}{\partial\rho_p^{\mathrm{ps}}}\right] \end{aligned} \tag{A.9}$$

$$\begin{aligned} m_\phi^2 \phi_0 &= \sum_b g_{\phi b}\rho_b + \sum_j g_{\phi j}\rho_j \\ &\quad +\frac{1}{\rho_0}\left(\frac{g_{\omega\Lambda}m_\phi^2}{2g_{\omega N}g_{\phi\Lambda}}\right)\left(\rho_{^2\mathrm{H}}^s + \rho_{^3\mathrm{H}}^s + \rho_{^3\mathrm{He}}^s + 2\rho_{^4\mathrm{He}}^s + 2\rho_{^6\mathrm{He}}^s\right. \\ &\quad \left. +\rho_{^3_\Lambda\mathrm{H}}^s + \rho_{^4_\Lambda\mathrm{H}}^s + \rho_{^4_\Lambda\mathrm{He}}^s\right)\left[\frac{\partial\epsilon_n^*}{\partial\rho_n^{\mathrm{ps}}} - \frac{m\partial\rho_n^*}{\partial\rho_n^{\mathrm{ps}}} + \frac{\partial\epsilon_p^*}{\partial\rho_p^{\mathrm{ps}}} - \frac{m\partial\rho_p^*}{\partial\rho_p^{\mathrm{ps}}}\right] \\ &\quad +\frac{1}{\rho_0}\left(\frac{g_{\omega\Lambda}m_\phi^2}{2g_{\omega N}g_{\phi\Lambda}}\right)\left(\rho_{^3\mathrm{H}}^s + 2\rho_{^6\mathrm{He}}^s + \rho_{^4_\Lambda\mathrm{H}}^s\right)\left[\frac{\partial\epsilon_n^*}{\partial\rho_n^{\mathrm{ps}}} - \frac{m\partial\rho_n^*}{\partial\rho_n^{\mathrm{ps}}}\right] \\ &\quad +\frac{1}{\rho_0}\left(\frac{g_{\omega\Lambda}m_\phi^2}{2g_{\omega N}g_{\phi\Lambda}}\right)\left(\rho_{^3\mathrm{He}}^s + \rho_{^4_\Lambda\mathrm{He}}^s\right)\left[\frac{\partial\epsilon_p^*}{\partial\rho_p^{\mathrm{ps}}} - \frac{m\partial\rho_p^*}{\partial\rho_p^{\mathrm{ps}}}\right] \\ &\quad -\frac{1}{\rho_0}\left(\frac{m_\phi^2}{g_{\phi\Lambda}}\right)\left(\rho_{^3_\Lambda\mathrm{H}}^s + \rho_{^4_\Lambda\mathrm{H}}^s + \rho_{^4_\Lambda\mathrm{He}}^s\right)\left[\frac{\partial\epsilon_\Lambda^*}{\partial\rho_\Lambda^{\mathrm{ps}}} - \frac{m_\Lambda\partial\rho_\Lambda^*}{\partial\rho_\Lambda^{\mathrm{ps}}}\right] \end{aligned} \tag{A.10}$$

References

[1] N. K. Glendenning, *Compact Stars: Nuclear Physics, Particle Physics, and General Relativity (Astron. Astrophys. Library)*. Springer, 2000.

[2] N. Chamel and P. Haensel, "Physics of Neutron Star Crusts," *Living Reviews in Relativity*, vol. 11, no. 1, p. 10, 2008.

[3] I. Vidaña, "A short walk through the physics of neutron stars," *The European Physical Journal Plus*, vol. 133, no. 10, p. 445, 2018.

[4] D. G. Ravenhall *et al.*, "Structure of Matter below Nuclear Saturation Density," *Physical Review Letters*, vol. 50, pp. 2066–2069, June 1983.

[5] G. Watanabe *et al.*, "Simulation of transitions between "pasta" phases in dense matter," *Physical Review Letters*, vol. 94, no. 3, p. 031101, 2005.

[6] H. Pais and J. R. Stone, "Exploring the nuclear pasta phase in core-collapse supernova matter," *Physical Review Letters*, vol. 109, no. 15, p. 151101, 2012.

[7] H. Pais and S. Typel, "Comparison of equation of state models with different cluster dissolution mechanisms," *arXiv*, 2016.

[8] J. Adam *et al.*, "Measurement of the mass difference and the binding energy of the hypertriton and antihypertriton," *Nature Phys.*, vol. 16, no. 4, pp. 409–412, 2020.

[9] A. Esser *et al.*, "Observation of ${}^{4}_{\Lambda}$H hyperhydrogen by decay-pion spectroscopy in electron scattering," *Phys. Rev. Lett.*, vol. 114, p. 232501, Jun 2015.

[10] T. O. Yamamoto *et al.*, "Observation of spin-dependent charge symmetry breaking in Λn interaction: Gamma-ray spectroscopy of ${}^{4}_{\Lambda}$He," *Phys. Rev. Lett.*, vol. 115, p. 222501, Nov 2015.

[11] P. Braun-Munzinger and B. Dönigus, "Loosely-bound objects produced in nuclear collisions at the LHC," *Nucl. Phys. A*, vol. 987, pp. 144–201, 2019.

[12] L. Qin *et al.*, "Laboratory Tests of Low Density Astrophysical Equations of State," *Phys. Rev. Lett.*, vol. 108, p. 172701, 2012.

[13] R. Bougault *et al.*, "Equilibrium constants of Hydrogen and Helium isotopes at low nuclear densities," *J. Phys. G*, vol. 47, no. 2, p. 025103, 2020.

[14] A. Arcones *et al.*, "Influence of light nuclei on neutrino-driven supernova outflows," *Phys. Rev. C*, vol. 78, p. 015806, 2008.

[15] T. Fischer *et al.*, "Medium modifications for light and heavy nuclear clusters in simulations of core collapse supernovae – Impact on equation of state and weak interactions," *Phys. Rev. C*, vol. 102, no. 5, p. 055807, 2020.

[16] S. Rosswog, "The multi-messenger picture of compact binary mergers," *Int. J. Mod. Phys. D*, vol. 24, no. 05, p. 1530012, 2015.

[17] M. G. Alford *et al.*, "Viscous Dissipation and Heat Conduction in Binary Neutron-Star Mergers," *Phys. Rev. Lett.*, vol. 120, no. 4, p. 041101, 2018.

[18] S. Fujibayashi *et al.*, "Mass Ejection from the Remnant of a Binary Neutron Star Merger: Viscous-Radiation Hydrodynamics Study," *Astrophys. J.*, vol. 860, no. 1, p. 64, 2018.

[19] M. Marques *et al.*, "New temperature dependent hyperonic equation of state: Application to rotating neutron star models and I-Q relations," *Phys. Rev. C*, vol. 96, no. 4, p. 045806, 2017.

[20] M. Fortin *et al.*, "Hyperons in hot dense matter: what do the constraints tell us for equation of state?," *Publ. Astron. Soc. Austral.*, vol. 35, p. 44, 2018.

[21] D. P. Menezes and C. Providência, "Hyperons in the nuclear pasta phase," *Phys. Rev. C*, vol. 96, no. 4, p. 045803, 2017.

[22] A. Sedrakian, "Light clusters in dilute heavy-baryon admixed nuclear matter," *Eur. Phys. J. A*, vol. 56, no. 10, p. 258, 2020.

[23] H. Pais *et al.*, "Light clusters in warm stellar matter: explicit mass shifts and universal cluster-meson couplings," *Phys. Rev. C*, vol. 97, no. 4, p. 045805, 2018.

[24] H. Pais *et al.*, "Low density in-medium effects on light clusters from heavy-ion data," *Phys. Rev. Lett.*, vol. 125, p. 012701, Jul 2020.

[25] H. Pais *et al.*, "Improved method for the experimental determination of in-medium effects from heavy-ion collisions," *J. Phys. G*, vol. 47, no. 10, p. 105204, 2020.

[26] T. Custódio *et al.*, "Light clusters in warm stellar matter: calibrating the cluster couplings," *Eur. Phys. J. A*, vol. 56, no. 11, p. 295, 2020.

[27] T. Custódio *et al.*, "Light hyperclusters and hyperons in low-density hot stellar matter," *Phys. Rev. C*, vol. 104, p. 035801, Sep 2021.

[28] P. Ribes *et al.*, "Interplay between delta particles and hyperons in neutron stars," *The Astrophysical Journal*, vol. 883, p. 168, oct 2019.

[29] M. Fortin *et al.*, "Hypernuclei and massive neutron stars," *Phys. Rev. C*, vol. 95, p. 065803, Jun 2017.

[30] J. Boguta and A. Bodmer, "Relativistic calculation of nuclear matter and the nuclear surface," *Nuclear Physics A*, vol. 292, pp. 413–428, Dec. 1977.

[31] H. Müller and B. D. Serot, "Relativistic mean-field theory and the high-density nuclear equation of state," *Nuclear Physics A*, vol. 606, no. 3, pp. 508–537, 1996.

[32] C. J. Horowitz and J. Piekarewicz, "Neutron star structure and the neutron radius ofp208b," *Physical Review Letters*, vol. 86, pp. 5647–5650, June 2001.

[33] W.-C. Chen and J. Piekarewicz, "Building relativistic mean field models for finite nuclei and neutron stars," *Phys. Rev. C*, vol. 90, p. 044305, Oct 2014.

[34] W.-C. Chen and J. Piekarewicz, "Searching for isovector signatures in the neutron-rich oxygen and calcium isotopes," *Physics Letters B*, vol. 748, pp. 284–288, 2015.

[35] F. Hofmann *et al.*, "Density dependent hadron field theory for asymmetric nuclear matter and exotic nuclei," *Phys. Rev. C*, vol. 64, p. 034314, Aug 2001.

[36] C. Fuchs *et al.*, "Density dependent hadron field theory," *Phys. Rev. C*, vol. 52, pp. 3043–3060, Dec 1995.

[37] S. Typel *et al.*, "Composition and thermodynamics of nuclear matter with light clusters," *Phys. Rev. C*, vol. 81, p. 015803, Jan 2010.

[38] H. Pais *et al.*, "Full distribution of clusters with universal couplings and in-medium effects," *Phys. Rev. C*, vol. 99, p. 055806, May 2019.

[39] NIST, "Atomic weights and isotopic compositions for all elements," 2021. Visited on 19/10/21.

[40] Z.-L. She *et al.*, "Predictions for production of ${}^{3}_{\Lambda}H$ and ${}^{3}_{\Lambda}\overline{H}$ in isobaric ${}^{96}_{44}$Ru+${}^{96}_{44}$Ru and ${}^{96}_{40}$Zr+${}^{96}_{40}$Zr collisions at $\sqrt{s_{NN}} = 200$ GeV," *Phys. Rev. C*, vol. 103, no. 1, p. 014906, 2021.

[41] S. Typel *et al.*, "Effects of the liquid-gas phase transition and cluster formation on the symmetry energy," *Eur. Phys. J. A*, 2014.

[42] G. A. Lalazissis *et al.*, "New relativistic mean-field interaction with density-dependent meson-nucleon couplings," *Phys. Rev. C*, vol. 71, p. 024312, Feb 2005.

[43] L. Tolos *et al.*, "The equation of state for the nucleonic and hyperonic core of neutron stars," *Publications of the Astronomical Society of Australia*, vol. 34, p. e065, 2017.

[44] L. Tolos *et al.*, "Equation of state for nucleonic and hyperonic neutron stars with mass and radius constraints," vol. 834, p. 3, Dec 2016.

[45] K. Sumiyoshi *et al.*, "Influence of density dependence of symmetry energy in hot and dense matter for supernova simulations," vol. 887, p. 110, Dec 2019.

[46] H. Shen *et al.*, "Effects of symmetry energy on the equation of state for simulations of core-collapse supernovae and neutron-star mergers," *The Astrophysical Journal*, vol. 891, p. 148, mar 2020.

[47] O. Boukari *et al.*, "Critical properties of calibrated relativistic mean-field models for the transition to warm, nonhomogeneous nuclear and stellar matter," *Phys. Rev. C*, vol. 103, p. 055804, May 2021.

[48] T. E. Riley *et al.*, "A NICER view of PSR J0030+0451: Millisecond pulsar parameter estimation," vol. 887, p. L21, Dec 2019.

[49] M. Oertel *et al.*, "Equations of state for supernovae and compact stars," *Rev. Mod. Phys.*, vol. 89, no. 1, p. 015007, 2017.

[50] I. Tews *et al.*, "Symmetry Parameter Constraints from a Lower Bound on Neutron-matter Energy," vol. 848, p. 105, oct 2017.

[51] J. Birkhan *et al.*, "Electric dipole polarizability of ^{48}Ca and implications for the neutron skin," *Phys. Rev. Lett.*, vol. 118, p. 252501, Jun 2017.

[52] S. Weissenborn *et al.*, "Hyperons and massive neutron stars: Vector repulsion and SU(3) symmetry," *Phys. Rev. C*, vol. 85, p. 065802, Jun 2012.

[53] A. Gal *et al.*, "Strangeness in nuclear physics," *Rev. Mod. Phys.*, vol. 88, p. 035004, Aug 2016.

[54] M. Fortin *et al.*, "Relativistic hypernuclear compact stars with calibrated equations of state," *Phys. Rev. D*, vol. 101, p. 034017, Feb 2020.

[55] C. Providência *et al.*, "Hyperonic stars and the symmetry energy," 2018.

[56] S. X. Nakamura *et al.*, "Dynamical model of coherent pion production in neutrino-nucleus scattering," *Phys. Rev. C*, vol. 81, p. 035502, Mar 2010.

[57] J. Koch and N. Ohtsuka, "Inclusive electron scattering from light nuclei at intermediate energies," *Nuclear Physics A*, vol. 435, no. 3, pp. 765–790, 1985.

[58] K. Wehrberger *et al.*, "Electromagnetic excitation of the delta-baryon in quantum hadrodynamics," *Nuclear Physics A*, vol. 504, no. 4, pp. 797–817, 1989.

[59] A. R. Raduta, "Δ-admixed neutron stars: Spinodal instabilities and durca processes," *Physics Letters B*, vol. 814, p. 136070, 2021.

[60] A. Drago *et al.*, "Early appearance of Δ isobars in neutron stars," *Phys. Rev. C*, vol. 90, p. 065809, Dec 2014.

[61] E. Kolomeitsev *et al.*, "Delta isobars in relativistic mean-field models with σ-scaled hadron masses and couplings," *Nuclear Physics A*, vol. 961, pp. 106–141, 2017.

[62] R. C. Tolman, "Static solutions of einstein's field equations for spheres of fluid," *Phys. Rev.*, vol. 55, pp. 364–373, Feb 1939.

[63] J. R. Oppenheimer and G. M. Volkoff, "On massive neutron cores," *Phys. Rev.*, vol. 55, pp. 374–381, Feb 1939.

[64] G. Baym *et al.*, "The ground state of matter at high densities: Equation of state and stellar models," *The Astrophysical Journal*, vol. 170, p. 299, Dec. 1971.

[65] F. Grill *et al.*, "Equation of state and thickness of the inner crust of neutron stars," *Phys. Rev.*, vol. C90, no. 4, p. 045803, 2014.

[66] H. Pais and C. Providência, "Vlasov formalism for extended relativistic mean field models: The crust-core transition and the stellar matter equation of state," *Physical Review C*, vol. 94, July 2016.

[67] M. Fortin *et al.*, "Neutron star radii and crusts: Uncertainties and unified equations of state," *Phys. Rev. C*, vol. 94, p. 035804, Sep 2016.

[68] F. Grill *et al.*, "Equation of state and thickness of the inner crust of neutron stars," *Phys. Rev. C*, vol. 90, p. 045803, Oct 2014.

[69] C. Providência *et al.*, "Hyperonic stars and the nuclear symmetry energy," *Frontiers in Astronomy and Space Sciences*, vol. 6, p. 13, 2019.

[70] M. C. Miller *et al.*, "The radius of PSR J0740+6620 from NICER and XMM-newton data," *The Astrophysical Journal Letters*, vol. 918, p. L28, sep 2021.

[71] J. Antoniadis *et al.*, "A massive pulsar in a compact relativistic binary," *Science*, vol. 340, no. 6131, p. 1233232, 2013.

[72] N. K. Glendenning and J. Schaffner-Bielich, "First order kaon condensate," *Phys. Rev. C*, vol. 60, p. 025803, Jul 1999.

[73] D. P. Menezes *et al.*, "Kaon condensation in the quark-meson coupling model and compact stars," *Phys. Rev. C*, vol. 72, p. 035802, Sep 2005.

[74] P. K. Panda *et al.*, "Effects of the symmetry energy on the kaon condensates in the quark-meson coupling model," *Phys. Rev. C*, vol. 89, p. 045803, Apr 2014.

[75] V. B. Thapa *et al.*, "Massive Δ-resonance admixed hypernuclear stars with antikaon condensations," *Phys. Rev. D*, vol. 103, p. 063004, Mar 2021.